

MASARYKOVA UNIVERZITA  
Přirodovědecká fakulta  
Ústav teoretické fyziky a astrofyziky

## Diplomová práce

Brno 2025

Anna Richterková

MASARYKOVA UNIVERZITA

Přírodovědecká fakulta

Ústav teoretické fyziky a astrofyziky

Diplomová práce  
Studium vícenásobných hvězdných systémů

Anna Richterková

Vedoucí práce:  
doc. RNDr. Miloslav Zejda, Ph.D.

Brno 2025

# Bibliografický záznam

**Autor:** Anna Richterková

**Název práce:** Studium vícenásobných hvězdných systémů

**Studijní program:** Fyzika

**Studijní plán:** Teoretická fyzika a astrofyzika

**Vedoucí práce:** doc. RNDr. Miloslav Zejda, Ph.D.

**Akademický rok:** 2024/2025

**Počet stran:** IX+84

**Klíčová slova:** zákrytové dvojhvězdy, čtyřhvězdy, O-C diagram, LiTE efekt, SILICUPS, PHOEBE

# Bibliographic entry

**Author:** Anna Richterková

**Title:** Study of multiple stellar systems

**Degree programme:** Physics

**Study plan:** Theoretical physics and astrophysics

**Supervisor:** doc. RNDr. Miloslav Zejda, Ph.D.

**Academic year:** 2024/2025

**Number of pages:** IX + 84

**Key words:** eclipsing binaries, quadruples, O-C diagram, LiTE effect, SILICUPS, PHOEBE

# Abstrakt

Tato práce se zabývá studiem zákrytových čtyřhvězd v uspořádání 2+2. Konkrétně zkoumá systémy ASAS J073054-1840.7, V0674 Pup a TYC 2201-991-1, které byly představeny jako kandidáti na zákrytové čtyřhvězdy. Pomocí fotometrických dat byly získány fázové křivky, fyzikální modely, okamžiky minim, O-C diagramy a modely O-C diagramů jednotlivých párů. O-C diagramy dále sloužily ke zpřesnění oběžných period a okamžiků základního minima. Ve spektroskopických měřeních byly zkoumány posuvy spektrálních čar a jejich štepení vlivem Dopplerova efektu. Na základě těchto pozorování byla potvrzena gravitační vazba u systémů V0674 Pup a TYC 2201-991-1. Pro potvrzení nebo vyvrácení gravitační vazby mezi páry v systému ASAS J073054-1840.7 by byla nutná další pozorování.

# Abstract

In this thesis, we study a multiply eclipsing system in the arrangement 2+2. Specifically we analyse the systems ASAS J073054-1840.7, V0674 Pup and TYC 2201-991-1, which were introduced as candidates for a quadruple. Using photometric measurements the phase curves, physical models, moments of initial minima, O-C diagrams, and the models of O-C diagrams were obtained. The O-C diagrams further served for specification of orbital periods and moments of initial minima. The shift of spectral lines and splitting due to the Doppler effect were examined in spectroscopic measurements. Based on these observations, the gravitational bond was proven in systems V0674 Pup and TYC 2201-991-1. To prove the gravitational bond between pairs in system ASAS J073054-1840.7, more observations are essential.

ZADÁNÍ  
DIPLOMOVÉ PRÁCE

Akademický rok: 2024/2025

---

**Ústav:** Ústav teoretické fyziky a astrofyziky

---

**Studentka:** Bc. Anna Richterková

---

**Program:** Fyzika

---

**Specializace:** Astrofyzika

Ředitel ústavu PŘF MU Vám ve smyslu Studijního a zkušebního řádu MU určuje diplomovou práci s názvem:

---

**Název práce:** Studium vícenásobných hvězdných systémů

---

**Název práce anglicky:** Study of multiple stellar systems

---

**Jazyk práce:** angličtina**Oficiální zadání:**

Vícenásobně zákrytové hvězdné soustavy představují relativně novou třídu objektů, která se nabízí jako významný zdroj informací o hvězdných systémech. Zatím je známo poměrně málo takových soustav a to zejména v severní části hvězdné oblohy. Cílem práce bude za pomoci dat z přehlídkových projektů, nově zejména TESS, vyhledávat další minimálně dvojkrytové soustavy a sestavit jejich katalog. Na takto získaném vzorku hvězdných soustav bude studovat obecné vlastnosti těchto soustav, například četnost určitých poměrů oběžných period složek systému. U alespoň jedné vybrané soustavy doplní případně sesbíraná data o vlastní fotometrická a spektroskopická pozorování a provede detailní analýzu systému s určením parametrů jednotlivých složek.

---

**Vedoucí práce:** doc. RNDr. Miloslav Zejda, Ph.D.

---

**Konzultant:** Mgr. Jakub Kolář

---

**Datum zadání práce:** 1. 11. 2023

---

**V Brně dne:** 22. 4. 2025

Zadání bylo schváleno prostřednictvím IS MU.

Bc. Anna Richterková, 28. 11. 2024

doc. RNDr. Miloslav Zejda, Ph.D., 28. 11. 2024

Mgr. Dušan Hemzal, Ph.D., 29. 11. 2024

# Poděkování

Na tomto místě bych chtěla poděkovat svému vedoucímu práce doc. RNDr. Miloslavu Zejdovi, Ph.D. a konzultantovi Mgr. Jakubu Kolářovi za cenné rady, ochotu vše vysvětlit, vstřícný přístup, čas, který mi věnovali i poskytnutá data. Velké díky patří také RNDr. Janu Janíkovi, Ph.D. za poskytnutá spektroskopická měření a cenné rady při jejich analýze. Dále bych ráda poděkovala Bc. Rudolfu Novákovi za zaučení práce s dalekohledy, pomoc při řešení technických problémů a vstřícnost při domluvě pozorovacího času.

# Prohlášení

Prohlašuji, že jsem svoji diplomovou práci vypracovala samostatně pod vedením vedoucího práce s využitím informačních zdrojů, které jsou v práci citovány.

Brno 2025

.....

Anna Richterková

# Contents

<b>1</b>	<b>Theory of quadruples</b>	<b>1</b>
1.1	Introduction to quadruples and eclipsing binaries . . . . .	1
1.2	Phenomena in spectra of eclipsing binaries . . . . .	2
1.2.1	Doppler effect . . . . .	2
1.2.2	Radial velocities . . . . .	2
1.3	Phenomena in lightcurves of eclipsing binaries . . . . .	3
1.3.1	Elliptical orbital trajectory . . . . .	3
1.3.2	Reflection effect . . . . .	4
1.3.3	Limb darkening . . . . .	4
1.3.4	O'Connell effect . . . . .	5
1.3.5	Transfer of mass . . . . .	5
1.3.6	Apsidal motion . . . . .	6
1.3.7	Stellar spots . . . . .	6
1.3.8	LITE effect . . . . .	7
<b>2</b>	<b>The process of analysis of light curves of eclipsing binaries</b>	<b>8</b>
2.1	Downloading TESS data . . . . .	9
2.2	Detrending . . . . .	13
2.3	Disentanglement by iterative method . . . . .	14
2.3.1	System of two binaries . . . . .	14
2.3.2	System of three binaries . . . . .	15
2.4	Disentanglement by Fourier method . . . . .	16
2.5	O-C diagrams . . . . .	19
2.6	Estimation of the physical parameters for the physical fit . . . . .	22
2.6.1	Mass ratio . . . . .	22
2.6.2	Temperature . . . . .	24
<b>3</b>	<b>S2 Pup</b>	<b>25</b>
3.1	Basic information . . . . .	25
3.2	Disentangled lightcurves . . . . .	27
3.2.1	Pair A . . . . .	30
3.2.2	Pair B . . . . .	30
3.2.3	Pair C . . . . .	32
3.3	O-C diagrams . . . . .	33
3.3.1	Pair A . . . . .	33
3.3.2	Pair B . . . . .	34
3.3.3	Pair C . . . . .	37
3.4	Spectra . . . . .	39

3.5	Physical models . . . . .	43
3.5.1	Pair A . . . . .	43
3.5.2	Pair B . . . . .	45
3.6	Summary . . . . .	47
<b>4</b>	<b>S1 Pup</b>	<b>48</b>
4.1	Basic information . . . . .	48
4.2	Disentangled lightcurves . . . . .	50
4.2.1	Pair A . . . . .	50
4.2.2	Pair B . . . . .	52
4.3	O-C diagrams . . . . .	53
4.3.1	Pair A . . . . .	53
4.3.2	Pair B . . . . .	55
4.4	Spectra . . . . .	56
4.5	Physical models . . . . .	59
4.5.1	Pair A . . . . .	59
4.5.2	Pair B . . . . .	61
4.6	Summary . . . . .	62
<b>5</b>	<b>S1 Peg</b>	<b>64</b>
5.1	Basic information . . . . .	64
5.2	Disentangled lightcurves . . . . .	66
5.2.1	Pair A . . . . .	66
5.2.2	Pair B . . . . .	68
5.3	O-C diagrams . . . . .	70
5.3.1	Pair A . . . . .	70
5.3.2	Pair B . . . . .	70
5.4	Physical models . . . . .	73
5.4.1	Pair A . . . . .	73
5.4.2	Pair B . . . . .	73
5.5	Summary . . . . .	76
	<b>Conclusion</b>	<b>78</b>
	<b>Bibliography</b>	<b>79</b>
	<b>Appendices</b>	<b>82</b>

# Chapter 1

## Theory of quadruples

### 1.1 Introduction to quadruples and eclipsing binaries

The increasing number of sky surveys, together with developing and financially available technologies, led to the discovery of a vast number of variable stars. This thesis will mainly concentrate on doubly eclipsing stellar objects (quadruples) in the arrangement of 2+2, which is one of the stable configurations. Arrangement 2+2 (see Figure 1.1) describes a system where 2 eclipsing binaries orbit around the common centre of mass and components are gravitationally bound.

The motivation for studying quadruples is the lack of yet proven systems. Most of the quadruple systems have not been studied in detail, and the gravitational bond between the components has not been proven. Therefore the formation and evolution of quadruples has not been explained yet. Analysing the systems in detail and determining the basic characteristics of quadruples in total (but also for individual components) will lead to the statistical sample essential for creating evolutionary models.

One of the first attempts at statistical analysis of the doubly eclipsing stellar objects was made by Kolář et al. (2025). In this article, the inner orbital period ratios of 781 candidates were analysed. Out of the 781 candidates, only 60 were confirmed as 2+2 quadruples. The period ratio  $R$  was calculated:

$$R = \frac{P_A}{P_B} \tag{1.1}$$

where  $P_A$  is the orbital period of pair A and  $P_B$  is the orbital period of pair B. The pairs were labeled A and B so that  $P_A \geq P_B$ .

Comparing the available data with the statistical model, there is a rise in the resonance 3:2. This may represent a configuration from which the system evolves with time or a stable configuration to which systems tend to evolve throughout time.

The lack of systems at higher period ratios can be influenced by the selection bias. For further detailed analysis, a more significant statistical sample is essential. This work should help with confirming of a possible candidates for doubly eclipsing systems. To understand how quadruples work and to analyse them properly, we first need to understand the topic of eclipsing binaries.

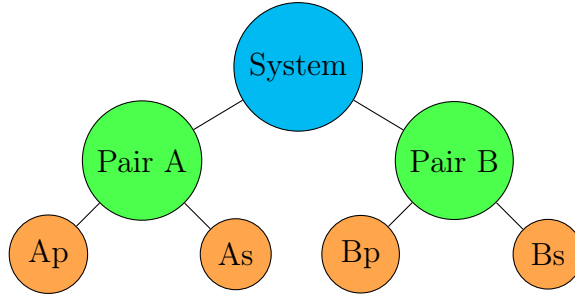


Figure 1.1: Scheme of doubly eclipsing quadruple star system.

## 1.2 Phenomena in spectra of eclipsing binaries

### 1.2.1 Doppler effect

In eclipsing binaries, two components orbit around the common centre of mass, therefore components periodically draw near and recede from us. The Doppler effect causes the emitted electromagnetic radiation to increase in frequency when the component gets near us, resulting in a lower wavelength observed (blueshift). On the other hand, when the component is moving away from us, the light emitted by the component encounters a decrease in frequency and, therefore, an increase in observed wavelength (redshift).

When the primary component draws near to us the secondary component becomes more distant and vice versa. The shift of spectral lines in opposite directions causes the spectral line to appear to be splitting into two lines, where each line corresponds to the individual component. In the time of an eclipse, no splitting is observed as the components are not moving toward us nor away from us.

### 1.2.2 Radial velocities

The measurements of the size of the shift of spectral lines caused by the Doppler effect correspond to the radial velocity. As the components periodically orbit around each other, the radial velocities curve is also periodic.

The shape of the radial velocity curve is dependent on the trajectory of both the components, eccentricity, and orientation with respect to the observer (Wilson, 1979). If the mass of the components is almost the same and the orbital trajectory is not far from being circular the radial velocities curve should be two sine curves that are in antiphase (shifted by  $180^\circ$ ) to each other (see Figure 1.2). If the components have very different masses or the trajectory is strongly elliptical, the radial velocity curve looks like a deformed sine curve with different amplitudes.

The previous section mentioned that in the time of an eclipse the splitting of spectral lines does not occur. We can see in radial velocities curve, that radial velocity is zero in the phases 0 and 0.5. Therefore, no shift in the position of spectral lines is observed.

The radial velocity curve is essential for determining the mass ratio, which is crucial for the successful physical model in PHOEBE (described in section 2.6). For determining the mass ratio in eclipsing binaries we can use the relation from (Mikulášek and Zejda, 2013):

$$q = \frac{m_2}{m_1} = \frac{a_1}{a_2} = \frac{K_1}{K_2}, \quad (1.2)$$

where  $q$  is the mass ratio,  $a_1$  and  $a_2$  are the distances of the components from the common centre of mass,  $K_1$  and  $K_2$  are the amplitudes of the radial velocity curves. From this relation, we can see that the higher the mass of the component, the lower the amplitude of the radial velocity curve. This corresponds well with the intuitive idea that the orbit of a more massive star will be less influenced by the less massive star.

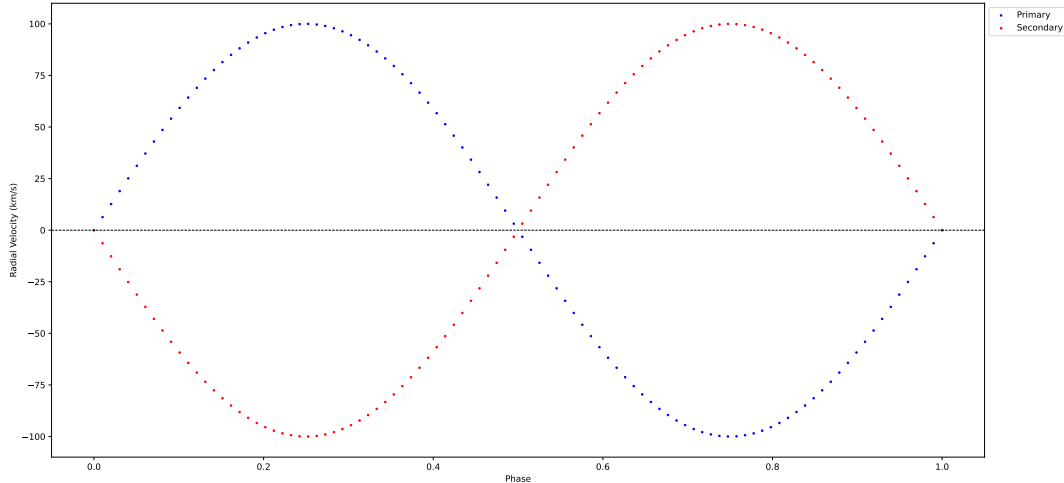


Figure 1.2: Synthetic radial velocity curve for an eclipsing binary with circular orbit.

## 1.3 Phenomena in lightcurves of eclipsing binaries

### 1.3.1 Elliptical orbital trajectory

In many studied eclipsing binaries the orbital trajectory is not a circle, but ellipse. If the secondary minima in a phase curve occur at a phase different from 0.5, the trajectory is an ellipse. Moreover, the eccentricity of the orbital trajectory is also imprinted in the mutual position of primary and secondary minima in the O-C diagram (see Figure 1.3). If they are horizontally shifted, the eccentricity of the orbital trajectory is non-zero.

The O-C diagram displays the difference between observed O and calculated C time of some periodically appearing event on y-axis. In eclipsing binaries, it is usually the time of the minima. On the x-axis there is either time or an epoch. Epoch defines the number of cycles from the initial moment of minima  $M_0$  and can be calculated using equation (Mikulášek and Zejda, 2013):

$$E = \text{floor} \left( \frac{t - M_0}{P} \right), \quad (1.3)$$

where  $E$  is the epoch,  $t$  is the time,  $M_0$  is the initial moment of minima and  $P$  is the period. The function floor rounds the calculated value down to the integer. Finally, the ellipticity influences the shape of the radial velocities curve. It will have the shape of an asymmetric sine curve.

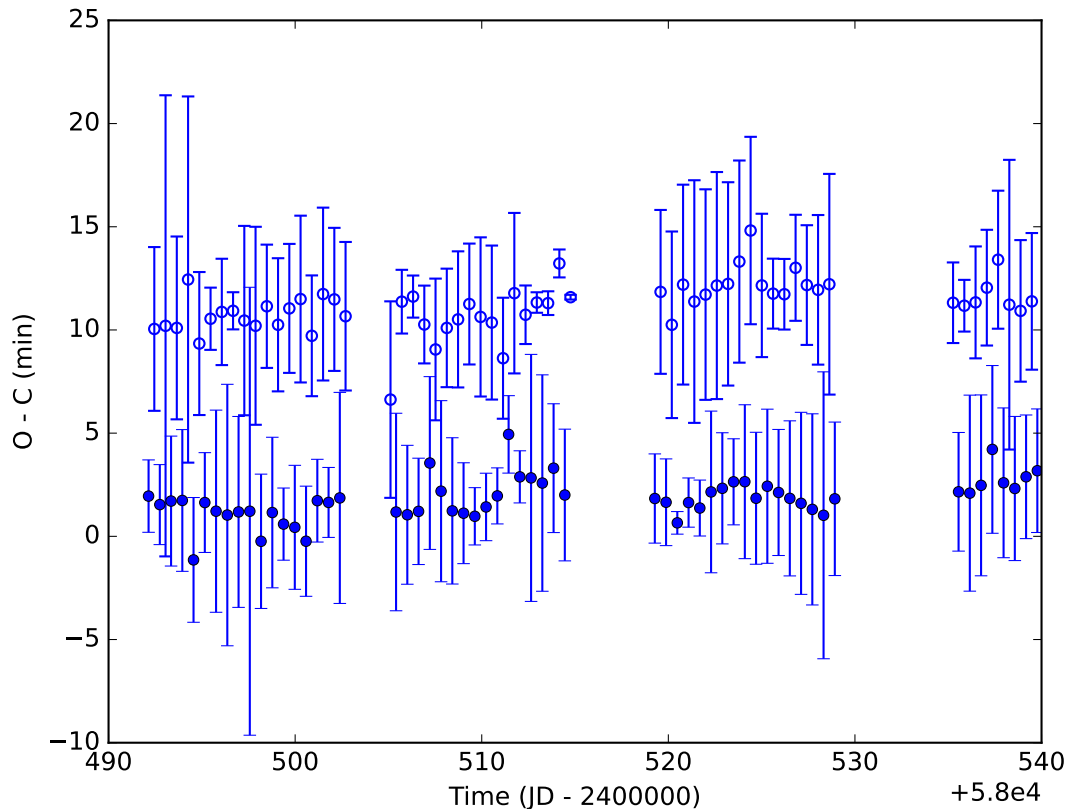


Figure 1.3: O-C diagram of eclipsing binary with elliptical orbit (S1 Pup - pairA). Empty points represent secondary minima, and full points primary.

### 1.3.2 Reflection effect

This effect occurs in close binary systems where one component has significantly higher temperature (component A) than the other (component B). The component B receives a huge amount of radiation that is absorbed and re-emitted back. The part of component B that is hit by this radiation is locally heated and its surface temperature rises.

The closer the components are to each other, and the bigger the difference between the temperatures of the components, the bigger the reflection effect.

### 1.3.3 Limb darkening

Limb darkening is an effect we observe in eclipsing binaries and in stars generally. The edges of the star appear darker compared to the centre. This effect is caused by the fact, that looking at the star's centre, we are looking into a greater depth and into denser areas with higher temperature than on the edges. The limb darkening influences the shape of the minima (mainly the entrance and exit from minima).

The value of limb darkening depends mainly on the spectral class of the star and its atmosphere. For cooler stars (spectral class K and M) are the values 0.8-0.9 and for stars with spectral class A0 the value of limb darkening is 0.5-0.6. Finally, for the spectral class B0 the value is in the range 0.25-0.35 (Harmanec and Zásche, 2023).

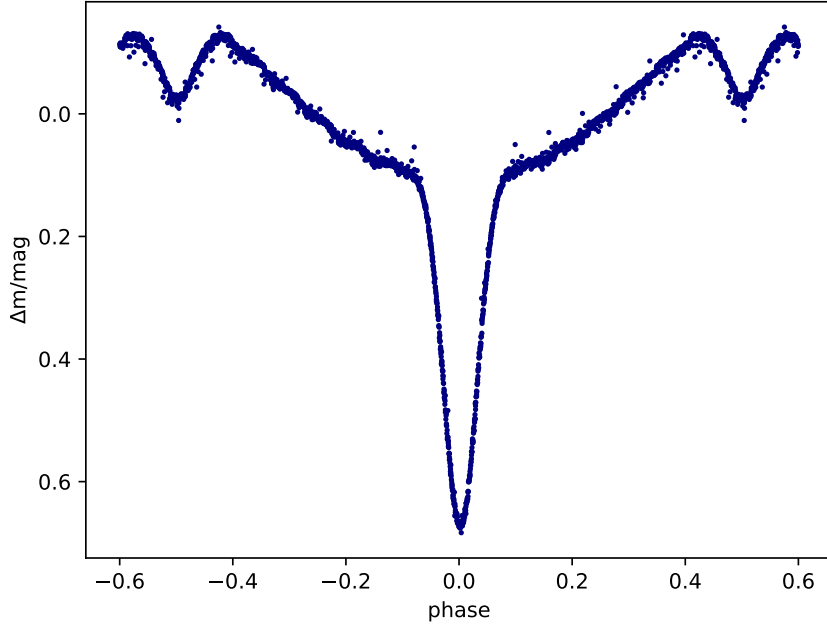


Figure 1.4: Lightcurve with reflection effect - HW Virginis, TESS data.

### 1.3.4 O’Connell effect

The O’Connell effect is called an asymmetry observed in the light curves of some eclipsing binaries (described in detail in O’Connell (1951)). The O’Connell effect appears mainly in the type W UMa type. The maxima in the light curve between the primary and secondary minima do not reach the same level. Similar variability in the light curves of eclipsing binaries can be caused by the stellar spots or ellipsoidal variability.

This effect causes problems with detrending data. It can be easily distinguished from a trend when we have data from more TESS sectors. If the variations in the level of maxima in the light curves are the same in all sectors, then it is caused by the O’Connell effect. On the contrary, if the variations are different in each sector or changes inside one sector, then it is caused by the trend or other above-mentioned effects.

### 1.3.5 Transfer of mass

The transfer of mass can be found in semi-detached and contact binaries. In semi-detached binaries, one of the stars fills up its Roche lobe, whereas the second star does not. In contact binaries, both components of the eclipsing binary fill their Roche lobe. When at least one Roche lobe in the system is filled up, mass transfer is allowed. This process causes the change in period, which can be observed in the O-C diagram.

The change in the orbital period due to the conservative mass transfer (no mass leaves the system and momentum is conserved) can be described by relation (Harmanec and Zaslavsky, 2023):

$$\frac{\Delta P}{P} = 3q \frac{1 - q^2}{M} \Delta M, \quad (1.4)$$

where  $P$  is the orbital period,  $\Delta P$  is the change in the orbital period,  $M_1$  is a donor star,  $M_2$  is the accretor,  $M$  is the total mass of the system ( $M = M_1 + M_2$ ),  $\Delta M$  is the amount of transferred mass and  $q = \frac{M_1}{M_2}$  is the mass ratio.

If the mass is transferred from a less massive star to a more massive star ( $q < 1$ ) the orbital period decreases. As the period decreases the points in the O-C diagram will create a downward-opening parabola. On the contrary, if the donor star is more massive than the accretor ( $q > 1$ ) the orbital period increases. In this case, the points in the O-C diagram will form a parabola open upward.

### 1.3.6 Apsidal motion

Apsidal motion is significant in eclipsing binaries whose orbital trajectory is an ellipse instead of a circle. This effect is mainly caused by the tidal forces between components of the eclipsing binary (the components no longer have a round shape), presence of another object in the system, and relativistic effects. In the O-C diagram, the apsidal motion causes the primary and secondary minima to be in antiphase (see Figure 1.5). The primary and secondary minima time will shift at different rates depending on which part of the ellipse will be its current position.

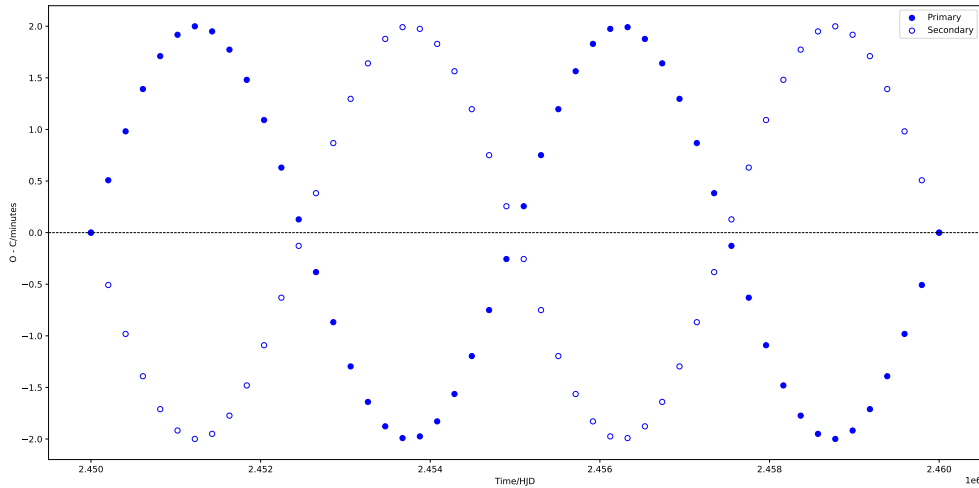


Figure 1.5: Synthetic O-C diagram showing apsidal motion.

### 1.3.7 Stellar spots

We can distinguish two main types of stellar spots. The first are temperature spots that characterize colder areas on the stellar surface. The second type of stellar spots, the colourful spots, are caused by the different chemical compositions.

The brightness variations in light curves come firstly from the rotation of the star with temperature spots itself. Secondly, if the components do not have a synchronous rotation, the eclipses will differ in shape depending on whether or not is the stellar spot blocked during the eclipse or not.

The modeling of the stellar spots can be very challenging, especially if we have only photometric data available. We can not determine the number of starspots from the photometric data alone.

### 1.3.8 LITE effect

LITE effect (= Light-Time Effect) in eclipsing binaries appears when another object is gravitationally bound to the system. Unlike in systems with a mass transfer, the orbital period itself remains unchanged. The apparent orbital period changes depending on whether the binary is drawing near to us or if it is moving away from us. This effect is also suitable for the discoveries of doubly eclipsing systems. Moreover, the first-ever discovered doubly eclipsing system V994 Her was identified due to the LITE effect (later studied in detail in Zasche et al. (2019)). The specific shape of O-C diagrams of doubly eclipsing systems will be discussed in detail in section 2.5).

# Chapter 2

## The process of analysis of light curves of eclipsing binaries

The process of analysis of individual multiply eclipsing systems that were used in this thesis starts with choosing the right candidates. As it is common for quadruples to have minima of one pair significantly deeper than for the second one, we first need to discuss if we can detect minima of both pairs with our observational equipment. Therefore, before analysing the measured data from terrestrial observatories the data from TESS were analysed. The reason for this was also practical. If we know the parameters of a light curve before we start the observation itself we can better adjust the measurement parameters such as the length of exposition, choose the most suitable comparison, check star, and others.

It is important to have both satellite and terrestrial measurements. It is essential to go through the previous publications that may contain the timings of minima to have as much data in the O-C diagram as possible. It is useful to collect all available measurements of the studied star to better understand of how the system evolves in time (for example, in the case of mass transfer). This thesis mainly used data from TESS satellite due to their easy access, continuity, and relatively low noise as they are measured outside of the atmosphere. Their biggest disadvantage is that we can not regulate the time of measurements. Another disadvantage is that they are only in one filter. For the determination of moments of minima, TESS data are sufficient, but for more precise physical models multicoloured data are desired as the depth of the eclipse may vary in every colour.

On the other hand, terrestrial data are not continuous and it may be more challenging to for example determine the moment of minima. On the contrary, if the weather is favourable, you can measure any night you want. This is crucial, especially when measuring some effect with longer periodicity or if we want to capture a specific minimum in the O-C diagram (for example, a turnoff point).

After thoroughly analysing the TESS and measuring our data we obtain the light curve using software Muniwin (Motl, 2010) for terrestrial data and Python for TESS data. Then via SILICUPS (=Simple Light Curve Processing System) software (Cagaš, 2025) or using the Fourier method we distinguish the contributions of individual pairs (discussed in detail in sections 2.3 and 2.4). Using SILICUPS software, we identify the moments of minima.

Comparing these with ephemeris (the moment of a basic minimum and the orbital period of the system) determined by Zbyněk Henzl (Henzl, 2023) we construct the O-C

diagram via OC-fit software (Gajdoš and Parimucha, 2019). If we had long-term data we can (only from the O-C diagram) propound that the observed system is a quadruple.

If the observed system was a quadruple, the distribution of points in the O-C diagram would oscillate around the mean value, which will also change over time. Moreover, if we construct O-C diagrams for individual pairs in a quadruple system, the distribution of points would look like (deformed) sine curves that are in antiphase (shifted by  $180^\circ$ ). This is the result of both pairs being gravitationally bonded and their orbits being synchronized around the common centre of mass.

An alternative way of proving the gravitational bond in doubly eclipsing systems are spectroscopic measurements. If the observed system is a quadruple the curves of radial velocities will resemble (deformed) sine curves that are in antiphase. The biggest disadvantage of this method is that the observational equipment in the Czech Republic can only measure bright systems, which is a very limiting restriction for yet-known candidates for quadruples.

## 2.1 Downloading TESS data

The data from the TESS satellite were downloaded and detrended via Python and the following code. A similar code was also used in my bachelor's thesis Richterková (2023). The main difference is in optimizing the automatic detrending of TESS data. For the best detrending, it is essential to choose the right value of parameter  $a$  that defines how much smoothing should be applied to the light curve to remove the trend. Higher the value of parameter  $a$ , the stronger the smoothing of the light curve and more slower trends are removed. The full code is presented here with the intention of making a manual for others and for the completeness of the code.

Firstly we import all packages that we are going to use later on.

```
import pandas as pd
import numpy as np
import matplotlib.pyplot as plt
import lightkurve as lk
```

Secondly, we will search for all data sets containing our star and we will download them.

```
search_results = lk.search_tesscut("ASAS J073054-1840.7")
search_results
tpfs = search_results.download_all(cutout_size=20,quality_bitmask='hardest')
```

Thirdly, we will define the ephemeris of a studied system.

```
perioda = 2.068435
MO = 2459245.65345
```

We will start with  $i = 0$  and continue this whole procedure for all  $i$  in range of `tpfs` (variable used in the previous step). The parameter  $i$  determines the number of analysed sector. We will plot the first capture of the data set from this sector and adjust the aperture accordingly so that we can later proceed with an aperture photometry. The aperture has a rectangular shape and can be changed by arguments in the variable `target_mask`. The

first argument is y-coordinate, second argument is x-coordinate of the aperture. Once we have defined the aperture, we plot it to check that it was done correctly.

```
i = 0
tpfs[i].plot()
target_mask = tpfs[i].create_threshold_mask(threshold = 150, reference_pixel =
'center')
target_mask[8:13,9:14] = 1
tpfs[i].plot(aperture_mask = target_mask, mask_color = 'r')
```

If the aperture was not done correctly, we have to delete the already existing aperture and repeat the previous step with altered coordinates. If the aperture was done correctly the first time around, we can skip this step. Deleting an aperture is done by the following code.

```
target_mask = tpfs[i].create_threshold_mask(threshold = 150, reference_pixel =
'center')
target_mask[8:13,9:14] = 0
tpfs[i].plot(aperture_mask = target_mask, mask_color = 'r')
```

In the next step, we will put the aperture to the variable and save it. (It is not necessary to save the picture of an aperture, but for the later control it can be useful.) Also, add all the pixels that are in the aperture, so that later we can normalize.

```
aperture = tpfs[i].plot(aperture_mask = target_mask, mask_color = 'r')
aperture_name = "aperture_star{}".format(i)+"cadence{}".format(a)+".jpg"
plt.savefig(aperture_name)
n_target_pixels = target_mask.sum()
n_target_pixels
target_lc = tpfs[i].to_lightcurve(aperture_mask = target_mask)
bg_mask = ~tpfs[i].create_threshold_mask(threshold = 0.001, reference_pixel =
None)
tpfs[i].plot(aperture_mask = bg_mask, mask_color = 'w')
n_bg_pixels = bg_mask.sum()
n_bg_pixels
```

In the following step, we will create a simple light curve without using any comparison star or detrending.

```
bg_lc_per_pixel = tpfs[i].to_lightcurve(aperture_mask = bg_mask)/n_bg_pixels
bg_estimate_lc = bg_lc_per_pixel * n_target_pixels
corr_lc = target_lc - bg_estimate_lc.flux
corr_lc.plot()
```

Detrending itself is done using the function `flatten`. To decide which argument of function `flatten` to use, we run following code that plots multiple light curves for different arguments of function `flatten` (if needed we can enlarge the range, but in most cases, it is not necessary). After analysing the plots, we put the chosen argument into variable `a`.

```

for a in range (1,1002,10):
    corr_lc.flatten(a).plot()
    picture = corr_lc.flatten(a).plot()
    picture_name = "star{}".format(i)+"cadence{}".format(a)+".jpg"
    plt.savefig(picture_name)
a = 101

```

In this step we will detrend the data and convert time to HJD.

```

lightcurve = corr_lc.plot()
lightcurve_name = "lightcurve_star{}".format(i)+"cadence{}".format(a)+".jpg"
plt.savefig(lightcurve_name)

corr_lc.flatten(a).plot()
flatten = corr_lc.flatten(a).plot()
flatten_name = "flatten_star{}".format(i)+"cadence{}".format(a)+".jpg"
plt.savefig(flatten_name)

corr_lc.time = corr_lc.time+tpfs[i].get_keyword('BJDREFI')+tpfs[i].get_keyword('BJDREFF')
name = "star{}".format(i)+"cadence{}".format(a)+".csv"
corr_lc.flatten(a).to_csv(name)
corr_lc.flatten(a).fold(perioda, t0 = M0).scatter()

phasecurve = corr_lc.flatten(a).fold(perioda, t0 = M0).scatter()
phasecurve_name = "phasecurve_star{}".format(i)+"cadence{}".format(a)+".jpg"
plt.savefig(phasecurve_name)

```

Almost the same process as for the variable star will be repeated for the comparison star.

```

search_results_cmp = lk.search_tesscut("TYC 5983-1709-1")
search_results_cmp
tpfs_cmp =search_results_cmp.download_all(cutout_size=20,quality_bitmask='hardest')

tpfs_cmp[i].plot()
target_mask_cmp = tpfs_cmp[i].create_threshold_mask(threshold = 150,
    reference_pixel = 'center')
target_mask_cmp[8:12,9:13] = 1
tpfs_cmp[i].plot(aperture_mask = target_mask_cmp, mask_color = 'r')

aperture_cmp = tpfs_cmp[i].plot(aperture_mask = target_mask_cmp, mask_color = 'r')
aperture_cmp_name = "aperture_star{}".format(i)+"cadence{}".format(a)+".jpg"
plt.savefig(aperture_cmp_name)

n_target_cmp_pixels = target_mask_cmp.sum()
n_target_cmp_pixels

target_cmp_lc = tpfs_cmp[i].to_lightcurve(aperture_mask = target_mask_cmp)

```

```

bg_mask_cmp = ~tpfs_cmp[i].create_threshold_mask(threshold = 0.001,
reference_pixel = None)
n_bg_cmp_pixels = bg_mask_cmp.sum()
bg_cmp_lc_per_pixel = tpfs_cmp[i].to_lightcurve(aperture_mask =bg_mask_cmp)/
n_bg_cmp_pixels
bg_estimate_cmp_lc = bg_cmp_lc_per_pixel * n_target_cmp_pixels
corr_cmp_lc = target_cmp_lc - bg_estimate_cmp_lc.flux
corr_cmp_lc.time = corr_cmp_lc.time+tpfs_cmp[i].get_keyword('BJDREFI')+
tpfs_cmp[i].get_keyword('BJDREFF')
name_cmp = "star_cmp_{}".format(i)+".csv"
corr_cmp_lc.flatten(a).to_csv(name_cmp)

```

Now, we will put everything we need for calculating the photometry into one dataset.

```

name = "star{}".format(i)+"cadence{}".format(a)+".csv"
name_cmp = "star_cmp_{}".format(i)+".csv"
variable = pd.read_csv(name, thousands = r"", sep = ",", decimal = ".")
comparison = pd.read_csv(name_cmp, thousands = r"", sep = ",", decimal = ".")
change_data =pd.concat([variable["time"],comparison["time"],variable["flux"],
comparison["flux"],variable["flux_err"],comparison["flux_err"]],axis =1)
change_data.columns = ["var_time", "comp_time", "var_flux", "comp_flux", "
var_flux_err", "comp_flux_err"]

```

In the following step, we will calculate the change in brightness and corresponding error.

```

change = -2.5*np.log10(change_data["var_flux"]/change_data["comp_flux"])
error = (((2.5*change_data["comp_flux_err"])/change_data["var_flux"])
**2+((2.5*change_data["var_flux_err"])/change_data["comp_flux"])**2)**0.5

```

Finally, we will save the data to file that is readable for SILICUPS software.

```

ch = change.tolist()
final_change = []
for j in range(len(ch)):
a = ch[j]
x = "%.17f" % a
final_change.append(x)
change = pd.Series(final_change)
err = error.tolist()
final_error = []
for k in range(len(err)):
b = err[k]
y = "%.17f" % b
final_error.append(y)
error = pd.Series(final_error)
time = variable["time"]
final_data = pd.concat([time, change, error], axis = 1)
final_name = "star{}".format(i)+"_final.txt"
np.savetxt(final_name,final_data,fmt='%s',delimiter='\t' )

```

## 2.2 Detrending

Sometimes, it is enough to stop at this point. In many cases, the downloaded data needs secondary detrending. The following code for detrending data was written by Jakub Kolář (Kolář, 2023) and the theory behind it was done by Zdeněk Mikulášek (Mikulášek and Zejda, 2013). The procedure of secondary detrending starts by importing all the packages that we are going to use.

```
import numpy as np
import math
from math import *
import scipy
import pandas as pd
import matplotlib.pyplot as plt
import scipy.optimize
from scipy.optimize import curve_fit
import pylab as pl
```

In the next step, the residua are plotted.

```
t, mag, err = np.loadtxt("rezidua.txt", unpack=True)
plt.figure(figsize=(18,12))
plt.tick_params(bottom=True, top=True, left=True, right=True)
plt.xticks(fontsize=26)
plt.yticks(fontsize=26)
plt.tick_params(axis="x", length=15, direction="in", pad=15)
plt.tick_params(axis="y", length=15, direction="in", pad=15)
plt.plot(t, mag, "o", color="blue")
plt.errorbar(t, mag, yerr=err, fmt='o', color="b", ecolor="b")
plt.gca().invert_yaxis()
```

Then the residua are fitted by Chebychev polynoms.

```
p = np.polynomial.Chebyshev.fit(t, mag, 30)
```

After that we plot the trend and save it.

```
y_tr = p(t)
plt.figure(figsize=(18,12))
plt.tick_params(bottom=True, top=True, left=True, right=True)
plt.xticks(fontsize=26)
plt.yticks(fontsize=26)
plt.tick_params(axis="x", length=15, direction="in", pad=15)
plt.tick_params(axis="y", length=15, direction="in", pad=15)
plt.plot(t, mag, "o", color="blue")
plt.plot(t, y_tr, "-", color="orange", linewidth=5)
#plt.ylim(-0.01,0)
plt.gca().invert_yaxis()
np.savetxt("trend_star9.txt",y_tr,delimiter=' ', fmt="%.5f")
```

The procedure continues with loading and plotting the original data containing the trend.

```
t, mag, err = np.loadtxt("star9_final_new.txt", unpack=True)
plt.figure(figsize=(18,12))
plt.tick_params(bottom=True, top=True, left=True, right=True)
plt.xticks(fontsize=26)
plt.yticks(fontsize=26)
plt.tick_params(axis="x", length=15, direction="in", pad=15)
plt.tick_params(axis="y", length=15, direction="in", pad=15)
plt.plot(t, mag, "o", color="blue")
plt.errorbar(t, mag, yerr=err, fmt='o', color="b", ecolor="b")
#plt.ylim(-0.01,0)
plt.gca().invert_yaxis()
plt.xlabel("$Phase$", fontsize=30, labelpad=20)
plt.ylabel("$\\Delta m$ [mag]", fontsize=30, labelpad=20)
```

In the following step, we will subtract the trend from the original data and plot the result (detrended data).

```
mag_novy = mag - y_tr
plt.figure(figsize=(18,12))
plt.tick_params(bottom=True, top=True, left=True, right=True)
plt.xticks(fontsize=26)
plt.yticks(fontsize=26)
plt.tick_params(axis="x", length=15, direction="in", pad=15)
plt.tick_params(axis="y", length=15, direction="in", pad=15)
plt.plot(t, mag_novy, "o", color="blue")
plt.errorbar(t, mag_novy, yerr=err, fmt='o', color="b", ecolor="b")
#plt.ylim(-0.01,0)
plt.gca().invert_yaxis()
plt.xlabel("$Phase$", fontsize=30, labelpad=20)
plt.ylabel("$\\Delta m$ [mag]", fontsize=30, labelpad=20)
```

Finally, we will save the detrended data into a format that is readable for SILICUPS.

```
np.savetxt("star.detrended.txt", np.c_[t,mag_novy,err], delimiter=' ', fmt="
%.5f")
```

## 2.3 Disentanglement by iterative method

### 2.3.1 System of two binaries

The first method of distinguishing the contributions of both the pairs in the measured light curve is based on the premise that if we add the contribution of pair A and the contribution of pair B, we will get the original light curve. The greatest advantage of this method is, that it can be used on noncontinuous data sets (so both on TESS data and ground-based measurements). Another advantage is that this method does not require high precision in the ephemeris value. The ephemeris are the only entrance conditions for

this method of disentanglement. The main disadvantage is that once we have a system where one pair is significantly dominant, the contribution of the less dominant pair will be hidden in the noise. Therefore, it will be harder and sometimes even impossible to disentangle.

The process starts with uploading the measured light curve into SILICUPS and phasing it according to the ephemeris of pair A. In the next step, we fit the contribution of pair A (as mentioned above one, of the pairs is usually dominating in the light curve, but sometimes it could be challenging) and subtract it from the original light curve. Assuming that the light curve contains only two pairs, we should obtain the contribution of pair B and save it.

Afterward, we will upload the contribution of pair B and phase it according to the ephemeris of pair B. Then we will fit pair B and subtract this fit from the original light curve. In this step, we should obtain the contribution of pair A in an ideal situation. In reality, the contribution of each pair also contains a little bit of the second one and also noise. We would have to repeat this process several times to get the most precise contributions of individual pairs.

To make sure that there are no other periodical eclipses in the system (suggesting, for example that it is not a quadruple but a sextuple in the arrangement 2+2+2 or quintuple 2+2+1) we will add the contribution of pair A and pair B and subtract it from the original light curve. If the result is points distributed around the line with a zero slope, the system contains only two pairs. However, if the result is points looking like a light curve of an eclipsing binary, we assume there is some other body in the system apart from pair A and pair B.

### 2.3.2 System of three binaries

If we have a system consisting of three binaries, the process of disentanglement by iterative method is rather more complicated. The beginning will be the same as if we had only two binaries. We will take a light curve containing all of the binaries (TABC) and phase it according to the ephemeris of pair A. Then, we will subtract this fit from TABC and get a light curve containing only pairs B and C (TBC). Accordingly, we will get a light curve containing only pairs A and C (TAC) by fitting and subtracting pair B from TABC. We will also get a light curve containing pairs A and B (TAB) by fitting and subtracting pair C from TABC.

Now, we will take TBC, fit and subtract pair B, and get a light curve containing only pair C (TC). We can also fit and subtract pair C from TBC and get a light curve containing only pair B (TB). We will do this process for TAC and TAB accordingly.

So, in the end, we will have twice TA (from TAC and TAB), twice TB (from TBC and TAB), and also twice TC (from TBC and TAC). Combining TA and phasing it according to the ephemeris of pair A, we will get the contribution of pair A. Accordingly, we will get the contributions of pairs B and C.

In the next iteration, fits of these contributions will be used at the very beginning of the procedure. In addition, in the case of a system containing two binaries, the contributions are more precise with every iteration. The whole process is schematically shown in Figure 2.1. If there were more than three binaries in the system, we would have to change the procedure accordingly.

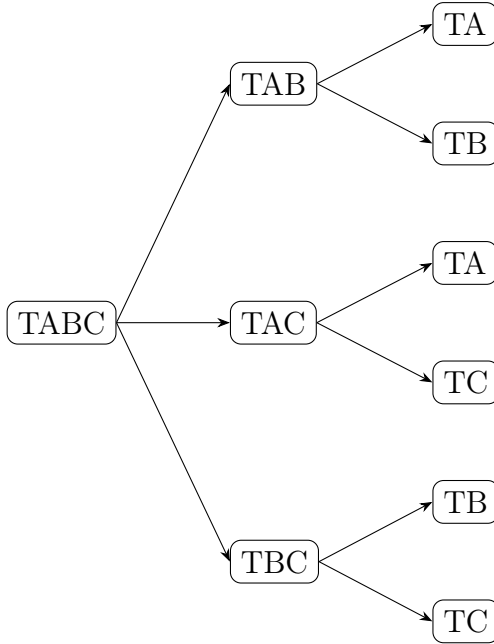


Figure 2.1: Scheme for three binaries-iterative method.

## 2.4 Disentanglement by Fourier method

This method of distinguishing the contributions of pairs from the original light curve is based on Fourier decomposition. Its most significant disadvantage is that it can be used only for continuous data sets. That is why this method was used only for analysing TESS data (containing 27-day continuous data), not ground-based measurements (containing only a few hours a day). This method also requires high precision in the ephemeris value. Both iterative and Fourier methods are less precise when trying to fit constant brightness.

As fitting the harmonics is an approximate method, disentangled light curves are less noisy than the iterative method, which makes them more suitable and precise for calculating the physical model. Another advantage of this method is that it can be used for higher multiple stars, whereas the iterative method would only get more complicated with the increasing the number of binaries in the system.

The entrance conditions for disentanglement by the Fourier method are knowledge of precise ephemeris and a number of binaries. Therefore, if we are not sure if the system consists of two or three binaries we have to make a Fourier transform with the assumption that there are two binaries, but also another one assuming that there are three binaries. By adding the disentangled individual pairs and subtracting them from the original light curve, we can proclaim which assumption was true.

The process (described in more detail the in article Powell et al. (2021)) starts with fitting harmonic series in the form:

$$F(t) = \sum_{m=1}^3 \left( \sum_{n=1}^{50} (\alpha_n^{(m)} \sin(\omega_n t) + \beta_n^{(m)} \cos(\omega_n t)) \right) + \gamma, \quad (2.1)$$

where

$$\omega_n(t) = \frac{2\pi n}{P_m} \quad (2.2)$$

is the  $n$ th orbital frequency of the  $m$ th binary, and  $\gamma$  is the constant background level. After fitting the harmonic series, we have to reconstruct the light curves for each binaries

using:

$$F_m(t_j) = \sum_{n=1}^{50} (\alpha_n^{(m)} \sin(\omega_n t_j) + \beta_n^{(m)} \cos(\omega_n t_j)) + \gamma, \quad (2.3)$$

where  $j$  is the  $j$ th data point.

Both above-mentioned methods have one common disadvantage. For binaries having orbital periods in resonance 1:1, the disentanglement is less precise and time consuming.

The whole disentanglement by the Fourier method was programmed in Python. If we assumed that there are two binaries in the system, we used the following code. If we assumed that there are three binaries, we would have to change the code accordingly (changing the range in a loop and adding one more orbital period). Firstly, we import all the packages that we will use later on.

```
import numpy as np
import matplotlib.pyplot as plt
from scipy.optimize import curve_fit
```

Secondly, we load the data set and put it into the variable.

```
data = np.loadtxt('data.txt')
time, brightness, error = data[:, 0], data[:, 1], data[:, 2]
```

Thirdly, we plot the original light curve.

```
plt.plot(time, brightness, 'o', markersize=2)
plt.xlabel('t / HJD')
plt.ylabel('\u0394m / mag')
plt.title('Original light curve')
plt.gca().invert_yaxis()
plt.grid(True)
plt.show()
```

Then, we define the Fourier series according to equation (2.1), where we loop over the number of binaries  $m$  and loop over the number of harmonics  $n$ . In the end, we also add the constant background level. In this case, we assume that there are two binaries in the system, which is why the range of  $m$  is two, if there were three binaries we would have to change the range to three.

```
def fourier_series(t, *coefficients):
    F = np.zeros_like(t)
    for m in range(2):
        for n in range(1, 51):
            omega = 2 * np.pi * n / periods[m]
            F += coefficients[m * 100 + 2 * (n - 1)] * np.sin(omega * t) +
                coefficients[m * 100 + 2 * (n - 1) + 1] * np.cos(omega * t)
    return F + coefficients[-1]
```

In the next step, we define the orbital periods of each binary. In this case, we assume that there are two binaries so there are only two periods listed. If we assumed that there are three binaries, we would have to add one more.

```
P_A = 2.0684350
P_B = 1.7285119
periods = np.array([P_A, P_B])
```

In the following step, we first make an initial guess for coefficients and then fit the coefficients. If we assumed that there are three binaries instead of two we would have to change the argument of  $p0$  to 301.

```
p0 = np.ones(201)
coefficients, _ = curve_fit(fourier_series, time, brightness, p0=p0)
```

Then we reconstruct the light curves of individual binaries according to equation (2.3).

```
reconstructed_light_curves = []
for i in range(2):
    Fm = np.zeros_like(time)
    for n in range(1, 51):
        omega = 2 * np.pi * n / periods[i]
        Fm += coefficients[i * 100 + 2 * (n - 1)] * np.sin(omega * time) +
        coefficients[i * 100 + 2 * (n - 1) + 1] * np.cos(omega * time)
    reconstructed_light_curves.append(Fm + coefficients[-1])
```

After that, we plot the reconstructed light curves of individual binaries.

```
plt.figure(figsize=(10, 6))
for i, light_curve in enumerate(reconstructed_light_curves):
    plt.subplot(2, 1, i + 1)
    plt.plot(time, light_curve)
    plt.xlabel('t / HJD')
    plt.ylabel('\u0394m / mag')
    plt.title(f'Reconstructed light curve for binary {chr(65+i)}')
    plt.gca().invert_yaxis()
    plt.grid(True)
    plt.legend()
plt.tight_layout()
plt.show()
```

In the following step, we save the light curves of individual binaries into txt file which will be used for the construction of the O-C diagram or the physical model later on.

```
for i, light_curve in enumerate(reconstructed_light_curves):
    filename = f'pair{chr(65+i)}.txt'
    np.savetxt(filename, np.column_stack((time, light_curve)), header='Time (
HJD) Brightness (Magnitude)', fmt='%.6f', delimiter='\t')
    print(f'Reconstructed light curve for binary {chr(65+i)} saved as {
filename}')
```

In this step, we will first normalize the reconstructed light curves, then add them together, scale them, and calculate the difference between the combined scaled light curve and the original light curve.

```

normalized_reconstructed_light_curves = [lc - np.mean(lc) for lc in
    reconstructed_light_curves]
combined_light_curve_normalized = normalized_reconstructed_light_curves[0] +
    normalized_reconstructed_light_curves[1]
scaling_factor = np.std(brightness) / np.std(combined_light_curve_normalized)
combined_light_curve_scaled = combined_light_curve_normalized * scaling_factor
    + np.mean(brightness)
difference = brightness - combined_light_curve_scaled

```

Finally, we will plot the original and combined light curve into one plot and we will also plot the calculated difference.

```

plt.figure(figsize=(15, 10))

plt.subplot(311)
plt.plot(time, brightness, 'o', markersize=2, label='Original Light Curve')
plt.plot(time, combined_light_curve_scaled, color='red', label='Combined
    Reconstructed Light Curve (Scaled)')
plt.xlabel('t / HJD')
plt.ylabel('\u0394m / mag')
plt.title('Original light curve and scaled combined reconstructed light curve'
    )
plt.gca().invert_yaxis()
plt.grid(True)
plt.legend()

plt.subplot(312)
plt.plot(time, difference, color='green')
plt.axhline(y=0, color='gray', linestyle='--', linewidth=0.8) # Add
    horizontal line at y=0 for reference
plt.xlabel('t / HJD')
plt.ylabel('\u0394m / mag')
plt.title('Difference between original light curve and reconstructed light
    curve')
plt.gca().invert_yaxis()
plt.grid(True)
plt.legend()

plt.tight_layout()
plt.show()

np.savetxt("rezidua.txt", np.column_stack((time, difference)), header='Time (
    HJD) Brightness (Magnitude)', fmt='%.6f', delimiter='\t')

```

## 2.5 O-C diagrams

The O-C diagrams will be essential in this work to prove of whether or not the studied system is a doubly eclipsing quadruple. After we have distinguished the contributions

of individual pairs, we have determined the moments of minima via SILICUPS software and plotted O-C diagrams for individual pairs. The O-C value in the diagrams should be in antiphase (the O-C diagram of pair A will be shifted by  $180^\circ$  when compared to pair B). The LITE effect is responsible for the characteristic shape of the O-C diagram of quadruples.

In all fits of O-C diagrams in this thesis the model LiTE3 was used. The model have following parameters:  $asin(i_3)$  in astronomical units,  $e_3$  (the eccentricity of the orbit of the third body),  $w_3$  in radians (longitude of the pericentre of the orbit of third body),  $t_{03}$  in HJD (time of pericentre passage of the third body) and  $P_3$  in days (period of the third body).

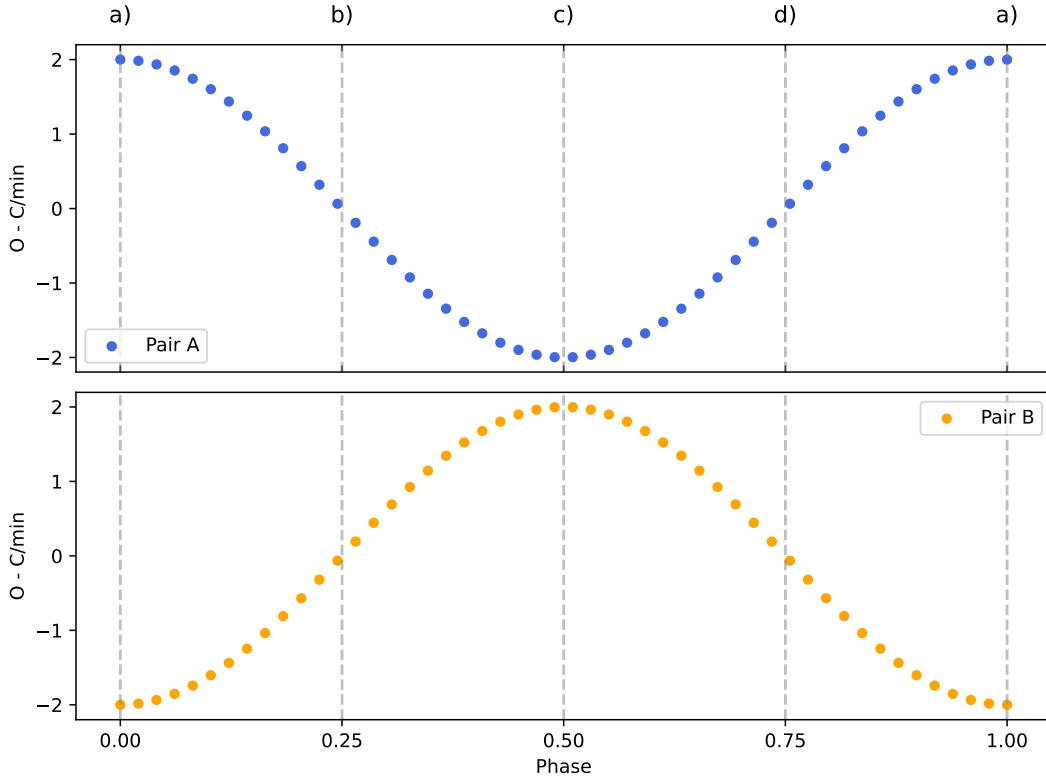


Figure 2.2: Synthetic O-C diagram for doubly eclipsing system.

The part a) in Figure 2.3 corresponds to the phase 0 in Figure 2.2. At this phase, pair A is further from the observer, the light from pair A has to pass a longer distance, therefore, it is delayed (compared to the expected time), and we observe a maximum in the O-C diagram of pair A. On the contrary, pair B is as close as possible to the observer, the light has to pass a smaller distance to reach the observer, and we observe a minimum in the O-C diagram of pair B earlier.

The parts b) and d) in Figure 2.3 correspond to phases 0.25 and 0.75 in Figure 2.2, where both the pairs are at the same distance from the observer, we observe the light at determined instances, which results in zero value in the O-C diagram.

Finally, the part c) Figure 2.3 corresponds to the phase, 0.5 in Figure 2.2. At this phase pair A is closer to the observer, so we observe a minimum at the O-C diagram for pair A. On the other hand, pair B is at the largest possible distance from the observer, which results in a maximum in the O-C diagram of pair B.

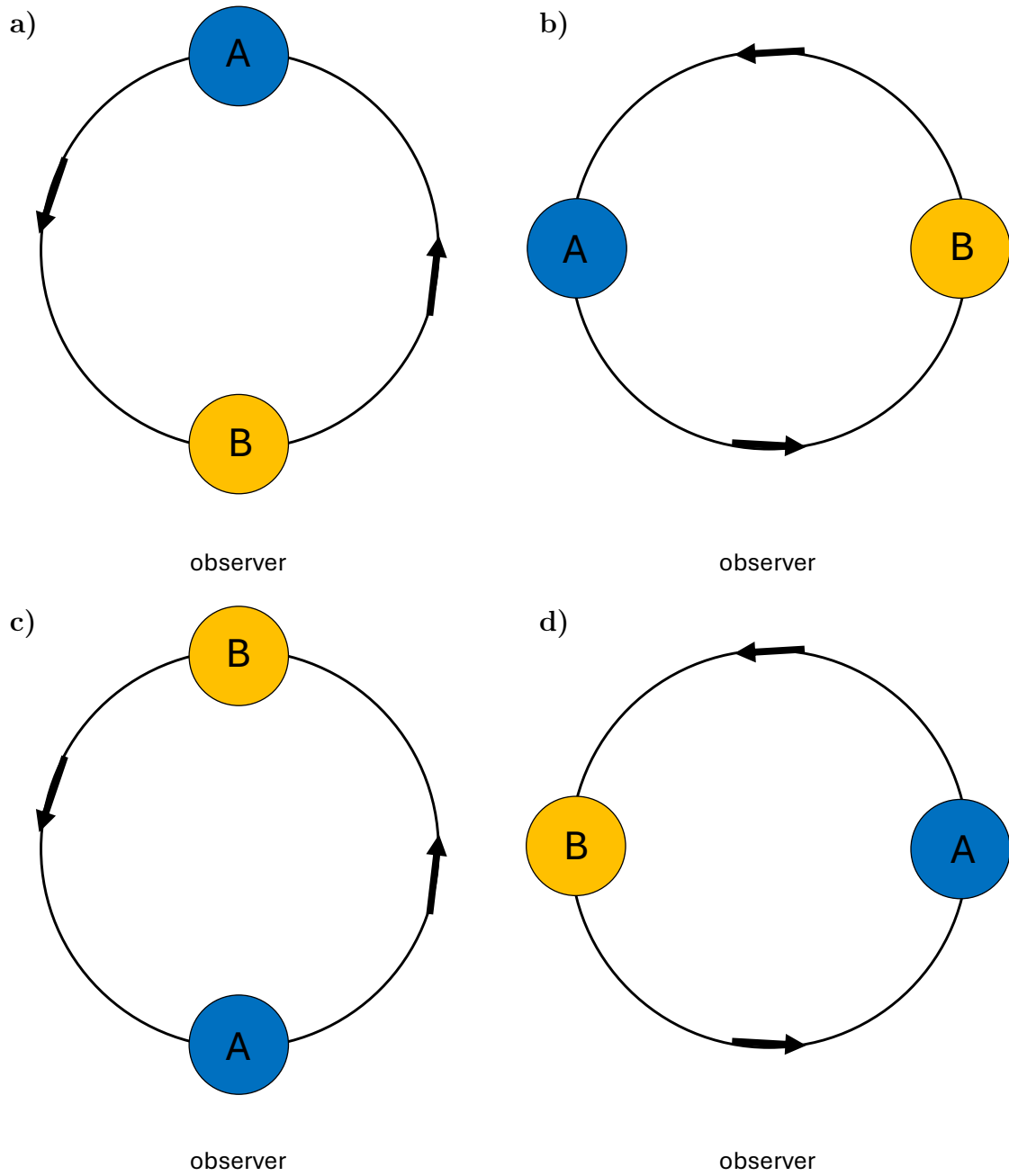


Figure 2.3: Position of pair A and pair B in specific phases in O-C diagram (in Figure 2.2): (a) Phase 0, (b) Phase 0.25, (c) Phase 0.5, and (d) Phase 0.75 .

## 2.6 Estimation of the physical parameters for the physical fit

The physical models were done in PHOEBE (=PHysics Of Eclipsing BinariEs) software (Prša et al., 2011). PHOEBE is eclipsing binary modeling software, using which we can determine the relative radii and temperatures of the primary and secondary components, mass ratio, inclination, and eccentricity of the orbital trajectory.

### 2.6.1 Mass ratio

The mass ratio significantly influences the physical fit. The best possible way to estimate the mass ratio is from the amplitude of the radial velocity curve. If we do not have the spectra at all or we have few points in the radial velocity graph, we can estimate the mass ratio only from the photometric measurements.

If the system is a detached binary where there is no transfer of mass, we can use relation (Graczyk, 2003):

$$\log(q) = \frac{(\log(L_1) - \log(L_2))}{3.664}, \quad (2.4)$$

where  $q$  is the mass ratio (primary/secondary),  $L_1$  is the absolute luminosity of a primary component, and  $L_2$  is the absolute luminosity of a secondary component.

On the contrary, if we want to estimate the mass ratio in overcontact binaries (where mass transfer occurs) we can use a process described in detail in the article Kouzuma (2023). This method is based on calculating the third derivative of a light curve (see Figure 2.4).

The factual reason why the third derivative was used is not clearly explained in the article, yet it gives an error of  $\pm 0.1$  for 97% of analysed systems. To be able to estimate the mass ratio correctly, the following conditions have to be fulfilled:

- the second derivative has two local maxima (symmetric with respect to eclipse)
- the third derivative has a local maximum and local minimum
- $w_{31} < w_{21} < w_{32} < w_{22} < 0.2P$  (where  $P$  is the orbital period and  $w_{ij}$  is the time interval between  $t_{ij}$  and the eclipse time)

The mass ratio can be estimated using the following equations:

$$q = 0.056W - 0.261, \quad (2.5)$$

where  $q$  is the mass ratio and  $W$  is

$$W = \frac{P}{t_{32} - t'_{32}} = \frac{P}{w_{32} + w'_{32}}. \quad (2.6)$$

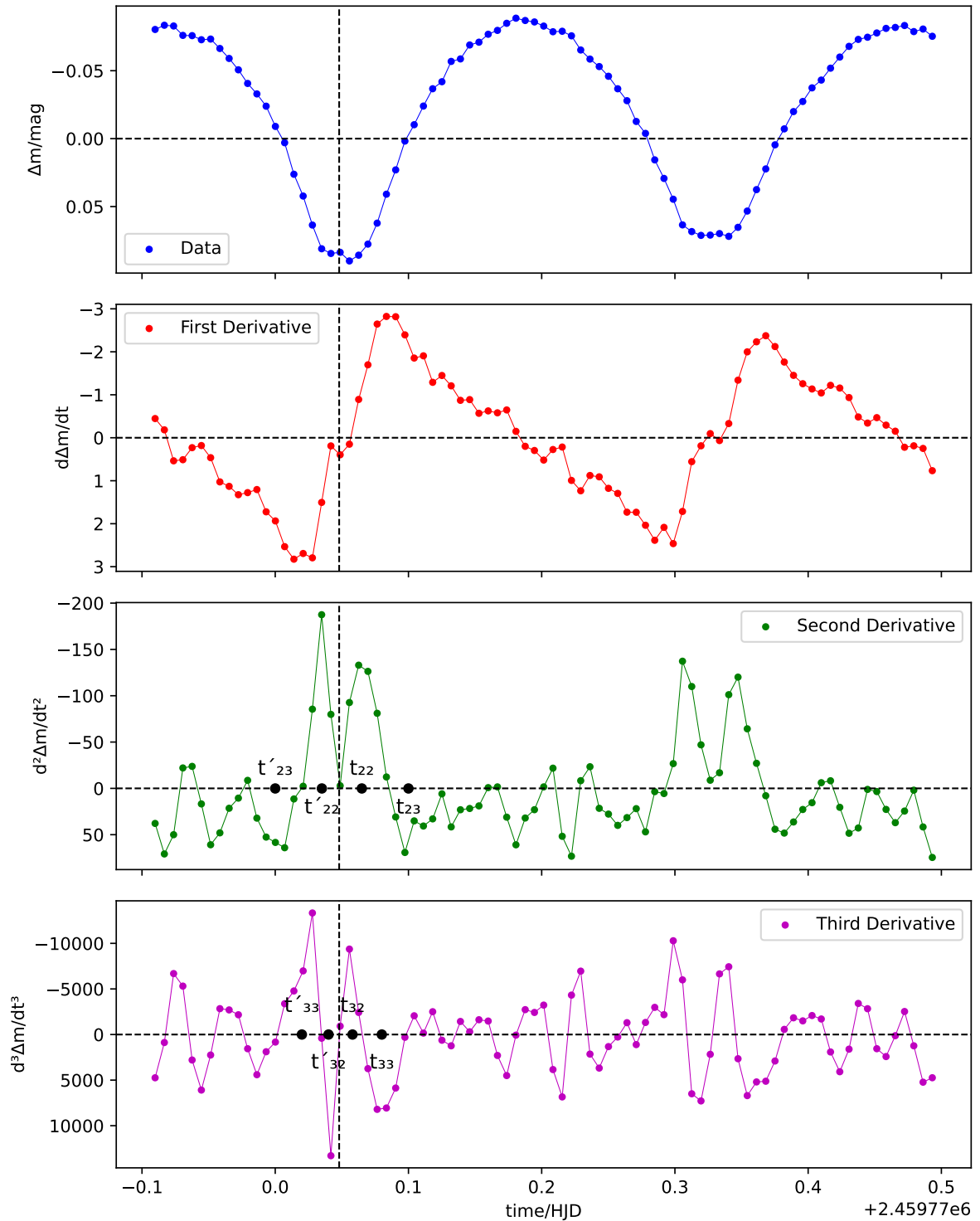


Figure 2.4: Example of estimation process of mass ratio for overcontact binaries - Brh V154, pair A.

## 2.6.2 Temperature

The common way of estimating the temperature is by using spectroscopic measurements. If we do not have spectroscopic data, the estimation of temperature can be challenging. The temperature value can be obtained from Gaia, but there is always only one value of temperature (for four components). Moreover, we do not know in which phase the temperature was measured.

To estimate the temperature by at least some statistical method, the VO SED analyzer (Bayo et al., 2008) was used. VO SED collects all available measurements of the temperature of the studied system (from different areas and filters) and makes a fit (see Figure 2.5). There are many options for the fit models, in this thesis the black body model is used.

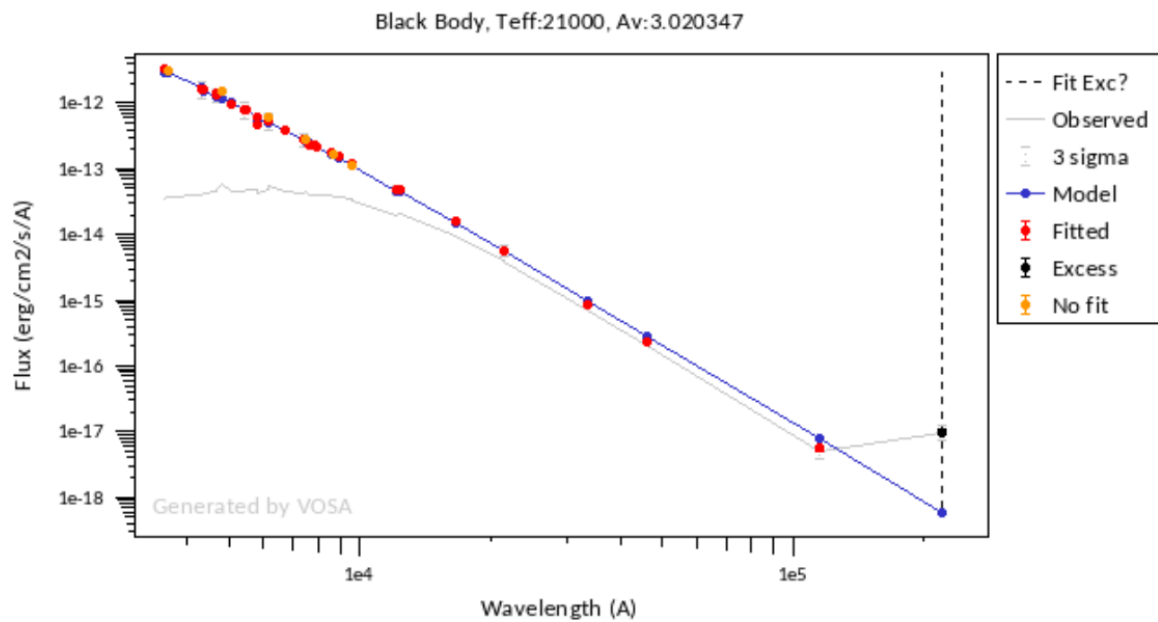


Figure 2.5: Example of estimation of temperature using SED of the star S2 Pup.

# Chapter 3

## S2 Pup

### 3.1 Basic information

In Table 3.1 there are the basic characteristics of the S2 Pup star and used comparison star. The choice of comparison star was very challenging because, in the closest neighborhood of this star, most of the stars are variable as well. The comparison star was selected as the star with the closest  $B - V$  value to the variable star even though variable and comparison star temperatures differ a lot.

For this star TESS data from years 2019, 2021, 2023, and 2025 were analysed, and data from other observers: Miloslav Zejda, Jan Janík, Jakub Kolář were collected. The list of these observations together with the photometric filter can be seen in Table 3.2. Besides the photometric data, the spectroscopic data were measured and processed (calibrated and normalized) by Jan Janík. Spectra were measured with SpUpNIC (Spectrograph Upgrade-Newly Improved Cassegrain) at SAAO (South African Astronomical Observatory).

Table 3.1: Basic information about S2 Pup star.

	<b>Variable star</b>	<b>Comparison star</b>
Name	ASAS J073054-1840.7	TYC 5983-1709-1
RA	07 <sup>h</sup> 30 <sup>m</sup> 54.25 <sup>s</sup>	07 <sup>h</sup> 30 <sup>m</sup> 57.2 <sup>s</sup>
DEC	-18° 40' 42.38''	-18° 44' 06.2''
T [K]	21800	5762
$B - V$ [mag]	0.744	0.970
$M_{0A}$ in HJD [days]	2459245.65345	
$P_A$ [days]	2.068435	
$M_{0B}$ in HJD [days]	2458508.99491	
$P_B$ [days]	1.728512	

Table 3.2: List of photometric observations of star S2 Pup.

<b>date</b>	<b>observer</b>	<b>filter</b>	<b>device</b>	<b>location</b>
18. 11. 2022	JJ	V	Cassegrain 1540	La Silla
18. 11. 2022	JJ	I	Cassegrain 1540	La Silla
24. 12. 2022	JJ	V	Cassegrain 1540	La Silla
24. 12. 2022	JJ	I	Cassegrain 1540	La Silla
10. 03. 2023	JK	V	Cassegrain 1540	La Silla
10. 03. 2023	JK	I	Cassegrain 1540	La Silla
05. 03. 2023	JK	V	Cassegrain 1540	La Silla
05. 03. 2023	JK	I	Cassegrain 1540	La Silla
09. 03. 2023	JK	V	Cassegrain 1540	La Silla
09. 03. 2023	JK	I	Cassegrain 1540	La Silla
25. 03. 2023	JK	V	Cassegrain 1540	La Silla
25. 03. 2023	JK	I	Cassegrain 1540	La Silla
06. 05. 2023	JK	V	Cassegrain 1540	La Silla
06. 05. 2023	JK	I	Cassegrain 1540	La Silla
07. 05. 2023	JK	V	Cassegrain 1540	La Silla
07. 05. 2023	JK	I	Cassegrain 1540	La Silla
05. 04. 2023	JK	V	Cassegrain 1540	La Silla
24. 12. 2023	MZ	V	Cassegrain 1540	La Silla
24. 12. 2023	MZ	I	Cassegrain 1540	La Silla
25. 12. 2023	MZ	V	Cassegrain 1540	La Silla
25. 12. 2023	MZ	I	Cassegrain 1540	La Silla
20. 01. 2024	MZ	V	Cassegrain 1540	La Silla
20. 01. 2024	JK	I	Cassegrain 1540	La Silla
19. 03. 2024	JK	V	Cassegrain 1540	La Silla
19. 03. 2024	JK	I	Cassegrain 1540	La Silla
21. 03. 2024	JK	V	Cassegrain 1540	La Silla
22. 03. 2024	JK	I	Cassegrain 1540	La Silla
26. 03. 2024	JK	V	Cassegrain 1540	La Silla
26. 03. 2024	JK	I	Cassegrain 1540	La Silla
23. 04. 2024	JK	V	Cassegrain 1540	La Silla
23. 04. 2024	JK	I	Cassegrain 1540	La Silla
24. 04. 2024	JK	V	Cassegrain 1540	La Silla
24. 04. 2024	JK	I	Cassegrain 1540	La Silla

## 3.2 Disentangled lightcurves

As the main goal of this thesis is the analysis of candidates for doubly eclipsing systems, the disentanglement method starts with the assumption that there are two pairs in the studied system. For both the methods mentioned in the chapters 2.3 and 2.4 were distinguished the contribution of pair A (see Figure 3.1) and pair B (see Figure 3.2).

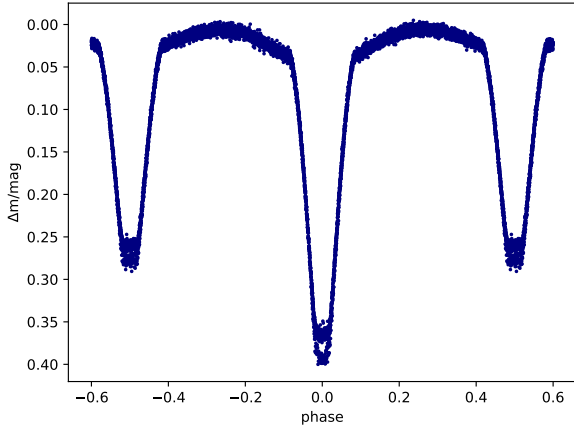


Figure 3.1: Pair A - iteration method.

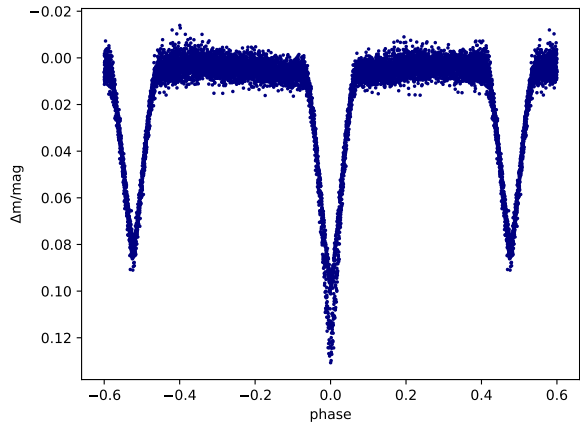


Figure 3.2: Pair B - iteration method.

Theoretically, if we sum up the contribution of pair A and pair B and subtract it from the original light curve (make the residuals) we should only get noise. If we apply this to the S2 Pup light curve, we can see some periodic signal throughout the whole sector. The shape of these periodic changes resembles eclipses (see Figure 3.3). The periodic signal may have many possible origins.

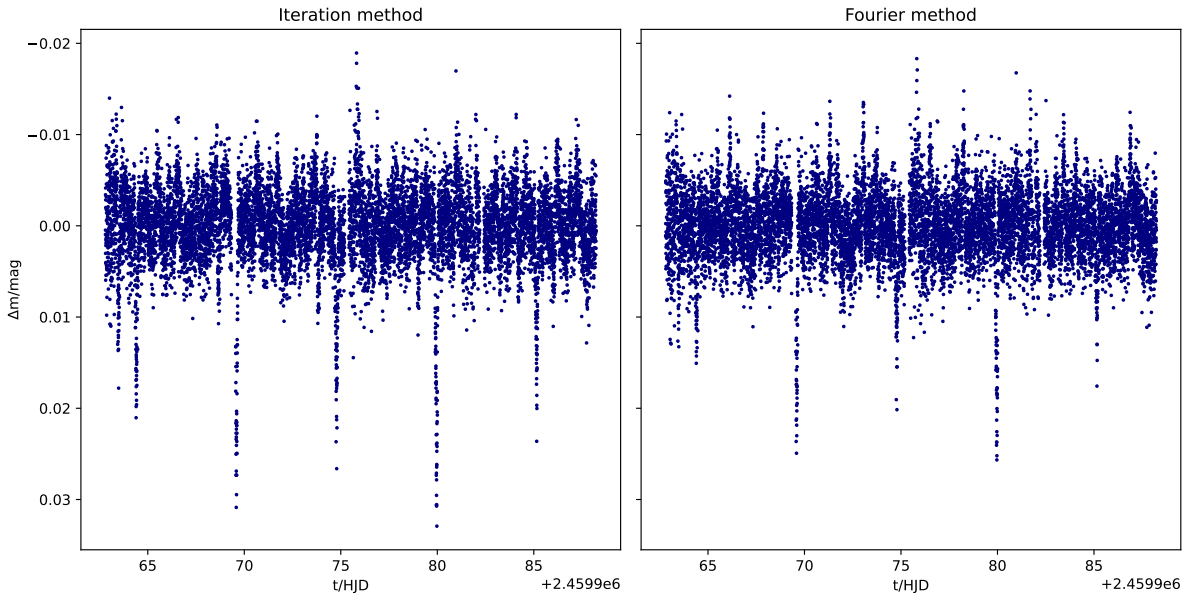


Figure 3.3: Residuals for 2 pairs in the system.

Firstly, it is necessary to check whether the additional changes are not due to a blend. In the TESS chart another star falls into the same pixel as S2 Pup, but in our measurements (see Figure 3.5), we can see that there is no star in the closest neighbourhood.

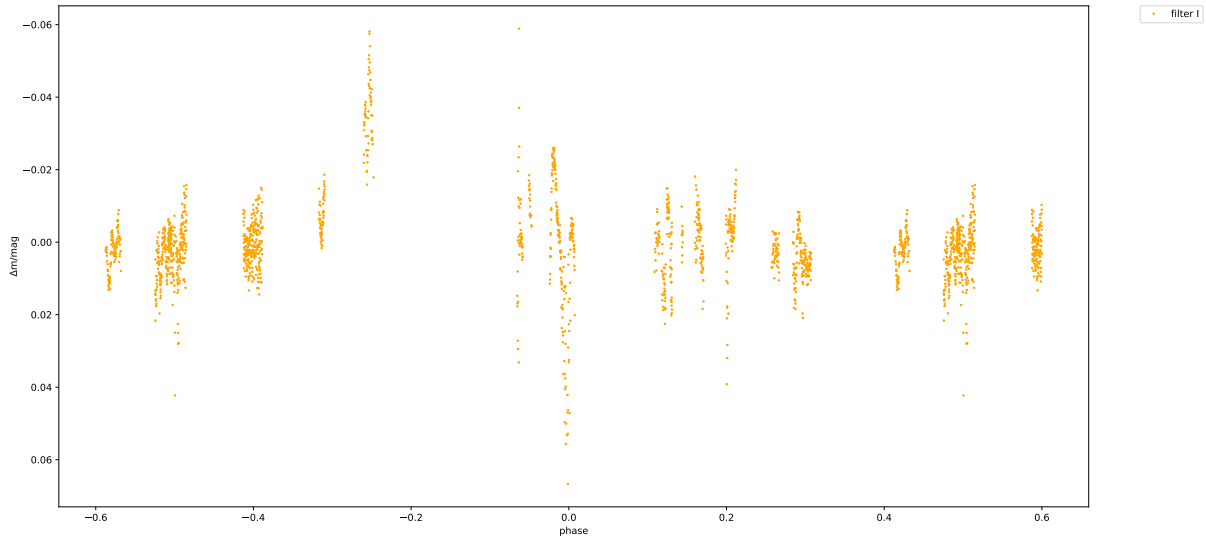


Figure 3.4: Residuals in ground-based data.

As we observe the periodic changes in residuals in ground-based data (see Figure 3.4), the periodic signal in the residuals is not caused by the blend.

The possibility that these eclipses were caused by pair A shadowing pair B and vice versa is very low. The eclipses occur multiple times in one TESS sector (27 days), whereas the typical outer period (for the yet-known doubly eclipsing systems) of these eclipses is in the order of years. Moreover, both pairs A and B are detached systems, so their mutual distance should be relatively high, resulting in a larger period of mutual motion.

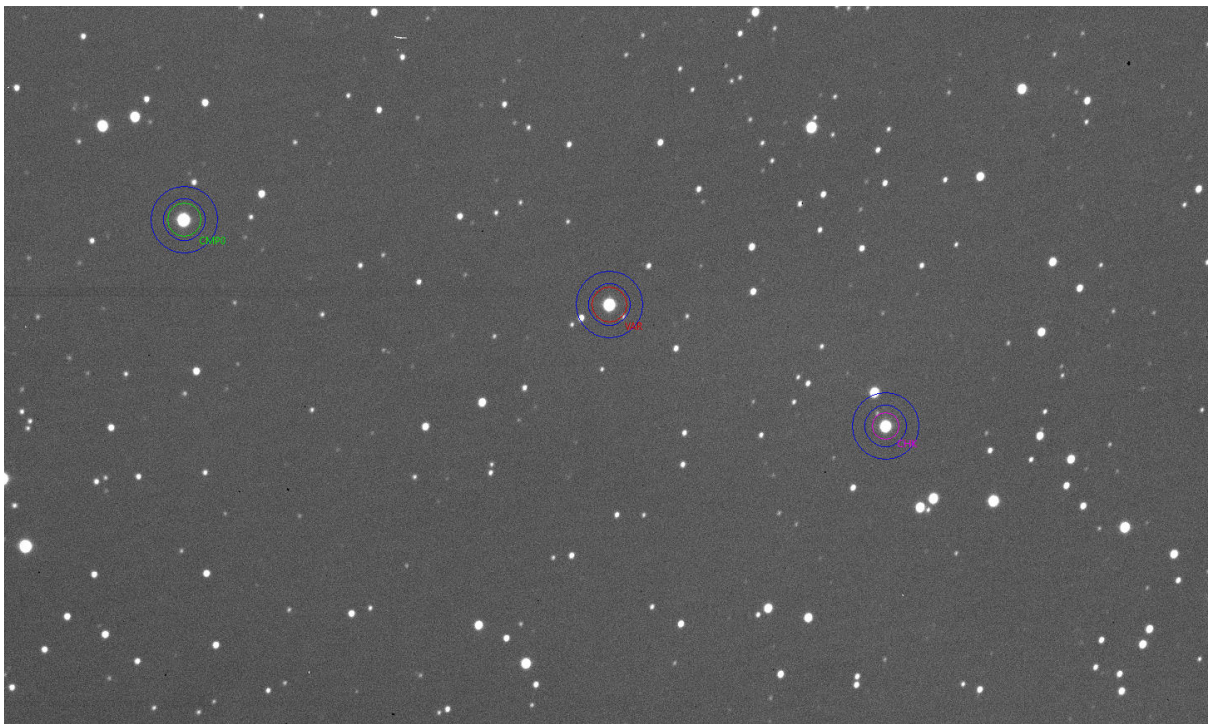


Figure 3.5: Chart of S2 Pup - La Silla.

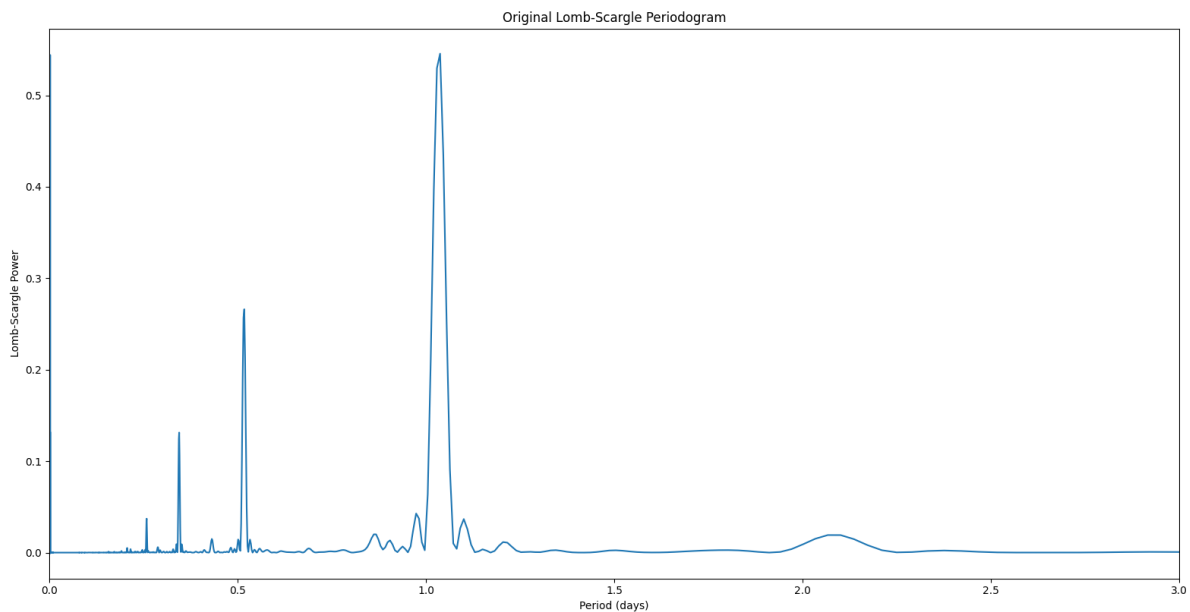


Figure 3.6: Lomb-Scargle periodogram, TESS 2.

Another possibility could be that the eclipses occur right at times when there are minima simultaneously in both pairs A and B. In this scenario, the value of the third light changes and the additional decrease in brightness is observed (Zasche, 2024). To be sure if they are just the sum of the minima, we have to know that the position of these eclipses does not change in time. Therefore, we have to analyse all available data and examine the position of points in the O-C diagram.

Finally, these eclipse-like structures appearing in the residuals could be caused by an exoplanet or another component in the system. However, the depth of these eclipses is too large to be caused by the transit of an exoplanet, and furthermore, the depth of these minima is comparable yet not the same every time it appears. This suggests that it may be caused by another eclipsing system (pair C), so there would be, in fact, three eclipsing pairs. According to the yet-known eclipsing sextuples, the stable arrangement would be a quadruple with a more distant eclipsing pair.

To prove whether the origin of these changes is another eclipsing pair in the system we have to use the disentanglement method with the initial assumption that there are three pairs in the system. We analyse the similarities and differences in the contributions of pairs obtained by iteration and the Fourier method. Afterwards, we look for a possible change in the O-C diagram of a pair C.

The crucial parameter for the disentanglement methods is the orbital period of all pairs and the moment of primary minima. The periods are usually determined from the Lomb-Scargle periodogram. However, if we try to plot one for S2 Pup (see Figure 3.6), we encounter the problem of pair A being so dominant that it overshadows even pair B (not to mention potential pair C). All the visible peaks in the periodogram are multiples of the orbital period  $P_A$ . To have at least some realistic value of the orbital period of a pair C we have to estimate it from the residuals ( $P_C=10.4$  d). That may result in the period not being maximally precise, but it can be more specified later on from the O-C diagram.

The contribution of individual pairs determined by the iterative method can be seen in 3.7, 3.9, and 3.11. The contribution determined from the Fourier method is depicted in Figures 3.8, 3.10, and 3.12. From a visual point of view, we can say that light curves determined by the Fourier method are less noisy but contain some wavelike structures. These are caused mainly by the fact that pair A is in resonance with the pair C ( $\frac{P_C}{P_A} \doteq 5$ ) and pair B is also in resonance with the pair C ( $\frac{P_C}{P_A} \doteq 6$ ).

There is a slight problem with using the Fourier method on the systems that are in resonance. The resonance is responsible for overlapping of higher harmonics, resulting in the wave-like structures in the light curve. Another reason for the imperfections in the light curves determined by the Fourier method could be the low precision in used orbital period  $P_C$ , because the Fourier method is very sensitive to the value of orbital period.

Nevertheless, the number, depth, shape, and duration of eclipses are the same regardless of the method of disentanglement used. That suggests that both the methods were processed correctly.

Even from the shape of the light curves of individual pairs, we can tell a lot about each pair. For example, if we compare the depth of the minima in each pair, we can determine which pair is the most dominant. The depth of the minima in pair A is in the order of 0.1 mag, in pair B, it is close to 0.1 mag, and in pair C, the primary minima are smaller than 0.05 mag. So the most dominant is pair A, and the least dominant is pair C. This gives us the initial estimation of the third light parameter. For pair A, the initial value of the third light will be 0.2, for pair B 0.7, and for pair C 0.9.

### 3.2.1 Pair A

In the phase curve of pair A (see Figure 3.7), we can say that it is a detached eclipsing binary. From the parts of the phase curve between minima, we can see that there are no changes yet the brightness is not perfectly constant (it has a bump-like shape). This suggests that the components of the pair are quite close to each other, and this bump-like structure may be a consequence of a reflection effect. The closer the components are, the more significant this reflection effect will be.

In both the primary and secondary minima, there is a phase of a constant brightness (total eclipses), which suggests that one component is significantly larger than the other one. As we can observe the total eclipses (phase of constant brightness in both the minima), the inclination should be high (around  $80^\circ$ - $90^\circ$ ). The secondary minima appear at phase 0.5, so the value of eccentricity will be close to zero. The depth of the primary minima is larger than the depth of the secondary one, so the primary component will have a higher temperature. The big difference in temperature and radii of individual components suggests that the mass ratio will be quite small (e.g., 0.4).

With these initially estimated parameters, the phase curve was fitted in PHOEBE software and the parameters of the fit are listed in the Table 3.5).

### 3.2.2 Pair B

When analysing pair A, we could have considered both the iteration and the Fourier method phase curves. If we look closer at the phase curves of pair B in the Fourier method (see Figure 3.10), we will notice significant wavelike structures that do not have a realistic base, so for guessing the initial values of parameters of pair B, we will take into account only phase curve determined by the iteration method.

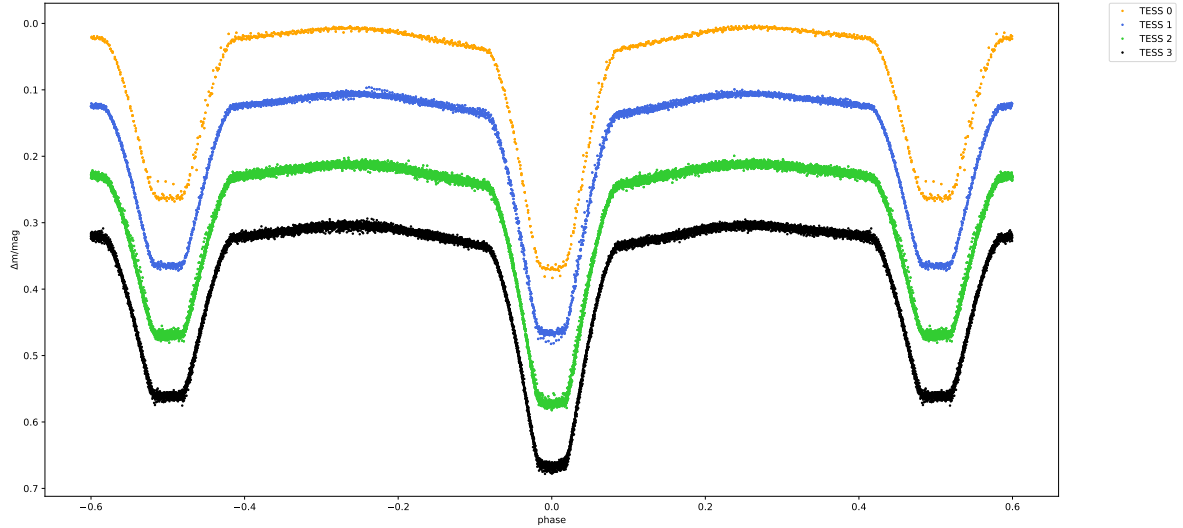


Figure 3.7: Pair A - TESS data, iteration method.

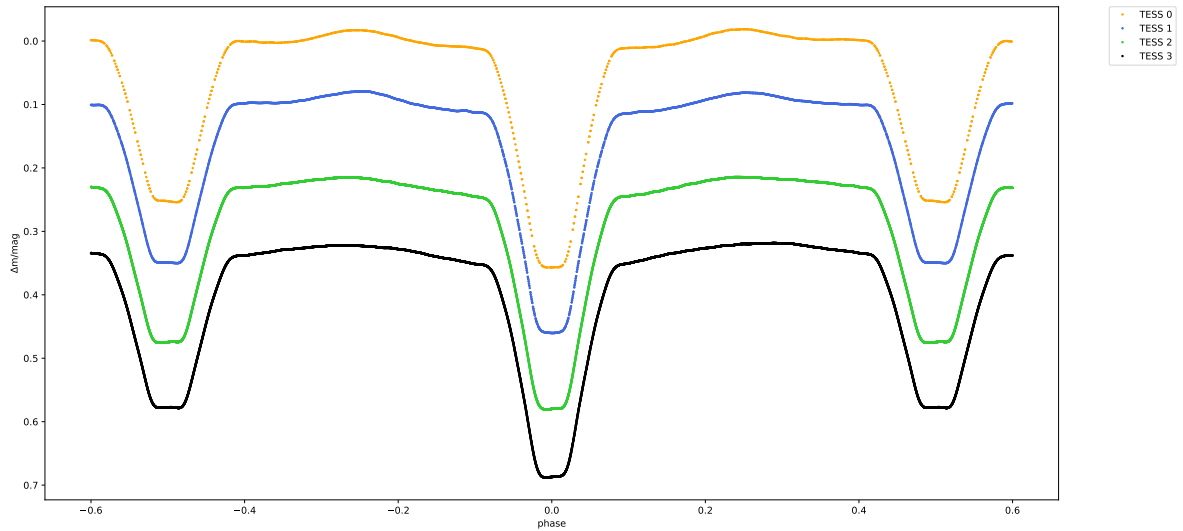


Figure 3.8: Pair A - TESS data, Fourier method.

As well as in the case of pair A, pair B is a detached eclipsing binary. In this case, there is no constant phase in the minima, so the size of the individual components will be comparable. The components will have approximately the same temperature and will be relatively close to each other as the duration of both the minima is quite large.

The inclination of this system will definitely be smaller than in pair A; therefore, our initial estimate is  $60^\circ$ - $70^\circ$ . In this case, the mass ratio will be much larger than for pair A, so we will take the initial estimate as 0.8.

The secondary minima do not appear at phase 0.5, but rather at phase 0.476. This suggests that the orbit will have non-zero eccentricity. Since the secondary minima phase is lower than 0.5, we can estimate the argument of periastron being close to  $180^\circ$ .

With these initially estimated parameters, we fitted the phase curve in PHOEBE software and got values of parameters (see Table 3.6).

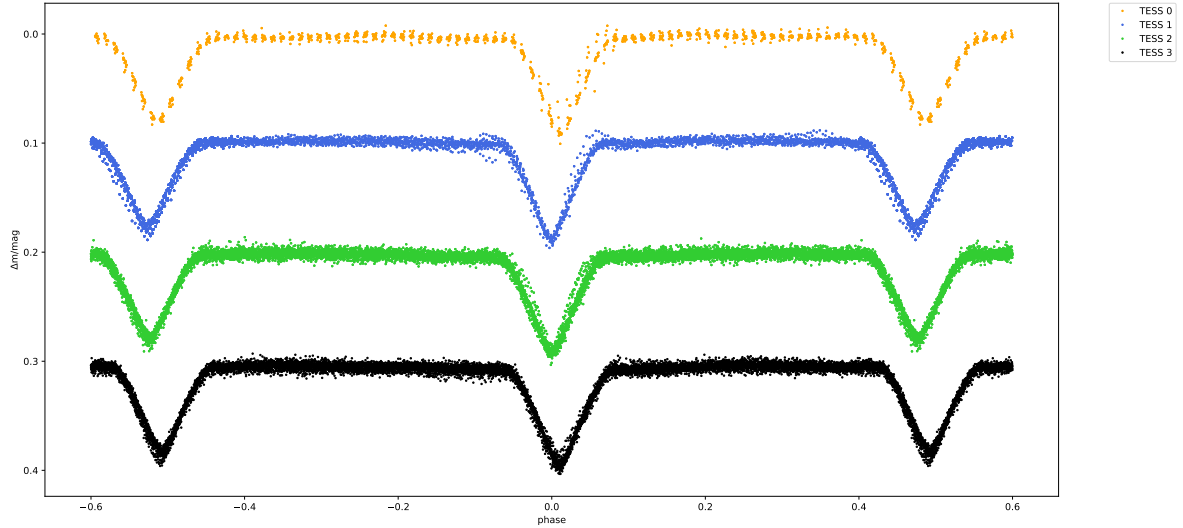


Figure 3.9: Pair B - TESS data, iteration method.

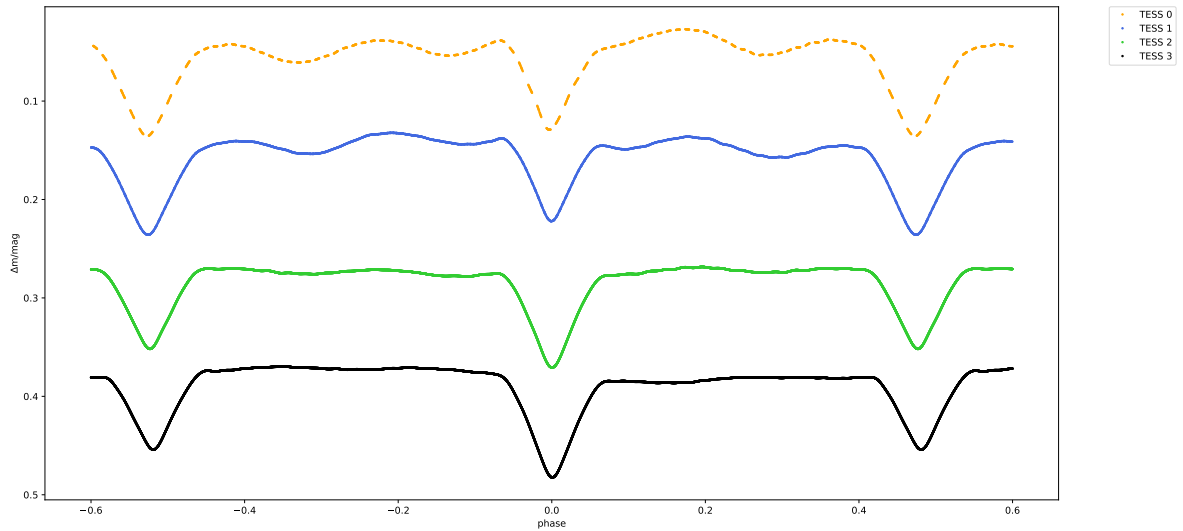


Figure 3.10: Pair B - TESS data, Fourier method.

### 3.2.3 Pair C

Similar to the case of pair B, here we can also analyse only the phase curve determined by the iteration method. If pair C is indeed another eclipsing binary in the system, then it is also a detached eclipsing binary of type Algol II. Both the primary and secondary minima have quite short duration, and there is no constant phase in the minima. The size of the individual components will be comparable and relatively far from each other.

The primary minima are deeper than the secondary ones, so the temperature of the individual components will be different. From the position of secondary minima (appearing at phase 0.5) the value of eccentricity will be close to zero. The initial estimate of the mass ratio will be definitely larger than in the case of pair B, so we will start with the value 0.8.

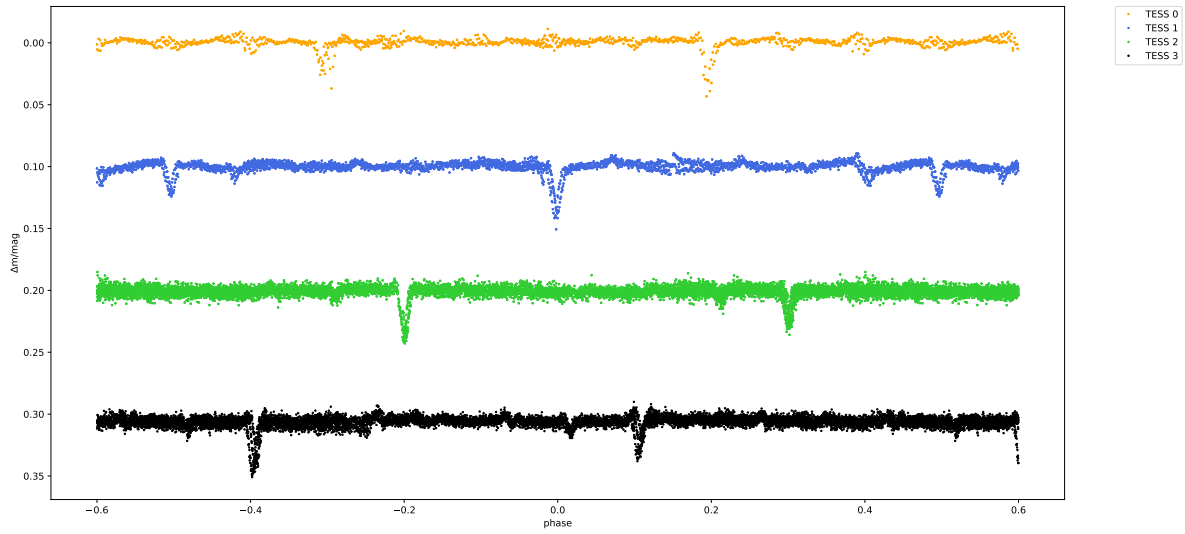


Figure 3.11: Pair C - TESS data, iteration method.

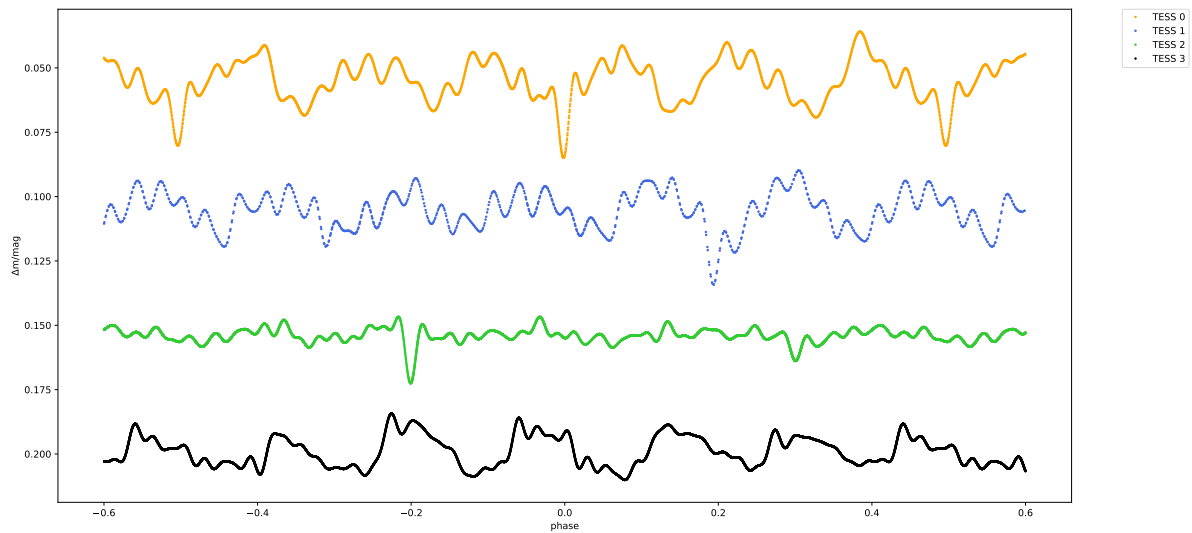


Figure 3.12: Pair C - TESS data, Fourier method.

### 3.3 O-C diagrams

In the O-C diagrams, the full points represent primary minima, and the empty points represent secondary minima.

#### 3.3.1 Pair A

If we look at the light curve of pair A, we can see that the secondary minimum is at phase 0.5, which suggests that pair A will have a rather circular orbit. As mentioned in the previous paragraphs, pair A is the most dominant of this system, which means that its orbital period could be well determined from the Lomb-Scargle periodogram or even

from the disentangled light curve itself. Thus, one would expect that the period used for disentangling should be determined quite precisely. And we can see that directly from the O-C diagram of pair A in Figure 3.13.

As pair A is the most dominant pair in the system, the amplitude of a potential sine curve in the O-C diagram should be small. Because the more massive the pair is, the smaller the motion about the barycentre it makes, and therefore, the smaller shift in the O-C diagram is observed. The points in the O-C diagram are positioned around the zero value on the y-axis (see Figure 3.13), so there is no need to correct the values of ephemerides. We will proceed with the fit of the O-C diagram, which can be seen in Figure 3.14, and the values of the parameters in the Table 3.3. The model LiTE3 was used in all fits of O-C diagrams in this thesis.

### 3.3.2 Pair B

From the light curve of a pair B (Figure 3.9) and the O-C diagram of pair B (Figure 3.15), we can see that there will be a significant value of eccentricity. The secondary minimum does not appear at phase 0.5 but rather at 0.476. In the O-C diagram, the secondary and primary minima are vertically shifted. The distribution of points in the O-C diagram indicates that the moment of initial minima should be determined more precisely.

Moreover, we can see that primary and secondary minima go in sine curves in antiphase. This indicates the apsidal motion. Before we proceed with the model of apsidal motion, it is necessary to change the value of  $M_0$  so that the positions of primary and secondary minima are symmetrical around the line  $y=0$ . The fit of apsidal motion can be seen in Figure 3.16 and the parameters of the model are in the Table 3.3.

Now that we have a model of the apsidal motion, we subtract it from the data and plot the residuals. We will look for a potential LiTE effect in the residuals. After lining up the primary and secondary minima in residuals and performing a linear fit to obtain more precise ephemerides:  $M_0 = (2458508.97300 \pm 0.00001)\text{HJD}$  and  $P = (1.728520 \pm 0.000001)\text{d}$ , we obtain the O-C diagram in Figure 3.17.

This graph shows no significant changes, which can be interpreted in several ways. There is no LiTE effect, indicating that the S2 Pup star is not a doubly eclipsing system. Another possible interpretation may be that as we do not have the whole phase of apsidal motion, it does not fit precisely, and therefore, we do not see the LiTE effect in the residuals even though it is present in pair B. Finally, it can be caused by the fact that not whole phase of the LiTE effect is captured in the O-C diagram, the period is long, and with more long-term observations, we would see the LiTE effect.

Table 3.3: Orbital parameters of pair A and pair B

LiTE3	Pair A	Error	Apsidal	Pair B	Error
$asin(i_3)$ [au]	0.30	0.01	$t_0$ [HJD]	2458508.973	0.001
$e_3$	0.00	0.01	P[d]	1.72852	0.0001
$\omega$ [rad]	5.33	0.01	$\omega_0$ [rad]	2.84	0.01
$t_{03}$ [HJD]	2457010	10	$d\omega_0$ [rad]	0.0009	0.00001
$P_3$ [d]	8720	10	$e$	0.043	0.01

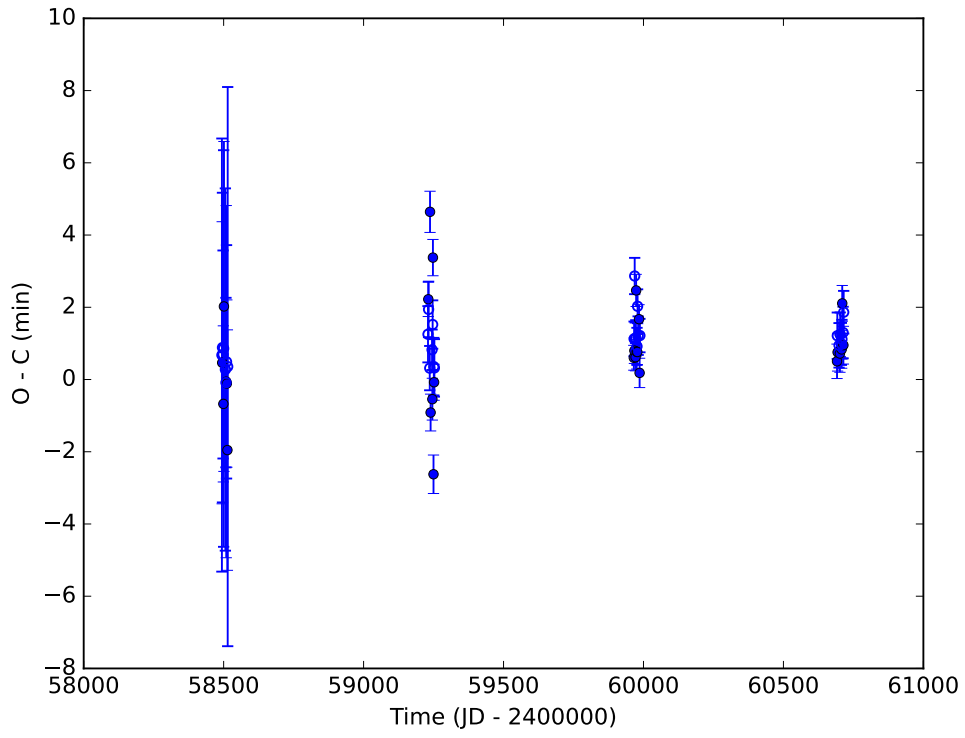


Figure 3.13: O-C diagram of pair A.

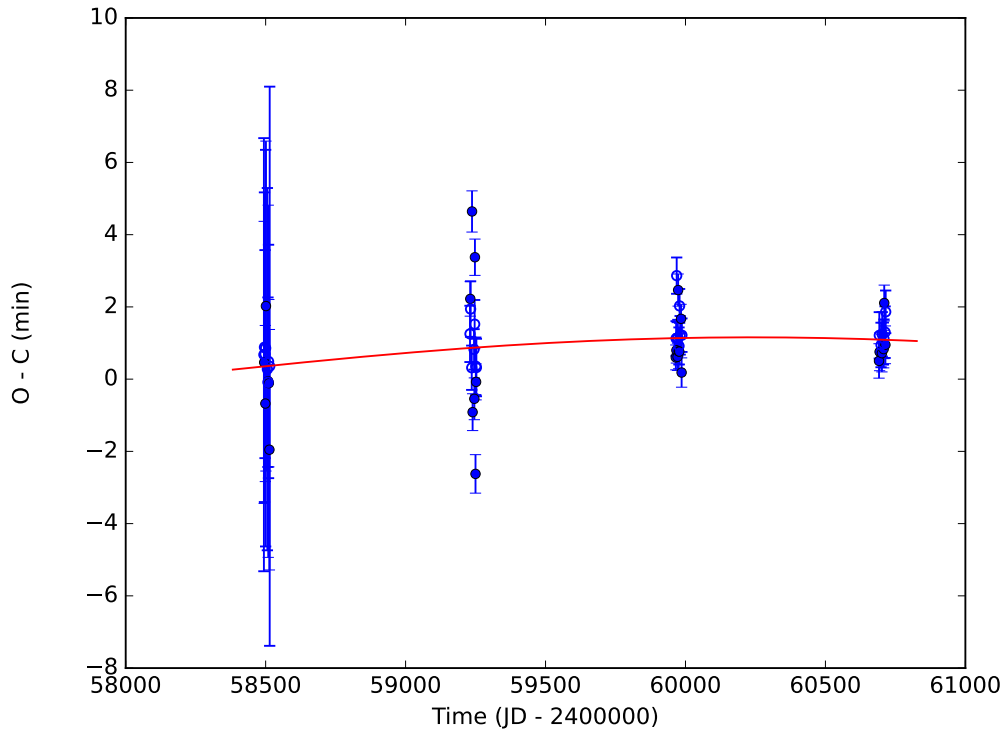


Figure 3.14: O-C diagram of pair A - corrected ephemerides, model.

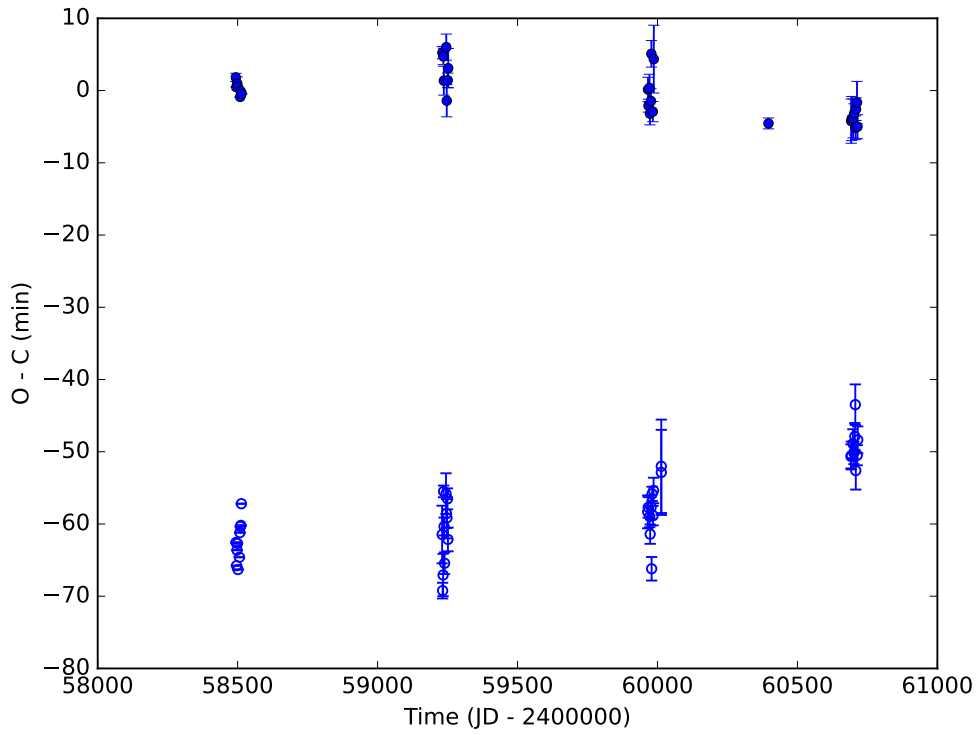


Figure 3.15: O-C diagram of pair B.

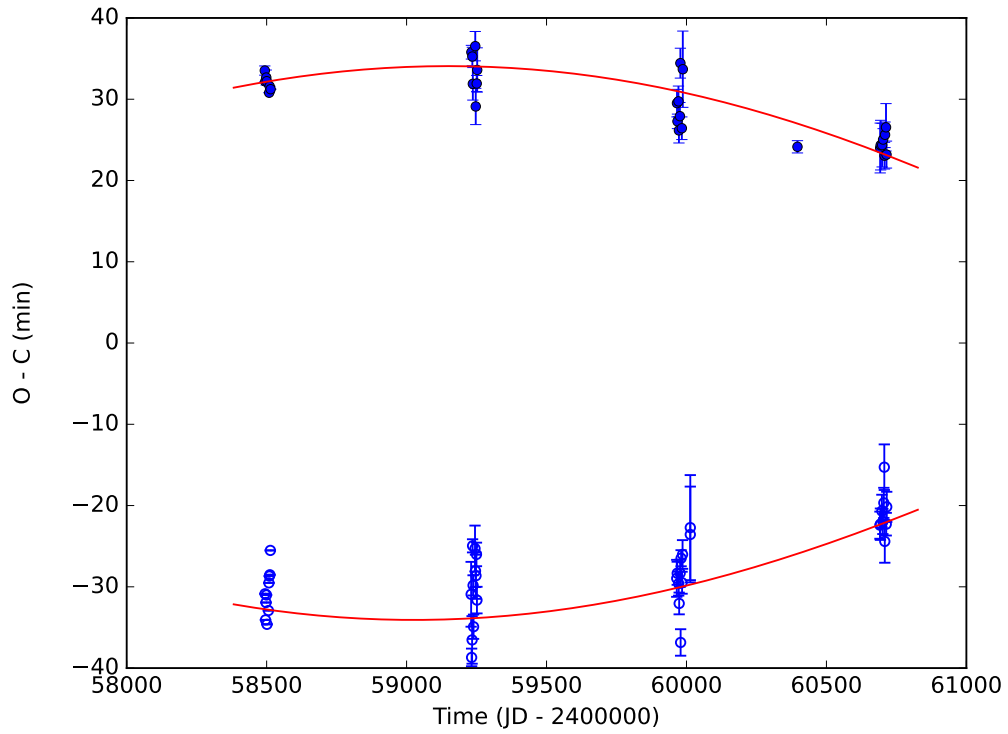


Figure 3.16: O-C diagram of pair B - apsidal motion, model.

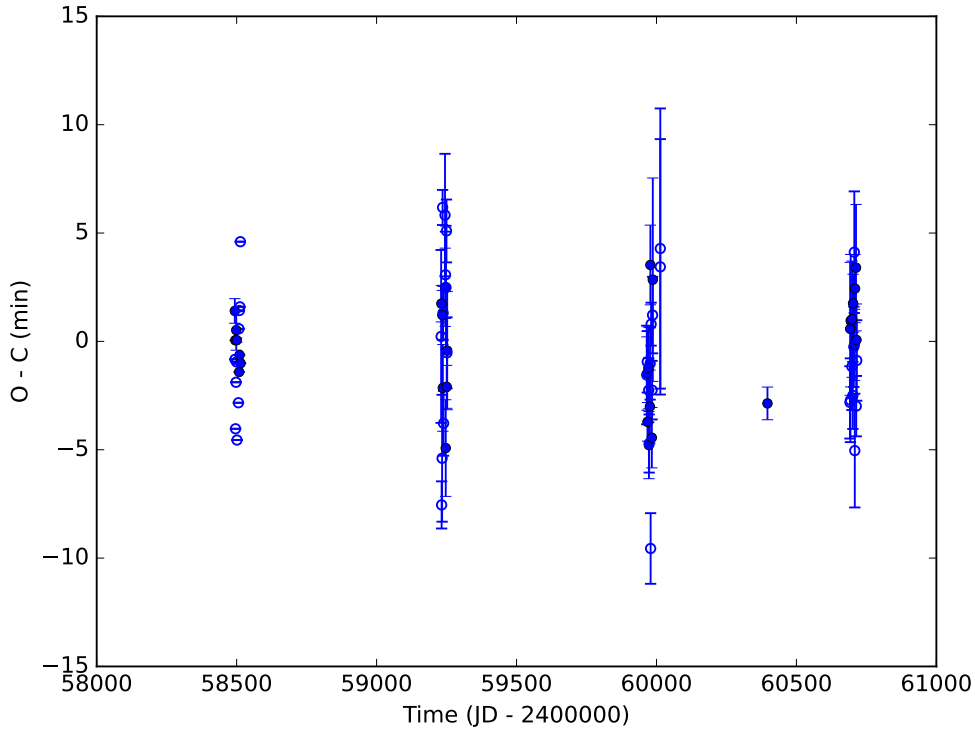


Figure 3.17: O-C diagram of pair B - residuals from apsidal motion.

### 3.3.3 Pair C

As expected from section 3.2, the position of points in the O-C diagram of a pair C (Figure 3.18) is around a line with a large negative slope. This means that the period used for plotting the O-C diagram is larger than the real period of the pair. That was caused by the fact that the original period was determined from the residuals and not from the periodogram. Thus, it is not precise. In the residuals, there were identified the moments of minima and afterward using the software SILICUPS from the times of minima, the period of pair C was obtained.

Using the linear fit, we specify the ephemerides  $P_C = (10.371118 \pm 0.000003)$  d and  $M_{0C} = (2459969.59331 \pm 0.00004)$  HJD and plot a corrected O-C diagram (see Figure 3.19). In the O-C diagram with new ephemerides, no trend is evident. From the shape of the phase curves of pair C (Figures 3.11 and 3.12), pair C is the less dominant in the system and, therefore, should move a lot around the barycentre. This movement should cause significant changes in the O-C diagram.

The fact that no significant changes can be seen in the O-C diagram of pair C suggests that pair C is not another binary in the system. Moreover, in the phase curve of pair C disentangled by the Fourier method (TESS 3 dataset), the eclipse-like shape is no longer observed. The possible explanation could be that as a period of pair A and pair B changes over time, the minima no longer happen simultaneously but are slowly getting out of the resonance. Therefore, the periodic changes in the residuals of light curves of pair A and B are most probably caused by simultaneous eclipses in pair A and pair B.

To be sure whether pair C is a real feature or not, we need long-term observations. But at this moment, everything suggests that there is no real pair C, therefore no physical fit for pair C will be done.

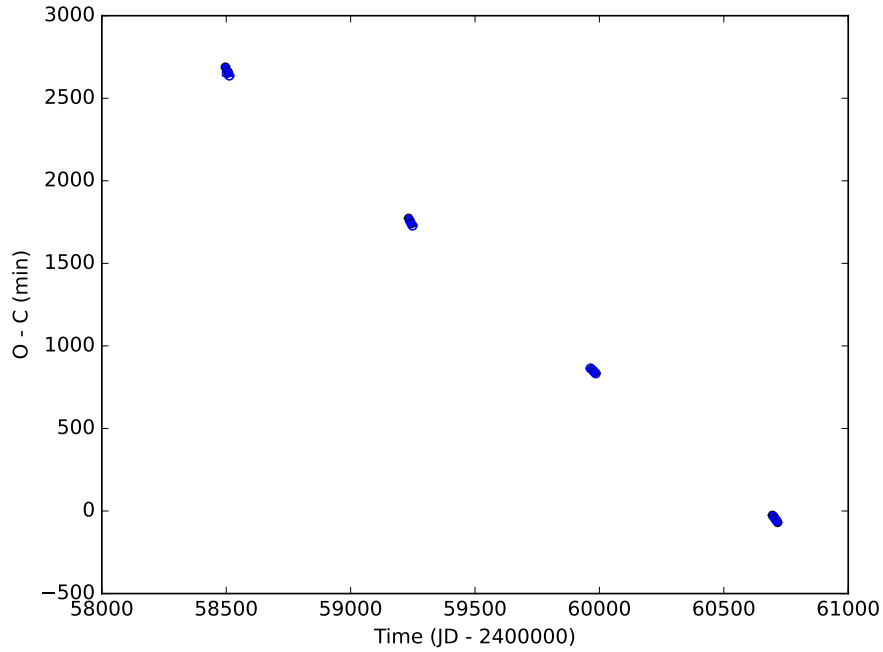


Figure 3.18: O-C diagram of pair C.

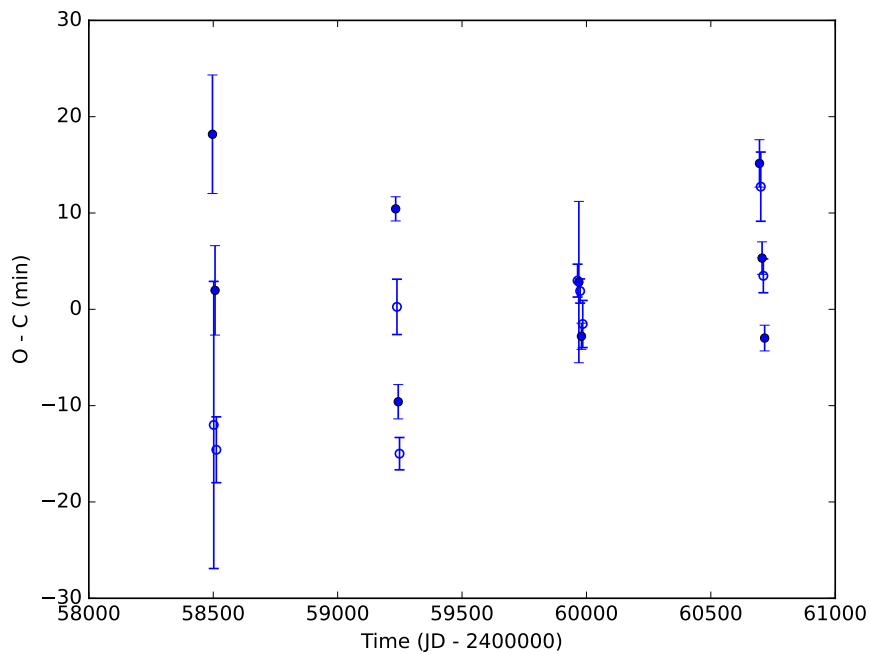


Figure 3.19: O-C diagram of pair C - corrected ephemerides, model.

## 3.4 Spectra

Besides the photometric measurements of the star S2 Pup, the spectra were also analysed. Ideally, we would see one spectral line splitting to four in the spectra caused by the Doppler effect. Due to the relatively small brightness and spectral resolution, we can not observe four systems of lines directly. Nevertheless, we can still see some features in the spectra which suggest (but not prove) that this system could be, indeed, a doubly eclipsing quadruple.

We have spectra measured in different phases for pair A and for pair B. Firstly, we take spectra, where pair B is in the brightness minima and pair A is not (see Figure 3.20). If we look at these spectra we can see directly that the position of spectral lines changes. This shift is caused by the motion of pair A, as pair A is the most dominant pair in this system, and the shift is well visible. Moreover, if we look at the spectral line at approximately 4380 Å at spectra 3 and 4 there is almost no splitting. On the contrary, there is a splitting in spectra 5 and 6. This gives us a basic idea of the shape of a curve of radial velocities. If the orbit is an ideal circle the radial velocity curve would have maxima at phases 0.25 and 0.75. The bigger the radial velocity the more visible the splitting of spectral lines should be. The ellipticity of the orbital trajectory causes the radial velocity curve to look like a deformed sine curve. Since we do not see any evidence of ellipticity in the O-C diagram, the presence of maximal splitting at phases 0.25 and 0.75, should be caused by different processes (such as tidal interactions, third body, or relativistic effects).

Now, if we subtract the spectra, the contributions of pair B should be subtracted as pair B is always in minima. What should remain is the contribution of pair A. As the analysed spectra differ a lot in phase for pair A, the motion of pair A can be directly seen from the comparison of spectra.

Therefore, we observe small waves at the positions of spectral lines in the subtracted spectra. To prove that the motion of pair A truly causes these, we will compare spectra 3, 4, 5, and 6 with spectra 14, where pair B is again in the minima, and pair A is in almost the same phase as in spectra 3 and 4. We can see the spectra in Figure 3.21. Now we subtract spectra 3, 4, 5, and 6 from spectrum 14 and compare the results. As spectra 3, 4, and 14 have nearly the same phase for pair A we observe almost no waves. On the other hand, spectra 5 and 6 differ a lot in the phase of pair A compared to pair 14, so the waves at the position of spectral lines are well visible.

Then we examine the spectra 18, 20, and 21, where pair A is always in the minima and pair B is not (see Figure 3.22). If we look at the hydrogen lines, we can see some small changes in their position. That is caused by the motion of pair B. If we subtract the spectra (see Figure 3.24) we should observe the motion of pair B, but because it is not as big as in the case of pair A it gets lost in the noise. We would need a higher spectral resolution to properly observe the motion of pair B.

Another step in the spectral analysis is searching for lines in spectra that appear when one pair is in the minima, and the other pair is not and disappear when both pairs are out of the minima. This should give us a basic idea about which spectral line belongs to which pair. However, if we look at the spectra, we do not see any new lines (see Figure 3.25).

Table 3.4: Values of phase for individual spectra.

<b>Spectrum</b>	<b>M0 [HJD]</b>	<b>Pair A</b>	<b>Pair B</b>
2	2460033.31061	0.798 out of minimum	0.862 out of minimum
3	2460034.27623	0.264 out of minimum	0.421 secondary minimum
4	2460034.37212	0.311 out of minimum	0.477 secondary minimum
5	2460035.27761	0.749 out of minimum	0.000 primary minimum
6	2460035.34762	0.782 out of minimum	0.041 primary minimum
7	2460036.25820	0.223 out of minimum	0.568 out of minimum
8	2460038.23042	0.176 out of minimum	0.709 out of minimum
9	2460038.32457	0.222 out of minimum	0.763 out of minimum
10	2460038.38268	0.250 out of minimum	0.797 out of minimum
11	2460039.23074	0.660 out of minimum	0.287 out of minimum
12	2460039.30587	0.696 out of minimum	0.331 out of minimum
13	2460040.30078	0.177 out of minimum	0.906 out of minimum
14	2460042.21976	0.105 out of minimum	0.017 primary minimum
15	2460042.31164	0.149 out of minimum	0.070 out of minimum
16	2460043.24251	0.599 out of minimum	0.608 out of minimum
17	2460043.28849	0.622 out of minimum	0.635 out of minimum
18	2460044.22587	0.075 primary minimum	0.177 out of minimum
19	2460044.31610	0.1183 out of minimum	0.229 out of minimum
20	2460045.22131	0.556 secondary minimum	0.753 out of minimum
21	2460046.23816	0.048 secondary minimum	0.341 out of minimum

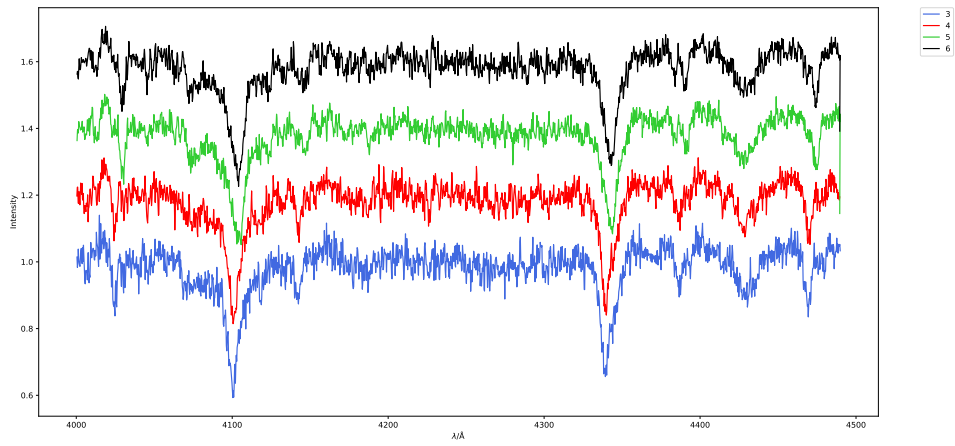


Figure 3.20: Spectra 3, 4, 5 and 6.

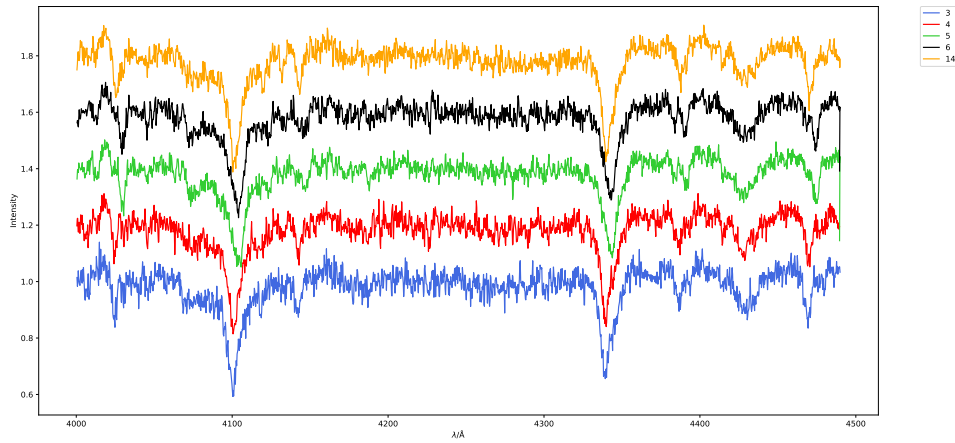


Figure 3.21: Spectra 3, 4, 5, 6 and 14.

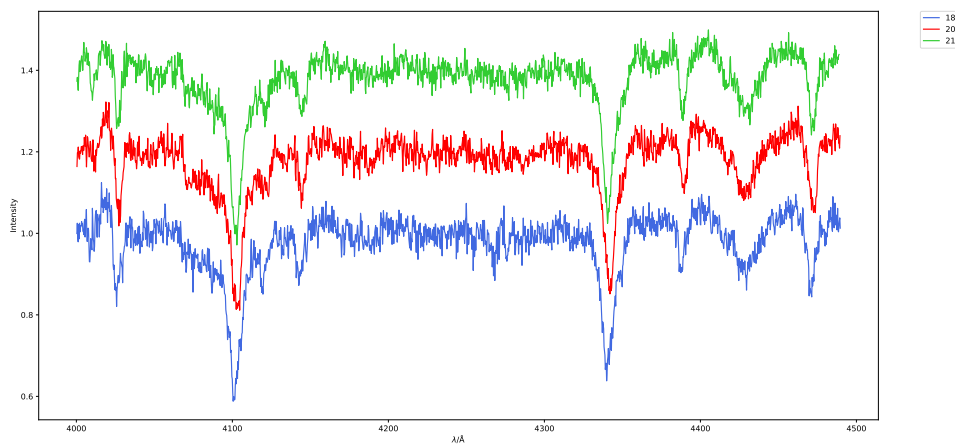


Figure 3.22: Spectra 18, 20 and 21.

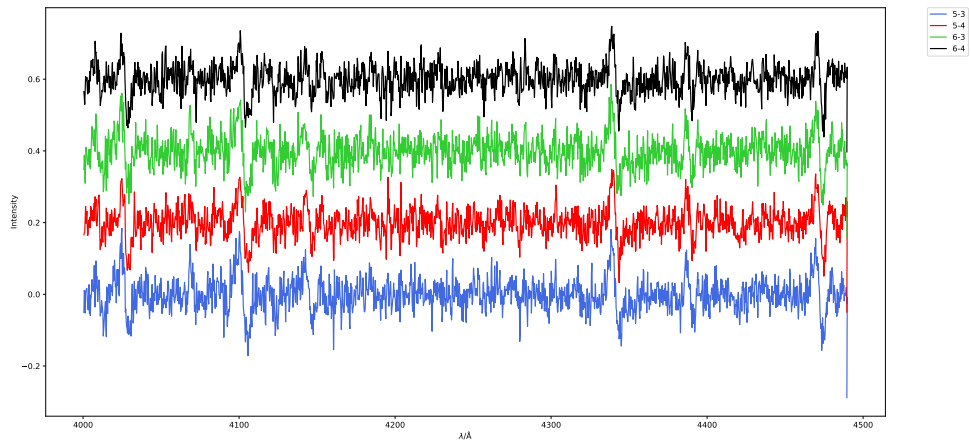


Figure 3.23: Subtraction of spectra 3, 4, 5, and 6.

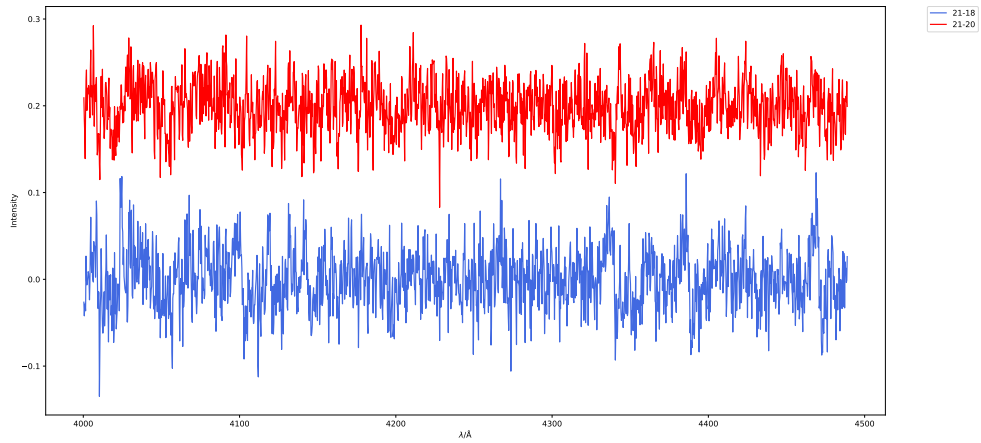


Figure 3.24: Subtraction of spectra 18, 20 and 21.

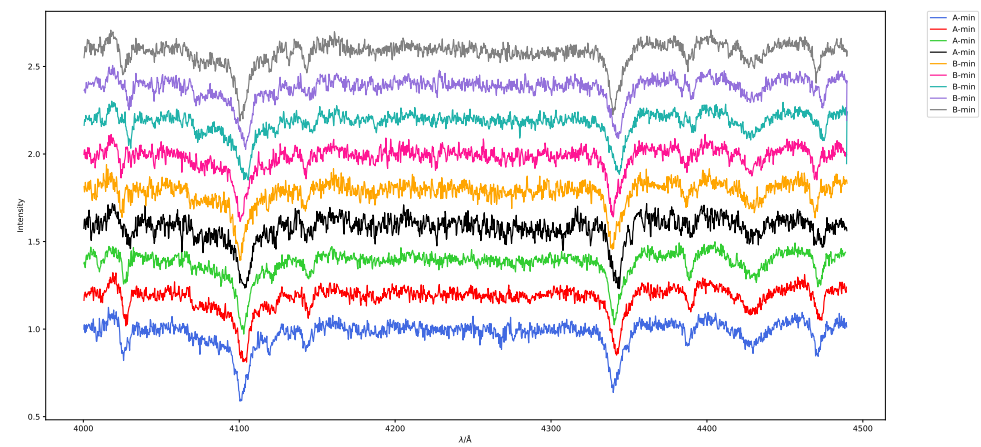


Figure 3.25: Spectra with pairs in minima.

## 3.5 Physical models

The parameters of the physical fit are listed in Tables 3.5 and 3.6 together with the error value which describes the value of a step with which were parameters fitted. The sets of fitting steps are the same for all stars studied in this thesis.

### 3.5.1 Pair A

If we look closely at the values in Table 3.5 we see that for both the TESS and observed data, the primary component is significantly greater than the secondary component. The values of temperature of both the components are approximately the same in both the TESS data and our measurements. The value of inclination (close to  $90^\circ$ ) corresponds well with our initial assumption (based on the observation of phase of constant brightness in both primary and secondary minima).

The reason for the mass ratio having different values in the TESS 2 and 3 dataset may be the cadence of analysed data. The TESS 0 dataset consists of frames with an exposure of 1426 s, the TESS 1 dataset with 475 s, and the TESS 2 and 3 datasets with 158 s frames. Therefore, the TESS 2 and 3 light curves show more detail than the TESS 0 and TESS 1 datasets. The mass ratio considerably influences the shape of the eclipses in the phase curve; therefore, its value may differ a bit with different cadence of data. On the other hand, the value of the mass ratio is far from 1 in all analysed datasets, as we estimated.

Table 3.5: Pair A – parameters of physical model.

Parameter	TESS 0	TESS 1	TESS 2	TESS 3	filter V	filter I	error
$\frac{R_1}{a}$	3.18	3.14	3.22	3.22	3.17	3.19	0.01
$\frac{R_2}{a}$	2.07	2.07	2.14	2.17	2.13	2.11	0.01
$M_{\text{bol1}}$ [mag]	-3.544	-3.516	-3.563	-3.568	-3.533	-3.541	0.001
$M_{\text{bol2}}$ [mag]	-1.777	-1.793	-1.848	-1.877	-2.052	-2.243	0.001
$T_{\text{ef1}}$ [K]	21 800	21 800	21 800	21 800	21 800	21 800	10
$T_{\text{ef2}}$ [K]	18 000	18 070	18 010	18 000	18 900	18 870	10
$i$ [ $^\circ$ ]	88.89	89.57	88.54	88.48	89.90	89.43	0.01
$q$	0.60	0.64	0.49	0.49	0.64	0.71	0.01
$e$	0.00	0.00	0.00	0.00	0.00	0.00	0.01

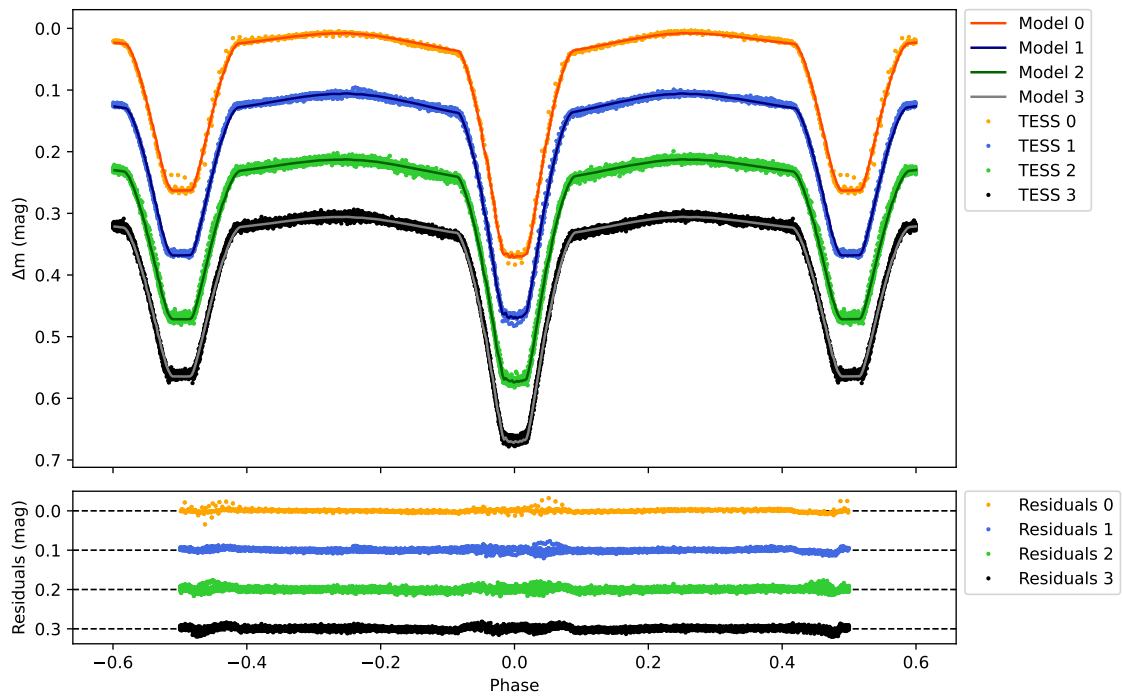


Figure 3.26: Pair A - physical model, TESS data.

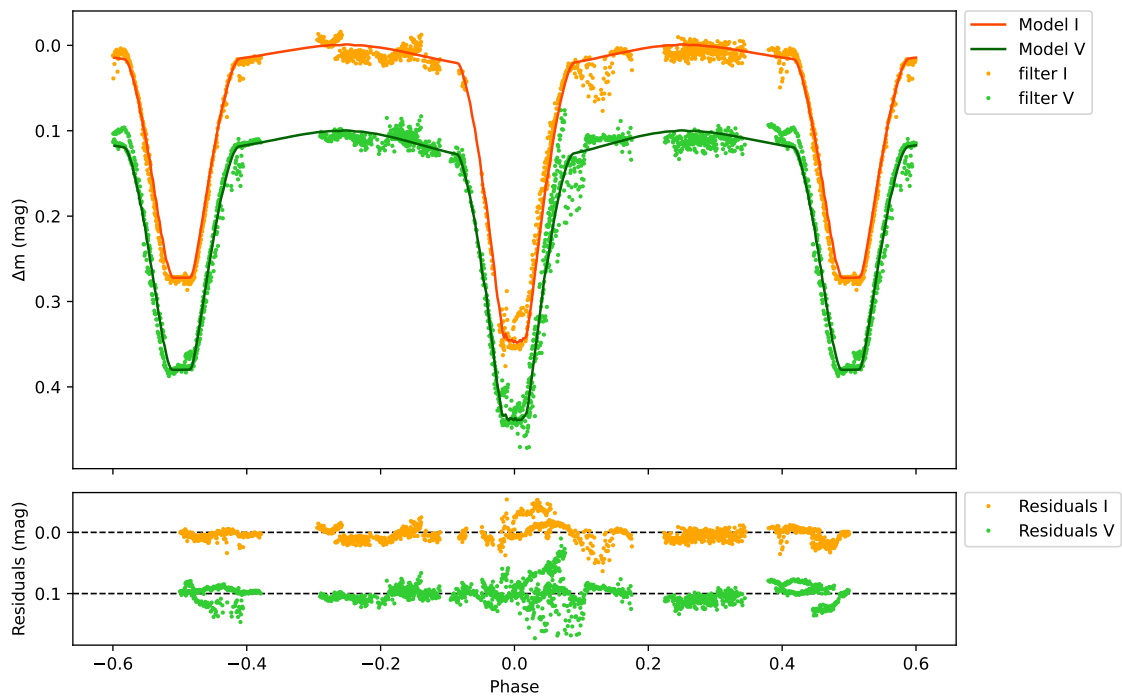


Figure 3.27: Pair A - physical model, ground-based data.

### 3.5.2 Pair B

Comparing the values in the Table 3.6, the sizes of both the components are comparable and are quite high, which corresponds with the duration of the eclipses. The temperature of secondary components is greater for TESS datasets than for our measurements.

As the temperature is the same for both the  $V$  and  $I$  filter, the discrepancy in the values of temperature between ground-based and TESS data will most likely be caused by the high noise in our data. As well as in the case of physical models of pair A (chapter 3.5.1), the mass ratio of TESS 2 datasets differs from other datasets. As it was suggested before, from the position of the secondary minima in the phase curve and the vertical shift of positions of the primary and secondary minima in the O-C diagram, the calculated value of orbital eccentricity is non-zero and has approximately the same value in all analysed datasets.

Table 3.6: Pair B – parameters of physical model.

Parameter	TESS 0	TESS 1	TESS 2	TESS 3	filter V	filter I	error
$\frac{R_1}{a}$	2.36	2.23	2.19	2.17	2.34	2.23	0.01
$\frac{R_2}{a}$	1.90	1.96	2.09	2.14	1.91	2.18	0.01
$M_{\text{bol1}}$ [mag]	-0.574	-0.451	-0.392	-0.417	-0.566	-0.456	0.001
$M_{\text{bol2}}$ [mag]	0.176	0.110	-0.032	-0.084	0.543	0.255	0.001
$T_{\text{ef1}}$ [K]	12 800	12 800	12 800	12 800	12 800	12 800	10
$T_{\text{ef2}}$ [K]	12 000	12 000	12 000	12 000	11 000	11 000	10
$i$ [°]	79.32	79.25	78.96	79.02	80.00	78.00	0.01
$q$	0.70	0.69	0.78	0.79	0.63	0.67	0.01
$e$	0.04	0.04	0.04	0.03	0.04	0.03	0.01

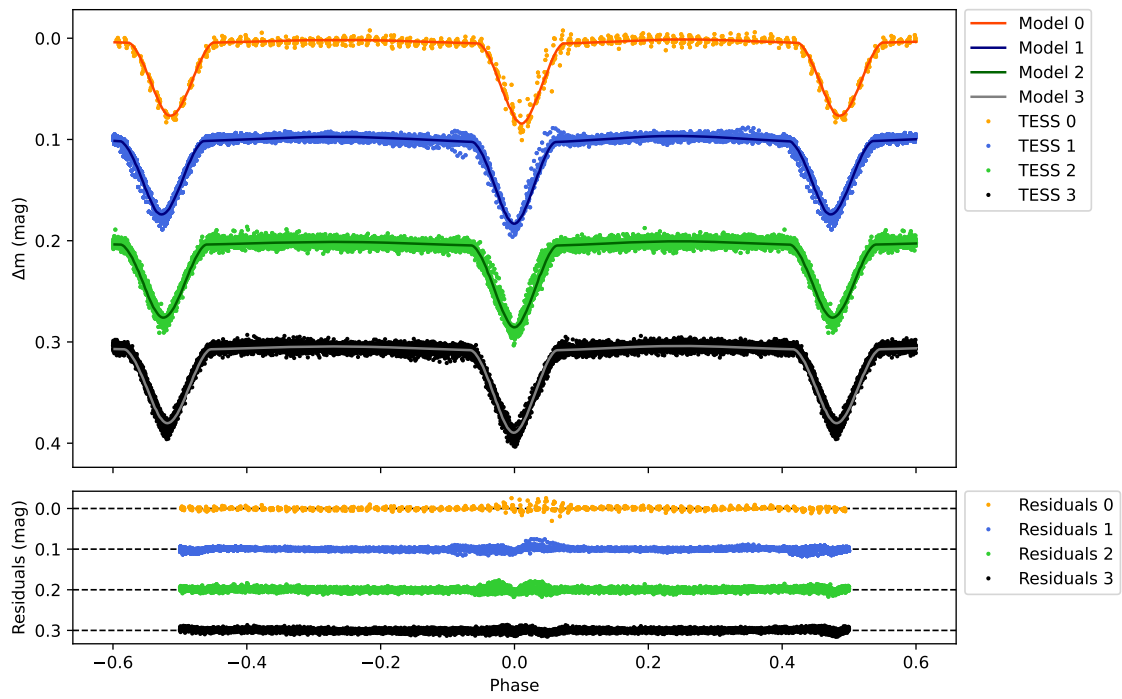


Figure 3.28: Pair B - physical model, TESS data.

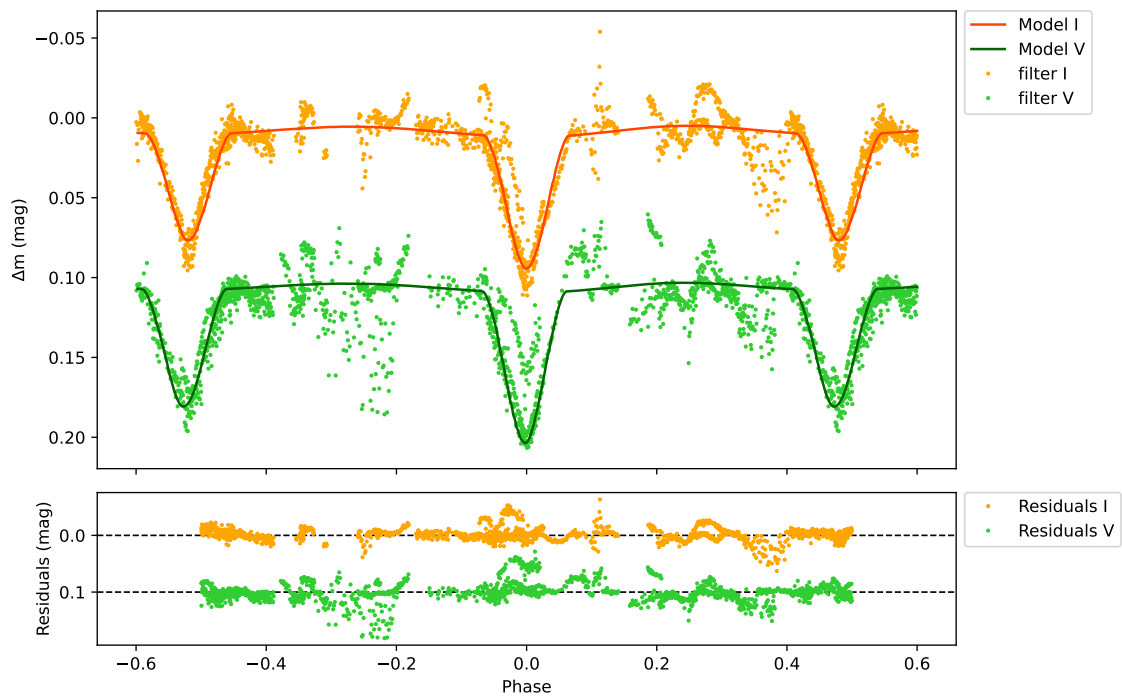


Figure 3.29: Pair B - physical model, ground-based data.

## 3.6 Summary

Both TESS and ground-based observations were analysed. Periodic changes in the brightness of system S2 Pup have the same course in both TESS and ground-based data. Moreover, the contribution of individual pairs is independent of the method of disentanglement used. Based on the photometric and spectroscopic analysis of S2 Pup, the periodic changes in residuals are most probably caused by the simultaneous eclipse in both pairs.

The physical fits for both the pairs were calculated independently for all datasets using PHOEBE software and have close, if not the same, values of parameters in all analysed datasets. The moments of minima were determined via SILICUPS software, and from them, O-C diagrams of individual pairs were obtained. In the O-C diagram of pair A, the LiTE effect was modeled. In the case of pair B, the apsidal motion was modeled, and no significant changes indicating the LiTE effect were identified. For both the pairs, the values of ephemerides were corrected (see Table 3.7).

In the spectroscopic measurements, splitting into four lines was not observed due to a poor spectral resolution. On the other hand, a shift in the position of spectral lines (hydrogen lines) is clearly seen when we analyse the spectra where one pair is in the minimum.

In conclusion, the spectroscopic measurements indicate that the system S2 Pup is indeed a doubly eclipsing stellar system, and photometric measurements do not exclude this arrangement but are not proving it. To prove the gravitational bond between both pairs, we need more long-term photometric observations. At least long enough to embrace the whole phase of the apsidal motion presented in pair B, to be sure that the apsidal motion was fitted correctly.

Table 3.7: Specification of ephemerides of pairs A and B.

<b>Parameter</b>	<b>Pair A - original</b>	<b>Pair A - new</b>
$M_0$ [HJD]	2459245.65345	$2459245.65345 \pm 0.00001$
$P$ [d]	2.068435	$2.068435 \pm 0.000001$
<b>Parameter</b>	<b>Pair B - original</b>	<b>Pair B - new</b>
$M_0$ [HJD]	2458508.99491	$2458508.97300 \pm 0.00002$
$P$ [d]	1.728512	$1.728520 \pm 0.000001$

# Chapter 4

## S1 Pup

### 4.1 Basic information

The basic characteristics of star S1 Pup and used comparison star are listed in the Table 4.1. The most suitable comparison star was chosen so that the  $B - V$  value was the closest. In the TESS chart, some other stars fall into the pixels containing the S1 Pup system. On the other hand, in ground-based observations, we can easily distinguish the S1Pup in the chart (see Figure 4.1) from other stars in the closest vicinity. The periodic changes in brightness were detected in both TESS and ground-based data so that we can rule out the blend.

The ground-based observations were measured by Martin Mašek (MM), Reinhold Fr. Auer (RFA), and Miloslav Zejda. (MZ). The list of observations is in Table 4.2. The TESS data were captured in the years 2019, 2023, and 2025. Besides the photometric data, the spectroscopic data were measured and processed (calibrated and normalized) by Jan Janík. Jan Janík also modeled the spectra, distinguished the contribution of individual components, and calculated the radial velocities. The spectra were measured with SpUpNIC (Spectrograph Upgrade-Newly Improved Cassegrain) at SAAO (South African Astronomical Observatory). The additional spectra with better spectral resolution were measured with PLATOSpec at La Silla.

Table 4.1: Basic information about S1 Pup star.

	Variable star	Comparison star
Name	V0674 Pup	TYC 7106-1554-1
RA	07 <sup>h</sup> 45 <sup>m</sup> 36.93 <sup>s</sup>	07 <sup>h</sup> 46 <sup>m</sup> 04.78 <sup>s</sup>
DEC	-31° 09' 32.0''	-31° 14' 41.06''
T [K]	6820	6070
$B - V$ [mag]	0.58	0.51
$M_{0A}$ in HJD [days]	2458497.5700	
$P_A$ [days]	0.6029032	
$M_{0B}$ in HJD [days]	2458510.9000	
$P_B$ [days]	6.5245459	

Table 4.2: List of photometric observations of star S1 Pup.

<b>date</b>	<b>observer</b>	<b>filter</b>	<b>device</b>	<b>location</b>
14. 01. 2023	MM	R	ODK 300/2040 + MII G4-16000	Los Leones
16. 01. 2023	MM	R	ODK 300/2040 + MII G4-16000	Los Leones
17. 01. 2023	MM	R	ODK 300/2040 + MII G4-16000	Los Leones
22. 01. 2023	MM	R	ODK 300/2040 + MII G4-16000	Los Leones
23. 01. 2023	MM	R	ODK 300/2040 + MII G4-16000	Los Leones
24. 01. 2023	MM	R	ODK 300/2040 + MII G4-16000	Los Leones
28. 01. 2023	MM	R	ODK 300/2040 + MII G4-16000	Los Leones
29. 01. 2023	MM	R	ODK 300/2040 + MII G4-16000	Los Leones
30. 01. 2023	MM	R	ODK 300/2040 + MII G4-16000	Los Leones
19. 02. 2023	MM	R	ODK 300/2040 + MII G4-16000	Los Leones
21. 02. 2023	MM	R	ODK 300/2040 + MII G4-16000	Los Leones
25. 02. 2023	MM	R	ODK 300/2040 + MII G4-16000	Los Leones
26. 02. 2023	MM	R	ODK 300/2040 + MII G4-16000	Los Leones
27. 02. 2023	MM	R	ODK 300/2040 + MII G4-16000	Los Leones
25. 10. 2024	RFA	C	SC 350/2236 + MI C3-26000	Boyden
05. 11. 2024	RFA	C	SC 350/2236 + MI C3-26000	Boyden
06. 11. 2024	RFA	C	SC 350/2236 + MI C3-26000	Boyden
23. 11. 2024	MZ	C	RL 350/2250 + C3-26000Pro	Boyden
30. 11. 2024	MZ	C	RL 350/2250 + C3-26000Pro	Boyden
12. 12. 2024	MZ	C	RL 350/2250 + C3-26000Pro	Boyden
02. 12. 2024	MZ	C	RL 350/2250 + C3-26000Pro	Boyden
05. 12. 2024	MZ	C	RL 350/2250 + C3-26000Pro	Boyden
27. 12. 2024	MZ	C	RL 350/2250 + C3-26000Pro	Boyden
28. 12. 2024	MZ	C	RL 350/2250 + C3-26000Pro	Boyden
06. 02. 2025	MM	R	ODK 300/2040 + MII G4-16000	Los Leones
07. 02. 2025	MM	R	ODK 300/2040 + MII G4-16000	Los Leones
08. 02. 2025	MM	R	ODK 300/2040 + MII G4-16000	Los Leones
18. 02. 2025	MM	R	ODK 300/2040 + MII G4-16000	Los Leones

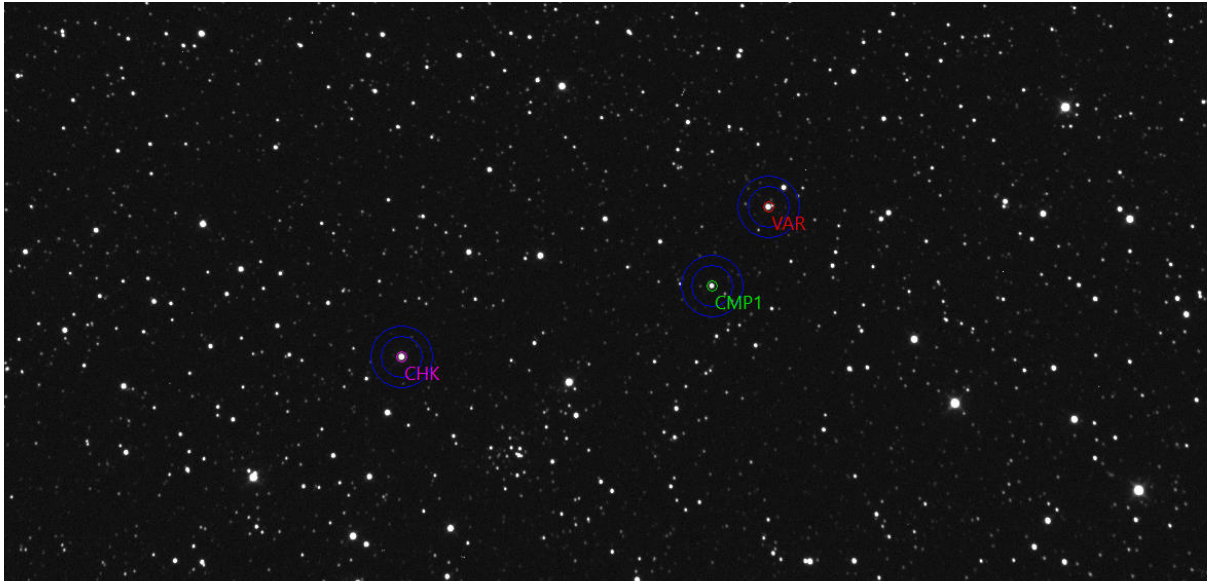


Figure 4.1: Chart of S1 Pup - Los Leones.

## 4.2 Disentangled lightcurves

### 4.2.1 Pair A

If we look at the phase curves of pair A obtained by the iteration method (see Figure 3.7) and pair A obtained by the Fourier method (see Figure 3.8), we can see some minor differences. The exposition times of frames in TESS datasets 0, 1, 3, and 4 are 1426 s, 1426 s, 158 s, and 158 s correspondingly. This means that the first two datasets were taken with a much smaller cadence, which results in less precise phase curves. In the case of the Fourier method, disentanglement more bump-like structures that are not based on real features.

Moreover, the light curves obtained by the iteration method contain the O’Connell effect, whereas the Fourier method assumes the symmetry in eclipses, so no O’Connell effect is observed. The O’Connell effect appears in the light curve of eclipsing binaries where the neighboring maxima do not have the same level, and this periodically repeats. For physical modeling, the datasets obtained by the iteration method were used.

The primary minima are deeper than the secondary, which suggests that the primary component has a higher temperature than the secondary one. If we look closer at the course of a phase curve in secondary minima, there is the phase of constant brightness, which suggests that one component is significantly larger than the other. In the primary minima, there is some asymmetry that may be caused by the presence of stellar spots on the primary component. This asymmetry only supports the presence of the O’Connell effect because the stellar spots are one of the possible reasons for the O’Connell effect.

The constant phase of brightness in secondary minima also indicates the relatively high value of inclination ( $80^\circ$ - $90^\circ$ ). The initial value of the mass ratio for physical fitting was 0.48. Unfortunately, we have no information from spectra about the number and position of stellar spots present on the primary or secondary component. That is why the physical model in PHOEBE can not be made precisely. To obtain at least some estimate of the parameters of physical fit, the phase curves of pair B will be fitted with

the assumption that there are no stellar spots. This means that the physical fit will not correspond to the phase curve well in all of the regions of the phase curve. However, it will be fitted in a way that corresponds well to the phase with the maximum brightness.

From the course of a phase curve of pair A, we can say that it is an eclipsing binary of type W UMa. These systems often (but not always) have a common envelope, so primary and secondary components share the same temperature. In the early stages of contact, the temperatures can differ a bit.

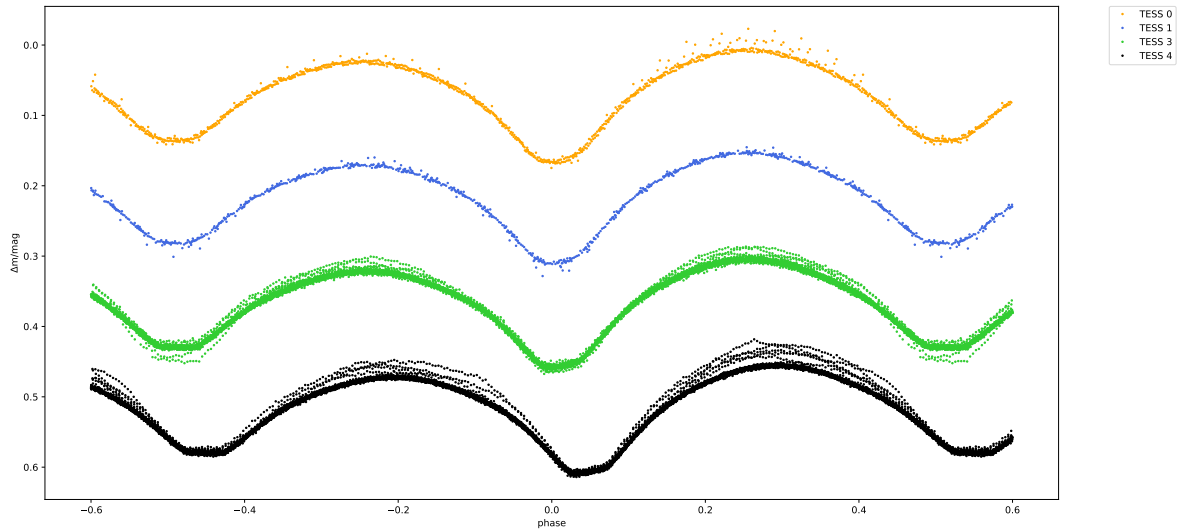


Figure 4.2: Pair A - TESS data, iteration method.

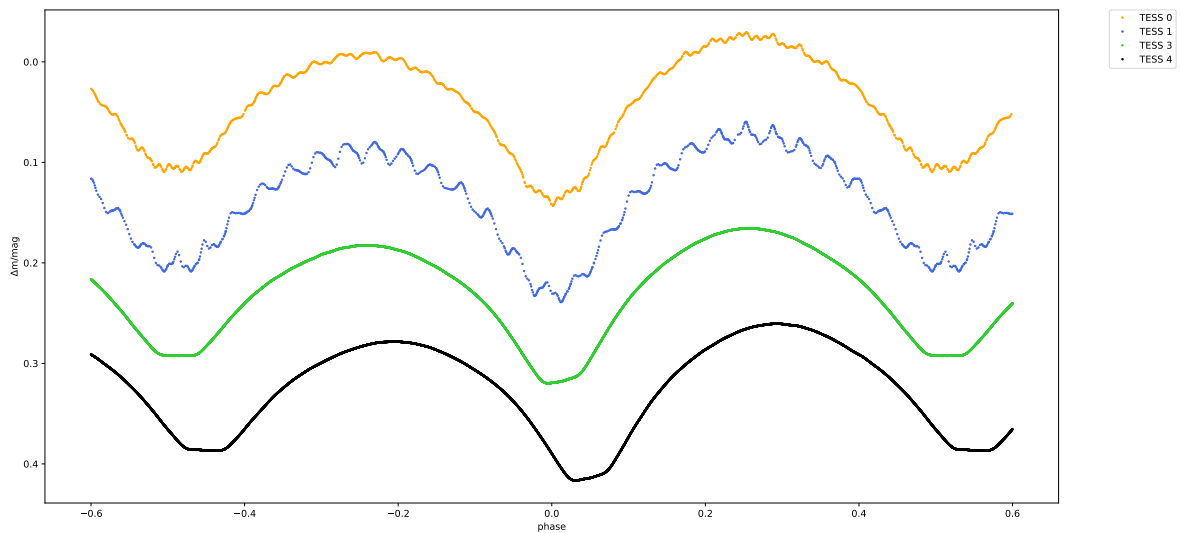


Figure 4.3: Pair A - TESS data, Fourier method.

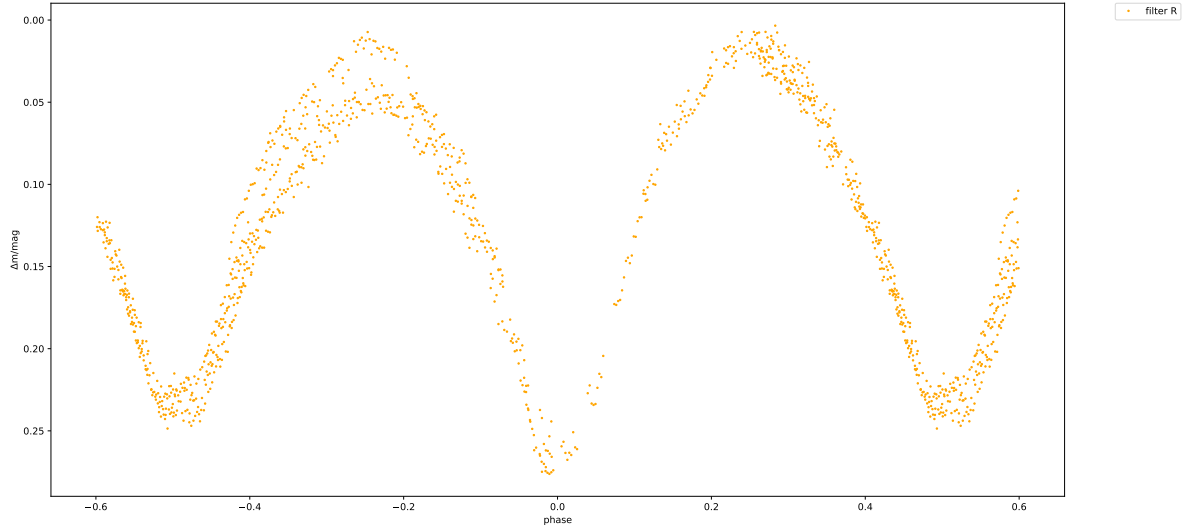


Figure 4.4: Pair A - ground-based data.

## 4.2.2 Pair B

From the phase curves of pair B (see Figures 4.5 and 4.7), we can say that pair B is an eclipsing binary of type Algol I type (primary and secondary minima have almost the same depth, which indicates the same temperature). As there is no phase of constant brightness in any minima and the duration of both primary and secondary minima are very similar, the inclination of this system will be smaller than  $90^\circ$ .

The secondary minima occur at a phase that is significantly smaller than 0.5, which suggests that the orbital trajectory will be an ellipse. As well as in the case of pair A (4.2.1) for physical fitting and any other further analysis, the datasets disentangled by iteration method were used.

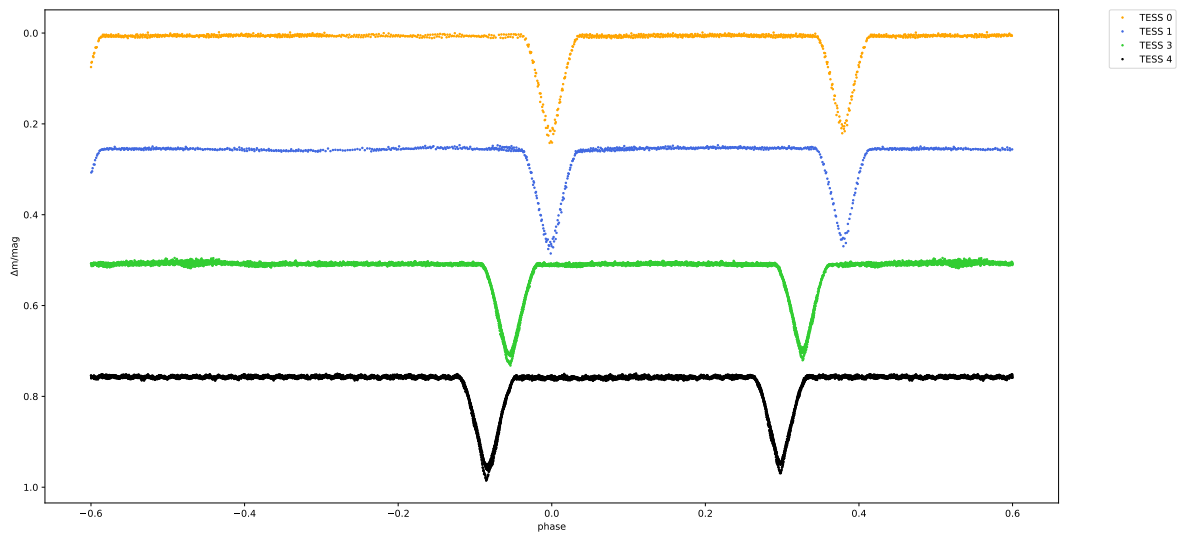


Figure 4.5: Pair B - TESS data, iteration method.

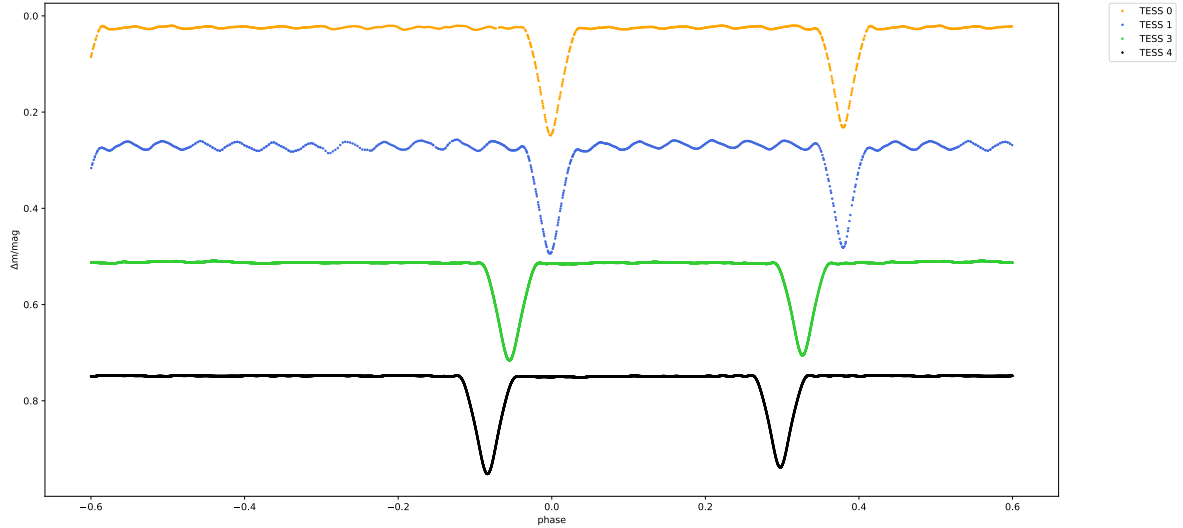


Figure 4.6: Pair B - TESS data, Fourier method.

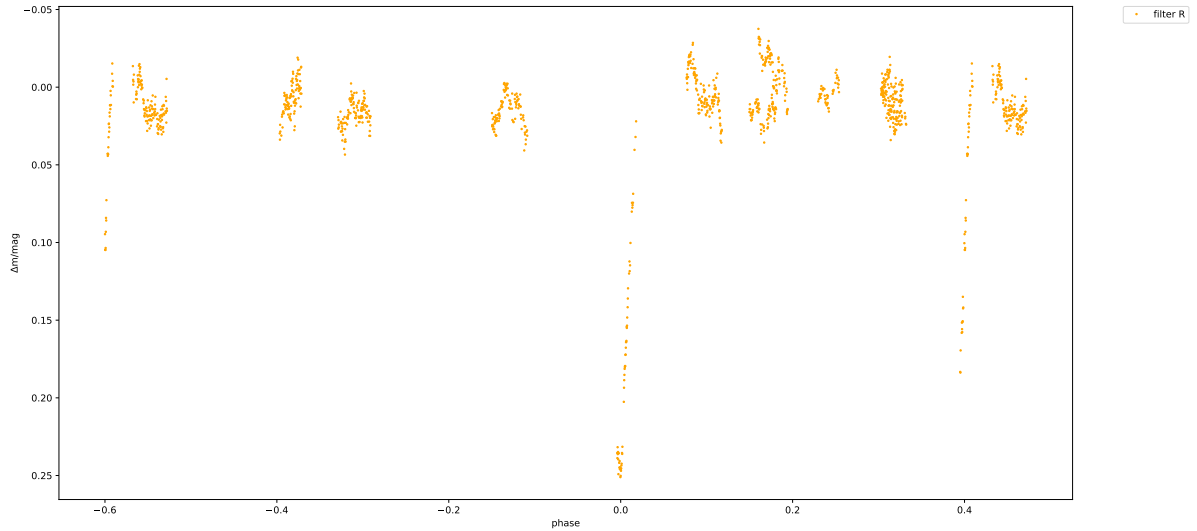


Figure 4.7: Pair B - ground-based data.

## 4.3 O-C diagrams

In the O-C diagrams, the full points represent primary minima, and the empty points represent secondary minima.

### 4.3.1 Pair A

The O-C diagram of pair A can be seen in the Figure 4.8. The points in the O-C diagram are positioned around a parabola open upwards, suggesting that the period of pair A is prolonging. First, the quadratic fit and then the linear fit was done to specify the ephemerides. O-C diagram with new ephemerides:  $P_A = (0.602915 \pm 0.000002)$  d and  $M_{0A} = (2458497.57501 \pm 0.00004)$  HJD, can be seen in Figure 4.9 together with the LiTE3 fit. The value of the parameters of the LiTE model is listed in Table 4.3.

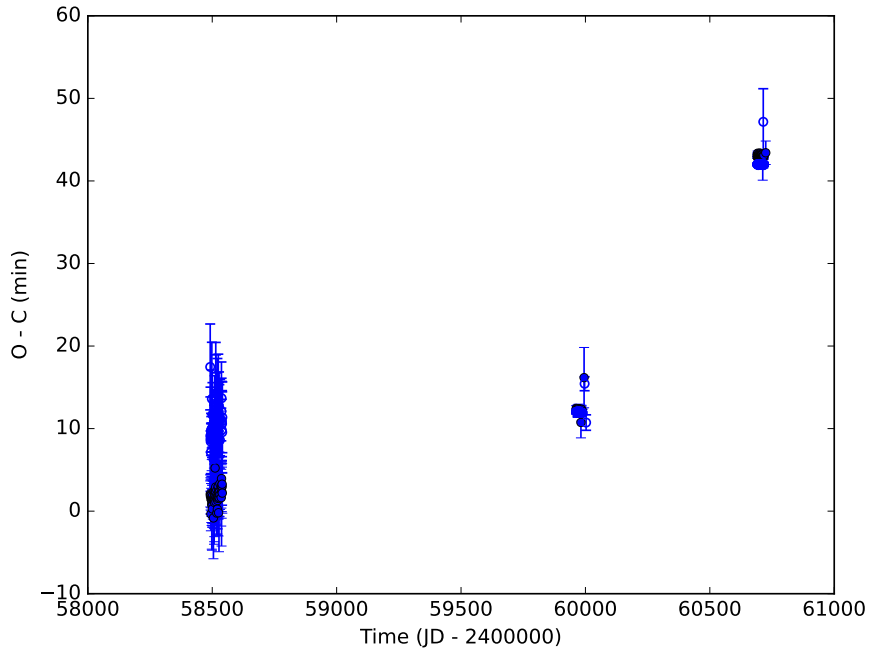


Figure 4.8: O-C diagram of pair A.

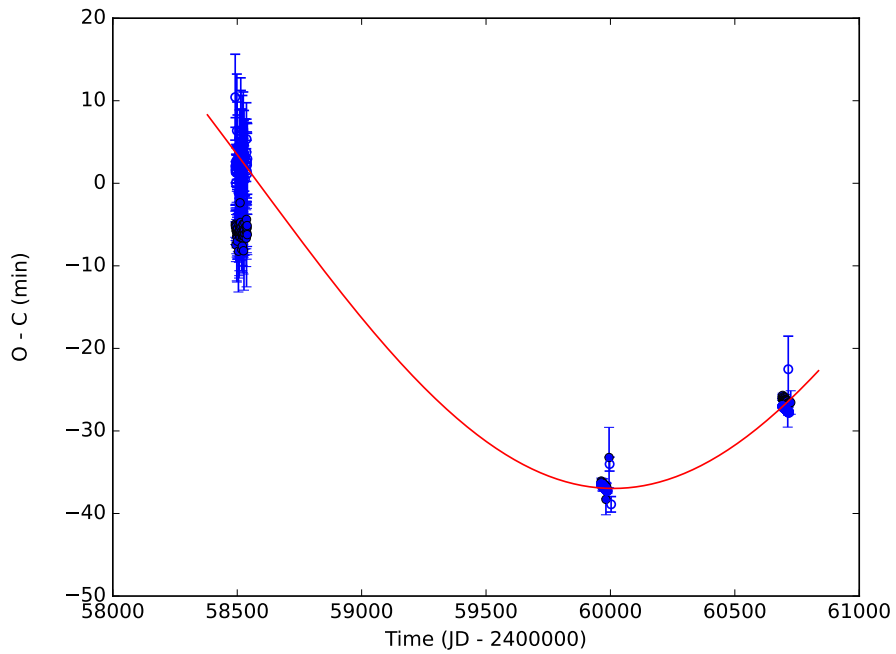


Figure 4.9: O-C diagram of pair A - corrected ephemerides, model.

Table 4.3: Orbital parameters of pair A and B of star S1 Pup.

Parameter	Pair A	Pair B	Error
$asin(i_3)$ [au]	4.44	2.17	0.01
$e_3$	0.00	0.00	0.01
$\omega$ [rad]	1.89	2.33	0.01
$t_{03}$ [HJD]	2457450	3246980	10
$P_3$ [d]	5700	3700	10

### 4.3.2 Pair B

The O-C diagram with the initial values of ephemerides (see Table 4.1) can be seen in Figure 4.10. The values are around the line with a negative slope, so the real period of the system is shorter than the period used to plot the O-C diagram.

In addition, the primary and secondary minima are vertically shifted. This shift is caused by the non-zero eccentricity of the orbital trajectory. This argument is also supported by the phase curves of pair B (Figures 4.5 and 4.7), where secondary minima occur at phase smaller than 0.5.

Before making the linear fit, we first need to align the primary and secondary minima. After that, by making the linear fit, we obtained the more precise values of ephemerides:  $M_{0A} = (2458511.44001 \pm 0.00004)$  HJD and  $P_A = (6.522901 \pm 0.000005)$  d. The O-C diagram with specified ephemerides and model can be seen in Figure 4.11.

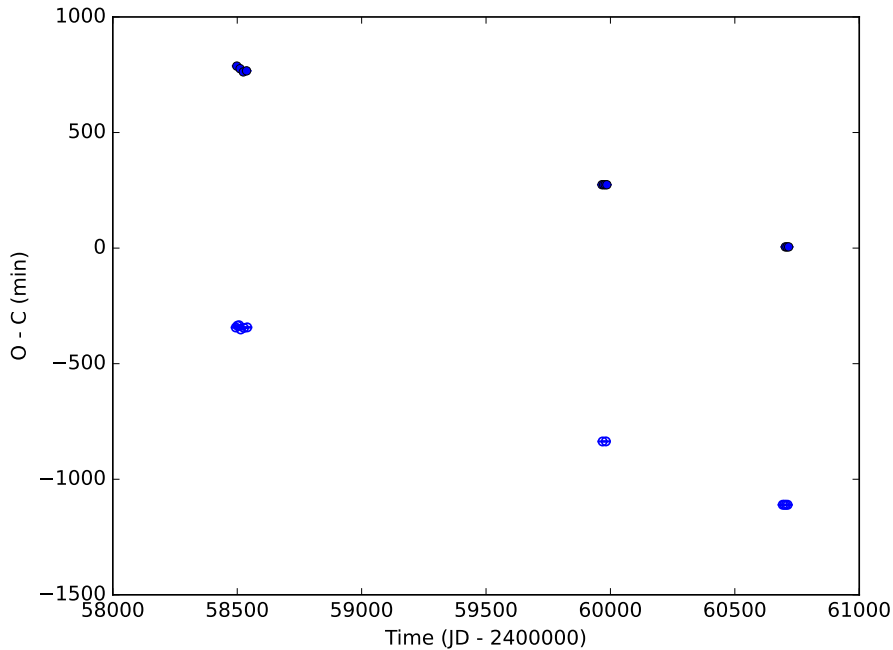


Figure 4.10: O-C diagram of pair B.

As both the O-C diagrams of pair A and B (Figures 4.9 and 4.11) have approximately the same amplitude in the O-C diagram, the masses of pair A and pair B are comparable. There is no strongly dominant pair in the system, and therefore, the value of the third light used in the physical modeling in PHOEBE should be around 0.5 for both pairs. The values of parameters of the LiTE model are listed in Table 4.3.

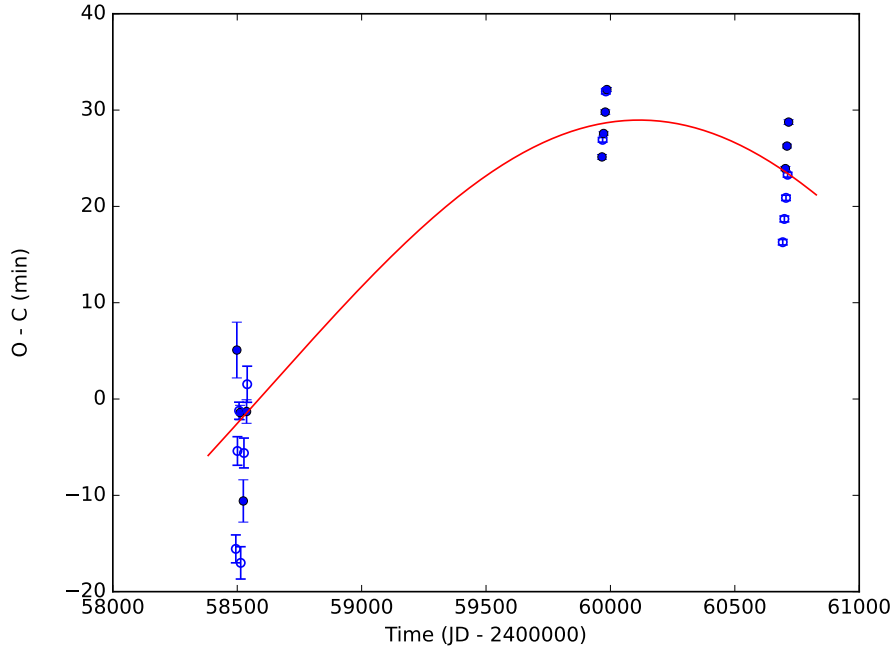


Figure 4.11: O-C diagram of pair B - corrected ephemerides, model.

## 4.4 Spectra

There were 22 spectra analysed. Unfortunately, in any of these spectra, splitting into four spectral lines is not observed. This can be caused by the limited spectral resolution together with the fact that components in pair A are most probably very close to each other (from the shape of the light curve in Figures 4.2 and 4.3). Although the splitting into 4 lines is not observed, we can tell a lot from analysing the spectra. In Table 4.4, there are listed phases for pair A and B for every measured spectrum.

Firstly, we will take spectra where pair A is in the minima and pair B is in different phases (spectra 5, 10, 12, and 17). By plotting these spectra (see Figure 4.12), we do not see any significant movement in any lines. This could suggest either that pair B is the more dominant out of the system or that the radial velocities have approximately the same value in phases of these spectra (0.019, 0.479, 0.624, 0.084 correspondingly) or that we would need a better spectral resolution to capture the shift.

If we subtract these spectra (see Figure 4.14), the contribution of pair A will cancel out as pair A is always in the minima. What will be left out will be the contribution of pair B. Ideally, we should observe a splitting into two lines (primary and secondary components of pair B). There is a splitting into two spectral lines at around 4310 Å.

Table 4.4: Values of phase for individual spectra.

<b>Spectrum</b>	<b>M0 [HJD]</b>	<b>Pair A</b>	<b>Pair B</b>
1	2460035.37656	0.670 out of minimum	0.571 out of minimum
2	2460035.41655	0.736 out of minimum	0.577 out of minimum
3	2460036.28331	0.174 out of minimum	0.710 out of minimum
4	2460036.37761	0.330 out of minimum	0.724 out of minimum
5	2460038.30392	0.525 secondary minimum	0.019 primary minimum
6	2460039.26012	0.111 out of minimum	0.166 out of minimum
7	2460040.25695	0.765 out of minimum	0.319 out of minimum
8	2460040.32510	0.878 out of minimum	0.329 out of minimum
9	2460041.25953	0.427 out of minimum	0.472 out of minimum
10	2460041.30290	0.499 secondary minimum	0.479 out of minimum
11	2460041.37144	0.613 out of minimum	0.489 out of minimum
12	2460042.24695	0.065 primary minimum	0.624 out of minimum
13	2460043.22077	0.680 out of minimum	0.773 out of minimum
14	2460043.36149	0.914 out of minimum	0.794 out of minimum
15	2460044.25284	0.392 out of minimum	0.931 out of minimum
16	2460044.37342	0.592 out of minimum	0.949 out of minimum
17	2460045.24811	0.043 primary minimum	0.084 out of minimum
18	2460045.31393	0.152 out of minimum	0.094 out of minimum
19	2460045.36272	0.233 out of minimum	0.101 out of minimum
20	2460046.21790	0.652 out of minimum	0.232 out of minimum
21	2460046.30342	0.794 out of minimum	0.245 out of minimum
22	2460046.39335	0.943 out of minimum	0.259 out of minimum

Secondly, we will take spectra, where both pairs A and B are out of minima, but pair B is in almost the same phase (0.084, 0.094, and 0.101 correspondingly). It would be ideal if pair B was in minima, but the duration of eclipses in pair B is so short, and the period is relatively long (see Table 4.1) that it was challenging to capture. A potential shift in the position of spectral lines would be caused by pair A; however, no significant shift is observed.

If we plot the subtraction of these spectra (19-17 and 18-17), we see the splitting of spectral lines, which correspond to the primary and secondary component of pair A, specifically, hydrogen lines  $H\delta$  (4102 Å) and  $H\gamma$  (4340 Å).

Finally, additional spectra with better spectral resolution were measured. From these spectra, radial velocity curves were constructed (see Appendices, Figures 5.15 and 5.16). Moreover, the splitting into 4 lines is present and the contribution of individual pairs in the spectra was distinguished (see Appendices, Figure 5.17).

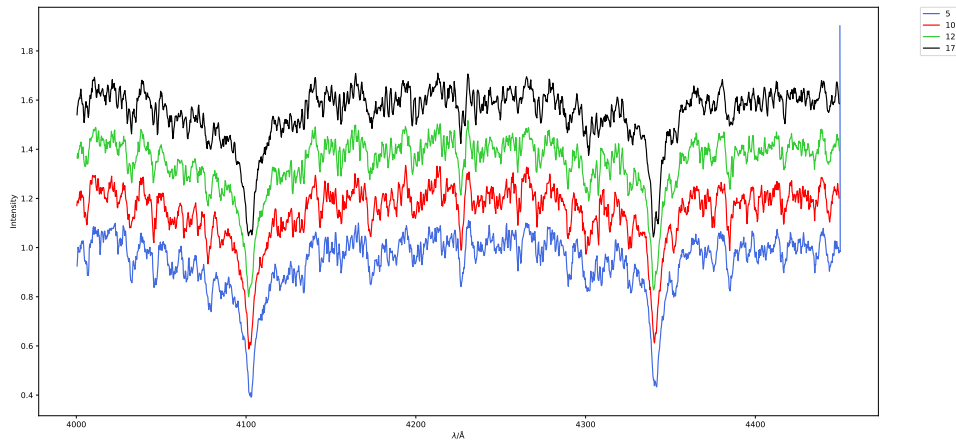


Figure 4.12: Spectra 5, 10, 12 and 17.

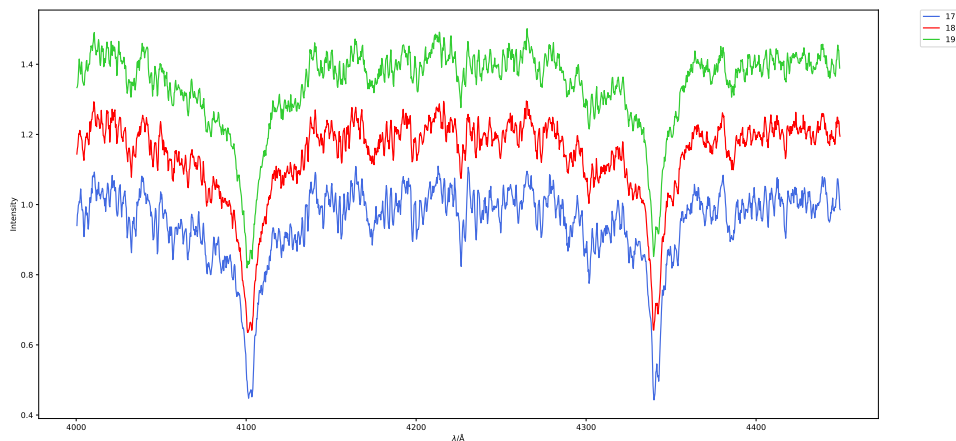


Figure 4.13: Spectra 17, 18 and 19.

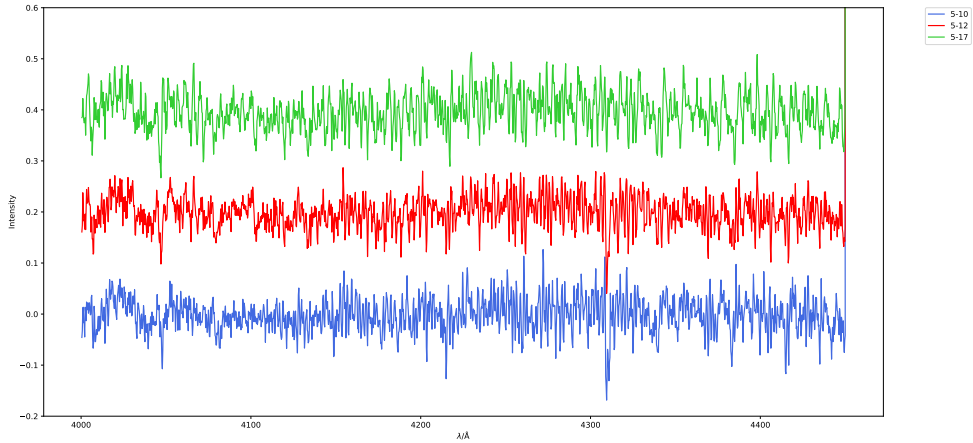


Figure 4.14: Subtraction of spectra 5, 10, 12 and 17.

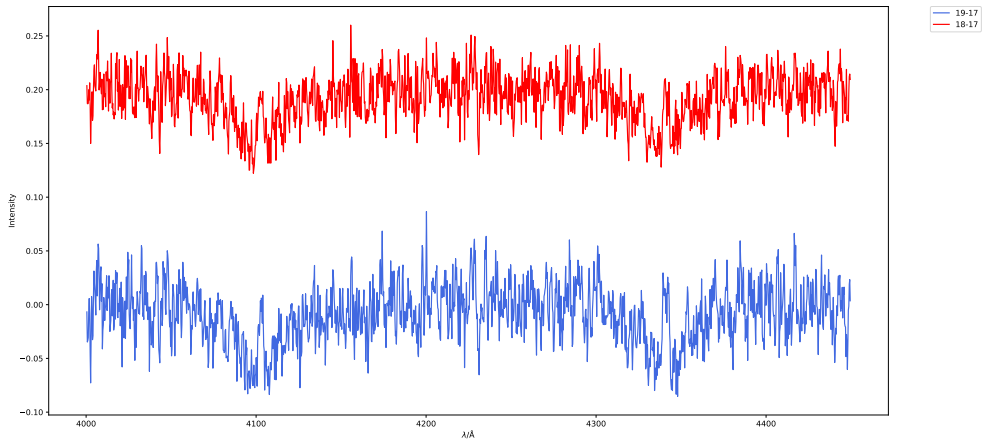


Figure 4.15: Subtraction of spectra 17, 18 and 19.

## 4.5 Physical models

### 4.5.1 Pair A

The values of parameters of physical fit in PHOEBE can be seen in Table 4.5 and the physical fit itself in Figures 4.16 and 4.17. When analysing the values of parameters obtained by the physical fit, we have to take into account that the fit is not precise as we lack information about the stellar spots. Moreover, the disentanglement by iteration method was influenced by the presence of the O'Connell effect.

The size of components is significantly different, as expected from the phase of constant brightness in secondary minima. The temperatures of components are very similar, which is typical for eclipsing binaries of type W UMa.

TESS 0 and TESS 1 have slightly different values of inclination and mass ratio than TESS 3 and TESS 4 datasets. This may be caused by the different exposure times. Therefore, phase curves from data TESS 3 and 4 are more detailed. Physical fits of TESS 3 and 4 are, therefore, more precise.

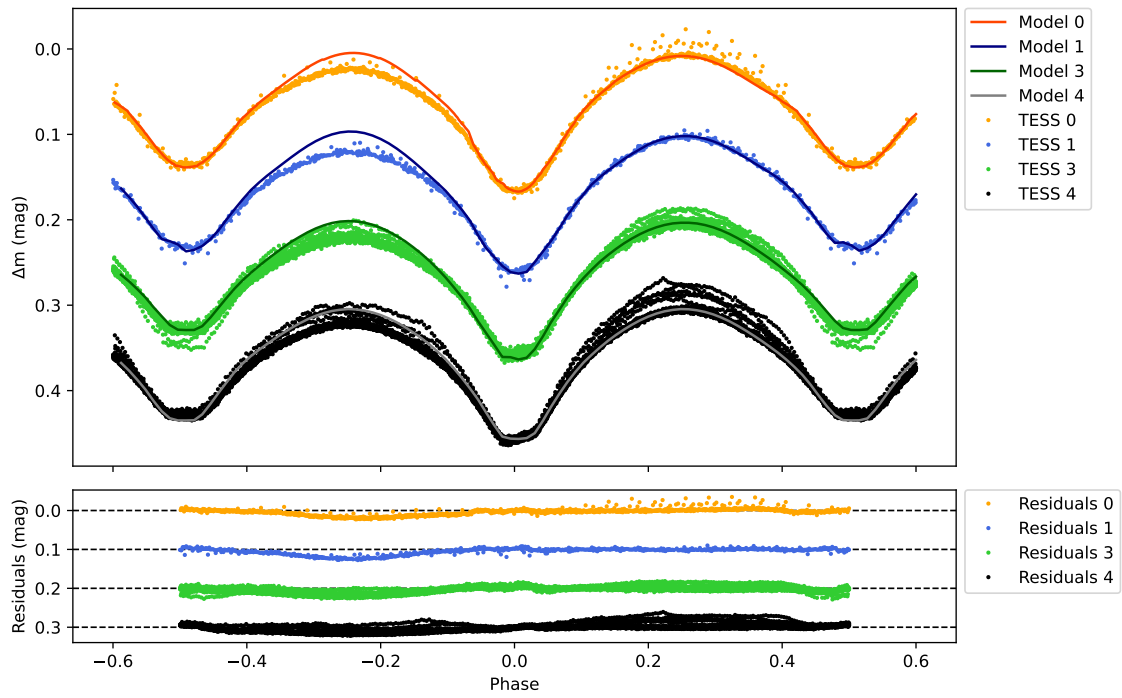


Figure 4.16: Pair A - TESS data, physical model.

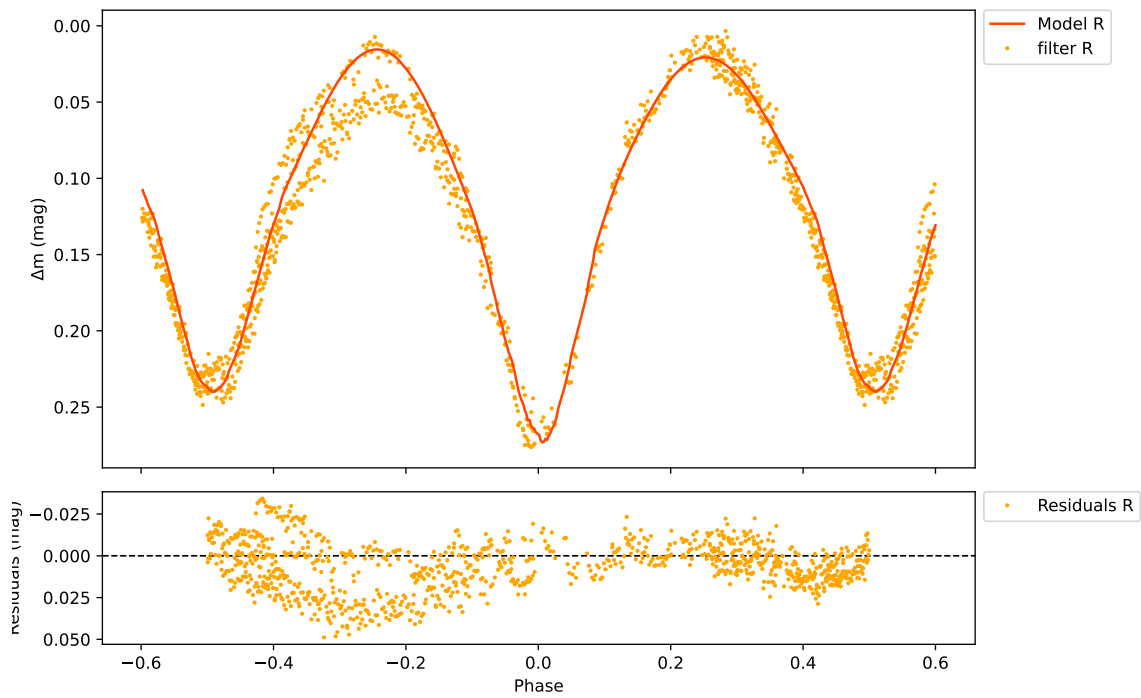


Figure 4.17: Pair A - ground-based data, physical model.

Table 4.5: Pair A – parameters of physical model.

Parameter	TESS 0	TESS 1	TESS 3	TESS 4	filter R	error
$\frac{R_1}{a}$	4.75	4.69	4.94	4.85	4.71	0.01
$\frac{R_2}{a}$	3.13	3.11	3.70	3.66	3.17	0.01
$M_{\text{bol1}}$ [mag]	0.641	0.672	0.555	0.589	0.655	0.001
$M_{\text{bol2}}$ [mag]	1.961	1.942	1.503	1.445	1.893	0.001
$T_{\text{ef1}}$ [K]	6 820	6 820	6 820	6 820	6 820	10
$T_{\text{ef2}}$ [K]	6 200	6 250	6 250	6 450	6 250	10
$i$ [°]	68.00	68.02	87.00	88.00	69.5	0.01
$q$	0.38	0.40	0.48	0.48	0.41	0.01
$e$	0.01	0.01	0.01	0.01	0.01	0.01

## 4.5.2 Pair B

The physical fit done in PHOEBE of pair B can be seen in Figure 4.18, and the values of parameters can be seen in the Table 4.6. The physical fit for ground-based data of Pair B was not done due to the insufficient coverage of the phase curve. Unlike in pair A, the sizes of primary and secondary components are almost the same, as are their temperatures. The value of inclination is high, as expected for all datasets. As well as in the case of pair A, the values of mass ratio for the first two TESS datasets are a bit different than for the remaining two.

Finally, the orbital eccentricity is non-zero, which is in unity with the vertical shift of primary and secondary minima in the O-C diagram (see Figure 4.10).

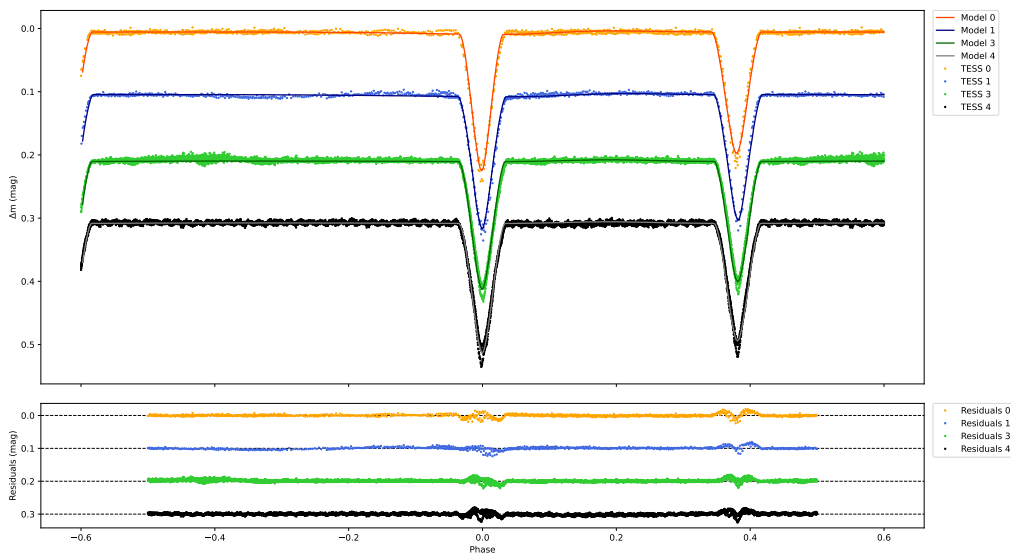


Figure 4.18: Pair B - TESS data, physical model.

Table 4.6: Pair B – parameters of physical model.

Parameter	TESS 0	TESS 1	TESS 3	TESS 4	error
$\frac{R_1}{a}$	1.21	1.18	1.18	1.18	0,01
$\frac{R_2}{a}$	1.09	1.18	1.17	1.16	0,01
$M_{\text{bol1}}$ [mag]	3.60	3.60	3.662	3.662	0,001
$M_{\text{bol2}}$ [mag]	3.87	3.69	3.720	3.720	0,001
$T_{\text{ef1}}$ [K]	6 820	6 820	6 820	6 820	10
$T_{\text{ef2}}$ [K]	6 750	6 750	6 750	6 700	10
$i$ [°]	85,90	86,56	84,80	84,80	0,01
$q$	0,68	0,75	0,73	0,73	0.01
$e$	0.20	0.19	0.19	0.19	0,01

## 4.6 Summary

For system S1 Pup, both ground-based data and data from the TESS satellite were analysed. The phase curves from iteration and Fourier method slightly differ due to the presence of the O’Connell effect. The physical fits for both pairs were calculated using PHOEBE software.

The moments of minima of both pairs have been determined via SILICUPS software, and the O-C diagrams for both pairs were plotted. From the O-C diagrams the values of ephemerides were corrected (see Table 4.7). The O-C diagrams were fitted by the LiTE model, and even though the full sine curve is not seen, the O-C diagrams clearly appear in the antiphase. While the O-C diagram of pair A is a parabola open upwards (the period is prolonging), the diagram of pair B is a downward open parabola (the period is getting shorter).

Moreover, from the spectroscopic measurements, there is clearly a shift in the position of spectral lines when comparing spectra with one pair in the minimum and the other one not. After subtracting the spectra, there is also a clear splitting into two spectral lines. Furthermore, the contribution of individual components was distinguished in the newest spectroscopic measurements with a better spectral resolution. The shapes of radial velocity curves support the doubly eclipsing quadruple model.

In conclusion, both spectroscopic and photometric measurements prove the gravitational bond between pair A and pair B. System S1 Pup is, therefore, a confirmed doubly eclipsing quadruple.

Table 4.7: Specification of ephemerides of pairs A and B.

<b>Parameter</b>	<b>Pair A - original</b>	<b>Pair A - new</b>
$M_0$ [HJD]	2458497.57000	$2458497.57501 \pm 0.00004$
$P$ [d]	0.6029032	$0.602915 \pm 0.000002$
<b>Parameter</b>	<b>Pair B - original</b>	<b>Pair B - new</b>
$M_0$ [HJD]	2458510.90000	$2458511.44000 \pm 0.00004$
$P$ [d]	6.524546	$6.522901 \pm 0.000005$

# Chapter 5

## S1 Peg

### 5.1 Basic information

The basic information about S1 Peg star is listed in the Table 5.1. The strongest criterion for the selection of optimal comparison star was again the value of  $B - V$ . In the TESS chart, another star falls into the same pixel. On the other hand, in ground-based observations, the star S1 Peg is easily distinguishible. The chart displaying the position of the variable and comparison star in the sky is shown in Figure 5.1.

The analysed TESS data were captured in 2019, 2022, and 2024. The ground-based observations for system S1 Pup were measured by František Lomoz (FL), Anna Richterková (AR), Rudolf Novák (RN), Miloslav Zejda (MZ), and Jakub Kolář (JK). The list of observations can be seen in Table 5.2.

For star S1 Peg, no spectroscopic measurements were available. S1 Peg was observed from the northern hemisphere, and it is not bright enough (12.3 mag in the visible range) for measuring spectra at available observatories (e.g., at Ondřejov). Therefore, only photometric measurements will be analysed.

As we lack the spectroscopic measurements, the only possible way in this thesis to prove whether or not there is a gravitational bond between individual pairs of star S1 Peg is the search for the LiTE effect in the O-C diagrams.

Table 5.1: Basic information about S1 Peg star.

	Variable star	Comparison star
Name	TYC 2201-991-1	UCAC4 592-128770
RA	21 <sup>h</sup> 38 <sup>m</sup> 04.77 <sup>s</sup>	21 <sup>h</sup> 38 <sup>m</sup> 12.32 <sup>s</sup>
DEC	28° 10' 07.8''	28° 13' 30.08''
T [K]	6200	4800
$B - V$ [mag]	1.38	1.31
$M_{0A}$ in HJD [days]	2459207.13900	
$P_A$ [days]	0.747245	
$M_{0B}$ in HJD [days]	2458726.71000	
$P_B$ [days]	2.083732	

Table 5.2: List of photometric observations of star S1 Peg.

date	observer	filter	device	location
05. 09. 2021	FL	C	Newton 300/1200+ST2000XM	
19. 10. 2022	AR, RN	R	Newton 400/1715 + G2-402	Prostějov
19. 10. 2022	AR, RN	V	Newton 400/1715 + G2-402	Prostějov
19. 10. 2022	AR, RN	C	RC 250/2000 + G2-4000	Úpice
05. 10. 2022	AR, RN	C	RC 250/2000 + G2-4000	Úpice
6. 10. 2022	AR, RN	C	RC 250/2000 + G2-4000	Úpice
17. 10. 2022	AR, RN	C	RC 250/2000 + G2-4000	Úpice
20. 10. 2022	AR, RN	C	RC 250/2000 + G2-4000	Úpice
31. 10. 2022	AR, RN	C	RC 250/2000 + G2-4000	Úpice
02. 11. 2022	AR, RN	C	RC 250/2000 + G2-4000	Úpice
05. 11. 2022	AR, RN	C	RC 250/2000 + G2-4000	Úpice
13. 11. 2022	AR, RN	C	RC 250/2000 + G2-4000	Úpice
14. 11. 2022	AR, RN	C	RC 250/2000 + G2-4000	Úpice
02. 10. 2023	MZ	V	AZ800/5480 + G4-16000	Ždánice
02. 10. 2023	MZ	R	AZ800/5480 + G4-16000	Ždánice
03. 10. 2023	MZ	V	AZ800/5480 + G4-16000	Ždánice
03. 10. 2023	MZ	R	AZ800/5480 + G4-16000	Ždánice
08. 10. 2023	MZ	V	AZ800/5480 + G4-16000	Ždánice
08. 10. 2023	MZ	R	AZ800/5480 + G4-16000	Ždánice
17. 10. 2023	MZ	V	Newton 600/2780 + G4-16000	Brno
17. 10. 2023	MZ	R	Newton 600/2780 + G4-16000	Brno
05. 08. 2024	AR, RN	V	Newton 400/1715 + G2-402	Prostějov
05. 08. 2024	AR, RN	R	Newton 400/1715 + G2-402	Prostějov
12. 08. 2024	MZ	g	AZ800/5480 + C5A-150M	Ždánice
12. 08. 2024	MZ	g	AZ800/5480 + C5A-150M	Ždánice
29. 08. 2024	AR, RN	R	Newton 400/1715 + G2-402	Prostějov
05. 09. 2024	AR, RN	R	Newton 400/1715 + G2-402	Prostějov
07. 09. 2024	AR, RN	R	Newton 400/1715 + G2-402	Prostějov
21. 10. 2024	MZ	r	AZ800/5480 + G4-16000	Ždánice
25. 12. 2024	JK	g	AZ800/5480 + G4-16000	Ždánice
25. 12. 2024	JK	r	AZ800/5480 + G4-16000	Ždánice

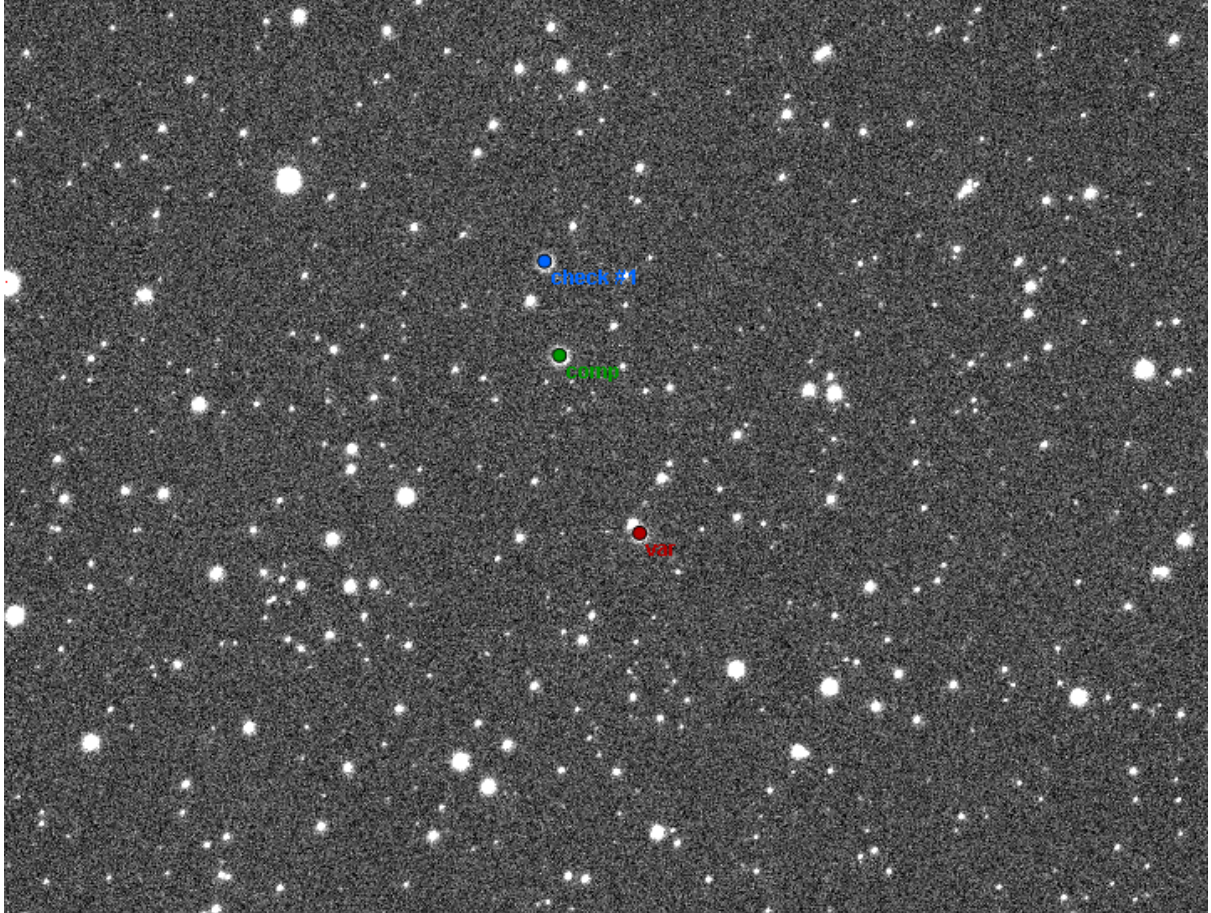


Figure 5.1: Chart of S1 Peg - Prostějov

## 5.2 Disentangled lightcurves

The contribution of individual pairs was distinguished by the iteration method (seen in Figures 5.2 and 5.5) and by the Fourier method (seen in Figures 5.3 and 5.6).

The contributions distinguished by the Fourier method are less noisy. This is caused mainly by the fact that pair A has a decrease in brightness in minima in the range of 0.1 and pair B in the order of 0.01. Therefore, when using the iteration method, the ability to fit precisely the shape of the minima for pair B is limited by the noise.

Comparing the contributions from iteration and the Fourier method, the depth and duration of the minima are the same. This suggests that the disentanglement was done correctly. For further analysis (O-C diagram and physical models), we will use the contributions obtained using the Fourier method.

### 5.2.1 Pair A

Just from the phase curve in Figures 5.2 and 5.3, we can say a lot about the pair. Pair A is the case of detached binary (type Algol). The depth of the primary minima is larger than the depth of the secondary minima yet is still comparable. Therefore, the primary component will have a higher surface temperature than the secondary component, but the temperatures will not differ much.

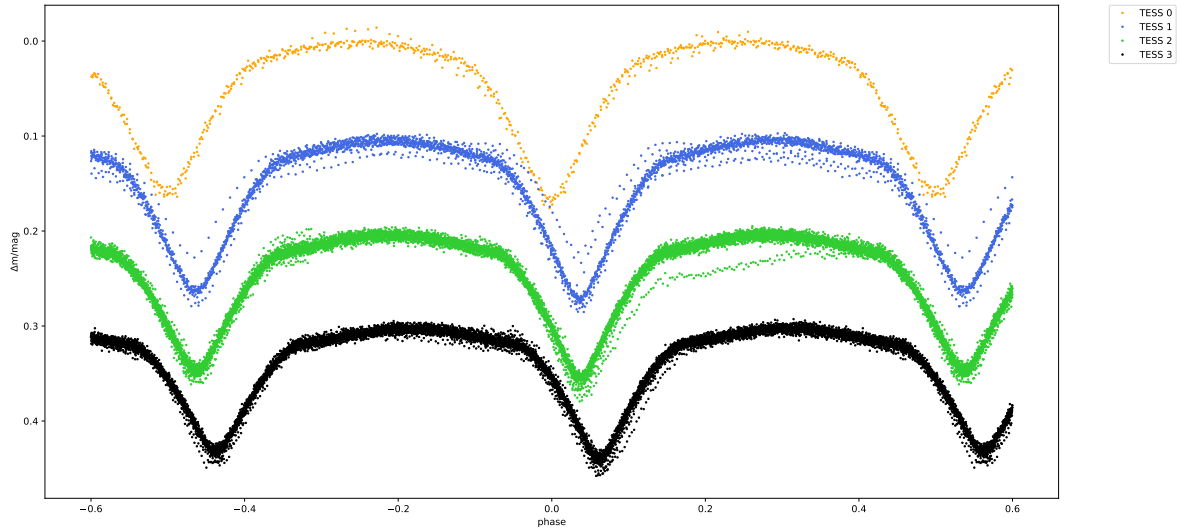


Figure 5.2: Pair A - TESS data, iteration method.

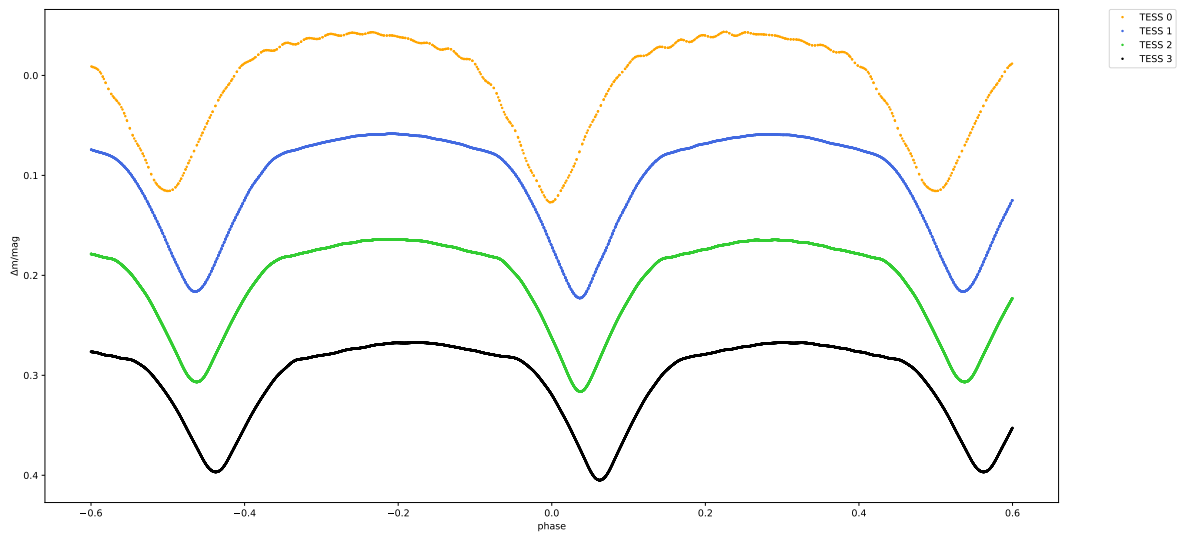


Figure 5.3: Pair A - TESS data, Fourier method.

There is no constant phase of brightness in primary nor secondary minima. Together with the fact that the duration of the eclipses is quite large, the distance of individual components is relatively small, and their sizes are comparable.

There is a slight bump between structures instead of the constant phase of brightness between the primary and secondary minima. This effect can be caused by the proximity effect. Due to gravitational interaction between components, the shape of the components changes, resulting in the different shape of the light curve.

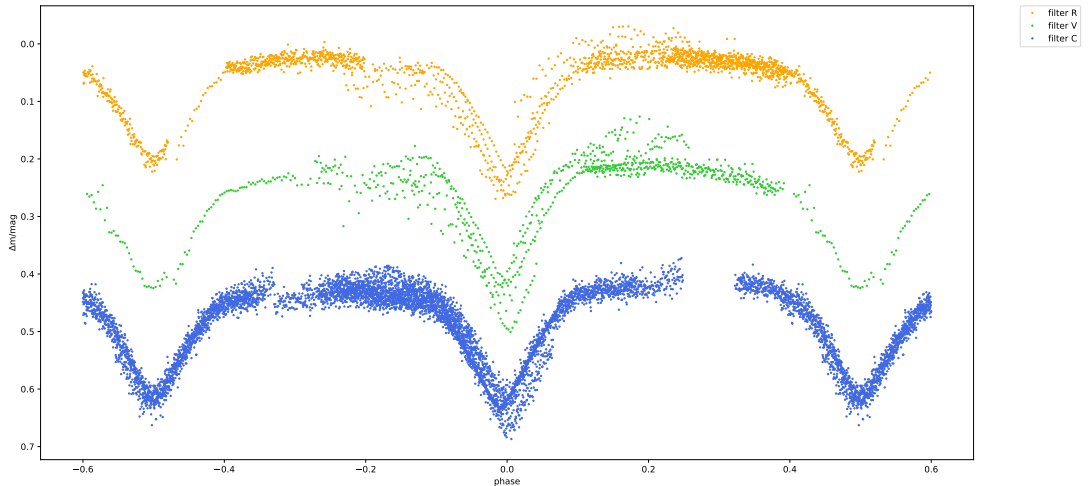


Figure 5.4: Pair A - ground-based data.

## 5.2.2 Pair B

In phase curves determined by both Fourier and iterative methods, there is an increase in brightness in both primary and secondary minima. This can be either caused by the presence of stellar spots (Oláh et al., 2025) or by the mid-eclipse brightening effect (Budaj, J., 2011). This effect is caused by a dust disc around one of the stars. The shape of the phase curve in minima suggests that the primary component is more dominant than the secondary one. The secondary component is surrounded by the dust disc. As the secondary component gets in front of the primary one (the moment of primary minima), the light from the primary component passes through the dust disc, where it is partially blocked and scattered. This scattered light is the source of the mid-eclipse brightening.

Unfortunately, we do not have any information about the number or position of potential stellar spots nor the size and orientation of potential dust discs surrounding the secondary component of pair B. Therefore, the physical fit of pair B will be done without them and will not correspond to the phase curve with high precision.

The iterative and Fourier methods of disentanglement result in the same shape, position, and duration of both primary and secondary minima. The contribution of individual pairs by the Fourier method will be used for further analysis (such as O-C diagrams and physical models) as it is less noisy.

The primary and secondary minima have different depths, so the primary component will have a higher temperature than the secondary. If there was no mid-eclipse brightening, there would be a phase of constant brightness in both primary and secondary minima, which indicates that the sizes of individual components will be significantly different. At the same time, in order to observe this, the value of inclination must be relatively high ( $80^\circ$ - $90^\circ$ ). The value of the mass ratio parameter should be small, around 0.4. The minima are separated; therefore, there is no mass transfer, and this eclipsing binary is of type Algol II.

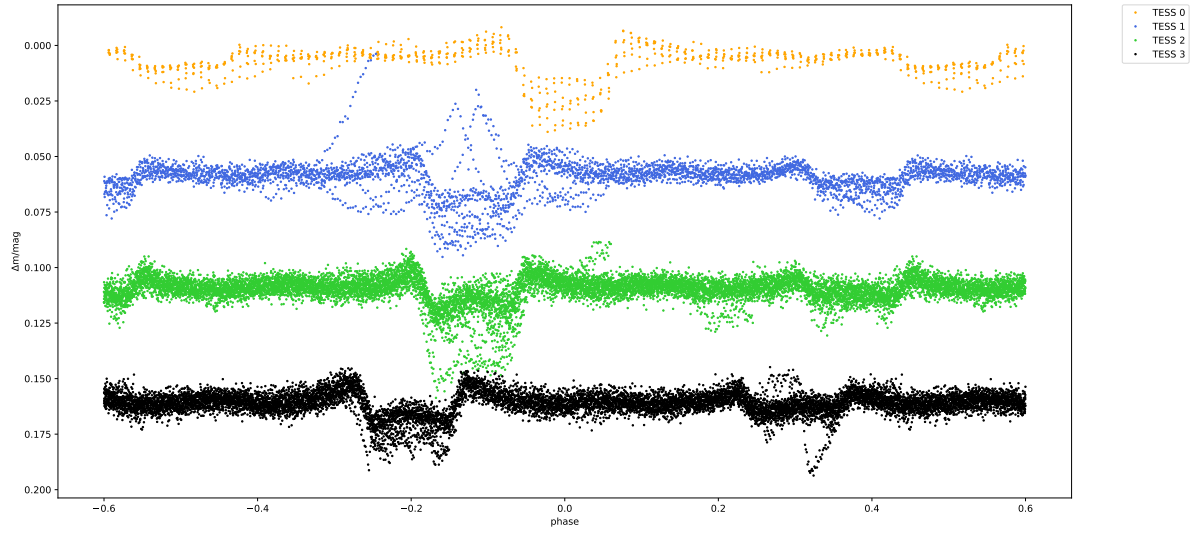


Figure 5.5: Pair B - TESS data, iteration method.

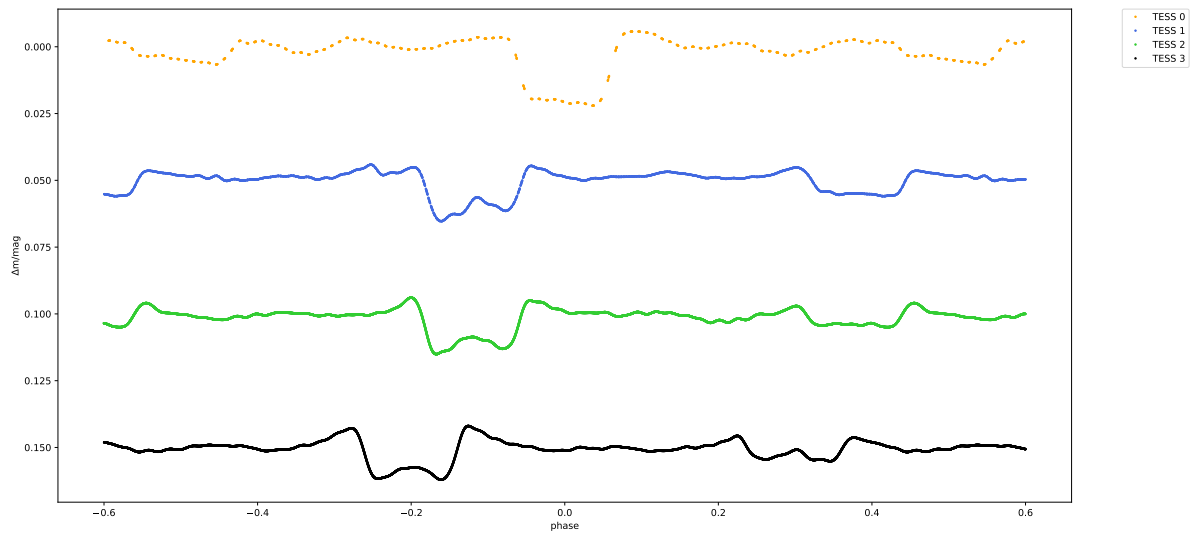


Figure 5.6: Pair B - TESS data, Fourier method.

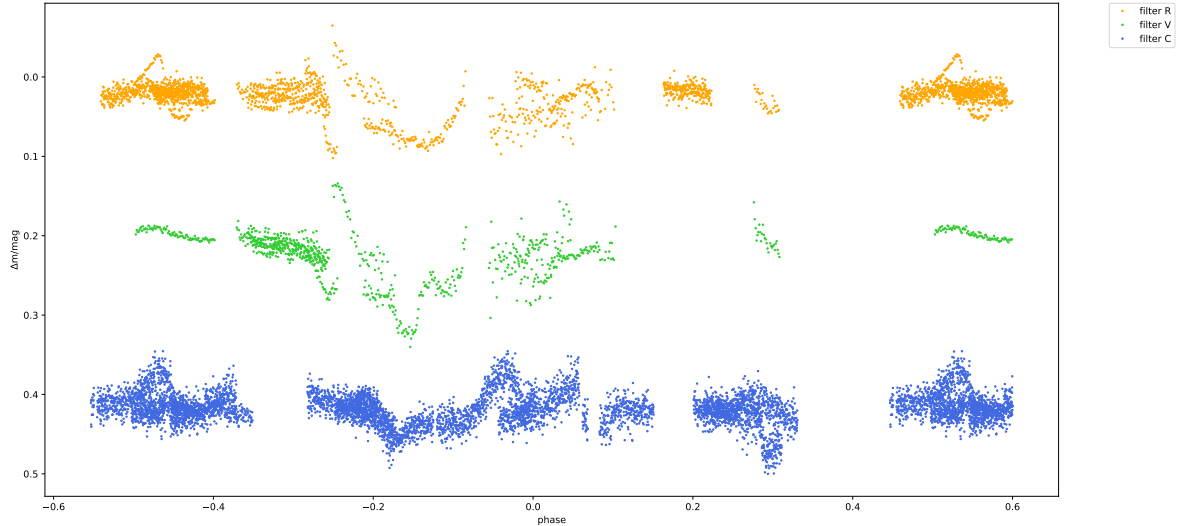


Figure 5.7: Pair B - ground-based data.

## 5.3 O-C diagrams

In the O-C diagrams, the full points represent primary minima, and the empty points represent secondary minima.

### 5.3.1 Pair A

The O-C diagram of pair A with initial values of ephemerides (see Table 5.1) can be seen in Figure 5.8. The points in the O-C diagram are along the line with a positive slope. It means that the real period of pair A is longer than the period from Table 5.1. The new values of ephemerides:  $P_A = (0.747264 \pm 0.000001)$  d and  $M_{0A} = (2459207.15103 \pm 0.00002)$  HJD, were obtained by a linear fit. The O-C diagram with corrected ephemerides and the model can be seen in Figure 5.9. The parameters of the LiTE model are in the Table 5.3.

Table 5.3: Orbital parameters of pair A and B of star S1 Peg.

Parameter	Pair A	Pair B	Error
$asin(i_3)$ [au]	0.11	0.81	0.01
$e_3$	0.00	0.00	0.01
$\omega$ [rad]	4.65	2.49	0.01
$t_{03}$ [HJD]	2459650	2457010	10
$P_3$ [d]	2940	3030	10

### 5.3.2 Pair B

If we look at the phase curves of pair B (Figures 5.5 and 5.6), we can see that the position of the minima changes in each sector. Moreover, the points in the O-C diagram with initial ephemerides (see Table 5.1) are located along the line with a negative slope. This suggests

that the real period of pair B is shorter than the period in Table 5.1. New, more precise ephemerides:  $P_B = (2.083265 \pm 0.000005)$  d and  $M_{0B} = (2458725.66000 \pm 0.000003)$  HJD were calculated using a linear fit. The O-C diagram with new ephemerides and LiTE model are plotted in Figure 5.11, and the parameters of the model are listed in the Table 5.3.

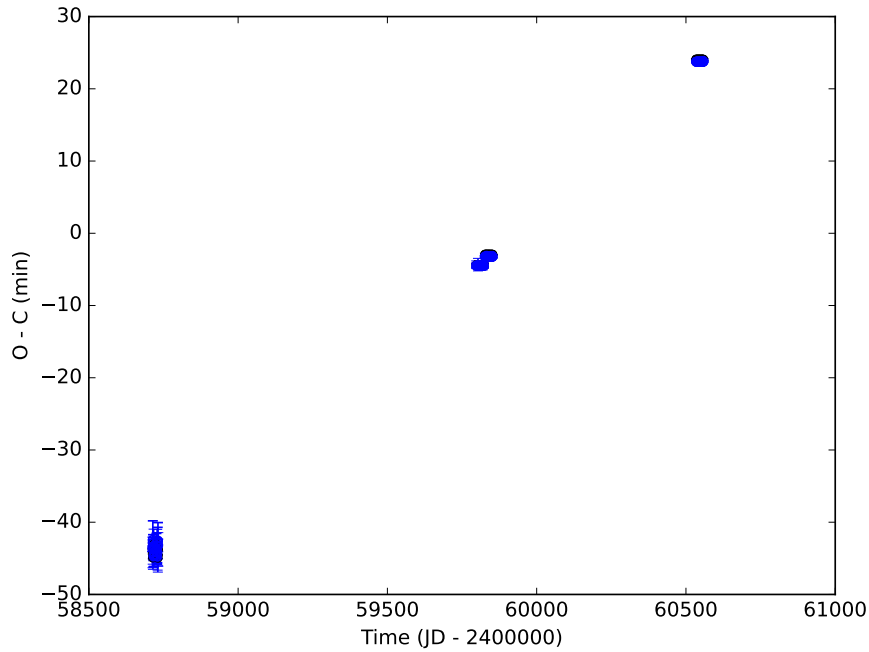


Figure 5.8: O-C diagram of pair A.

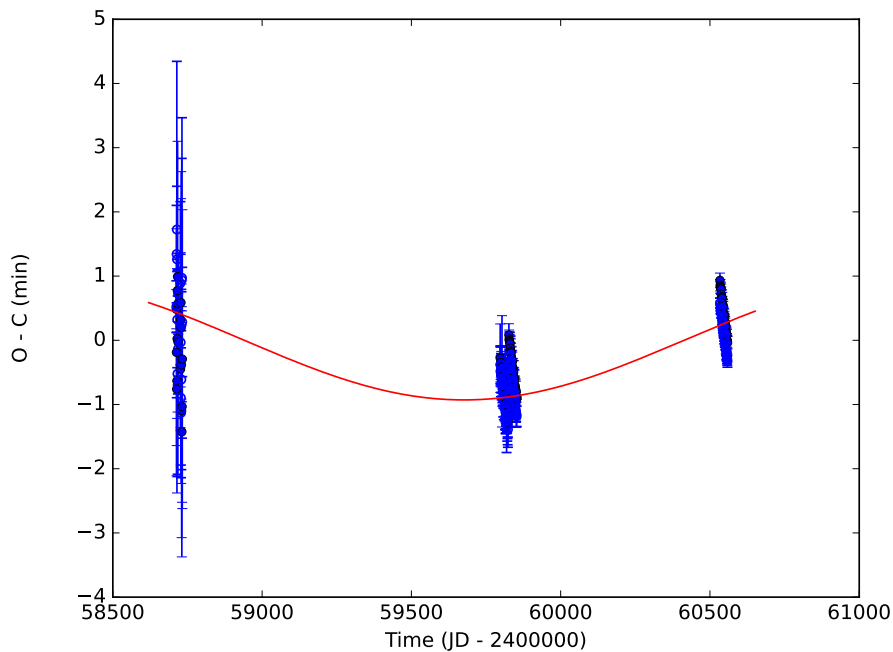


Figure 5.9: O-C diagram of pair A - corrected ephemerides, model.

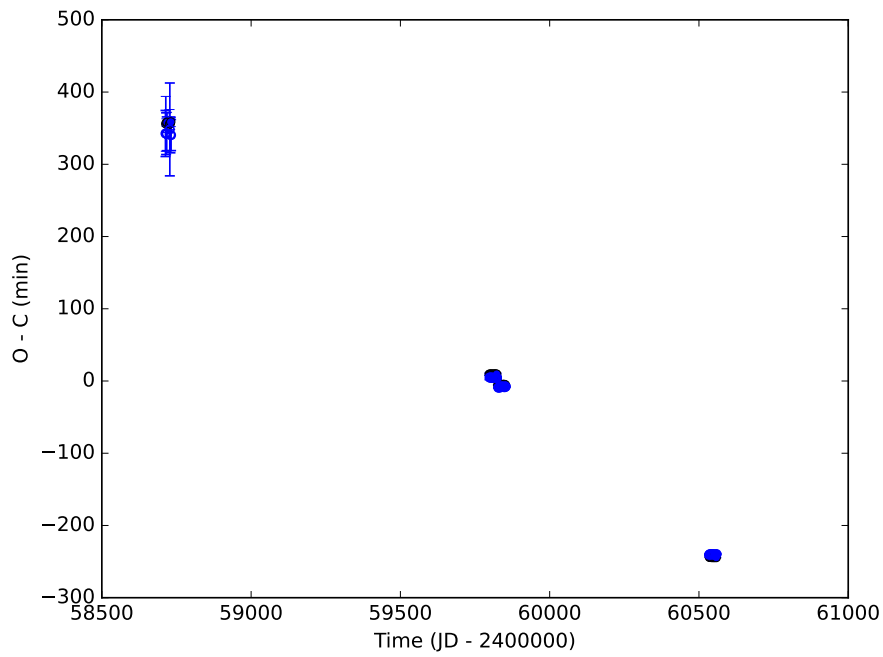


Figure 5.10: O-C diagram of pair B.

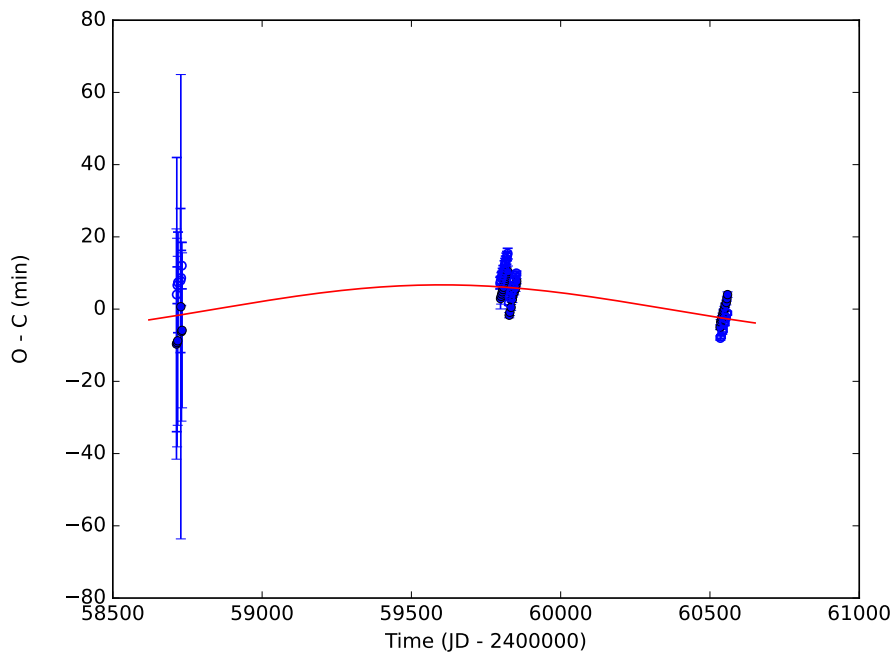


Figure 5.11: O-C diagram of pair B - corrected ephemerides, model.

## 5.4 Physical models

### 5.4.1 Pair A

The physical fit calculated by PHOEBE software can be seen in Figures 5.12 and 5.13. Comparing the values of parameters of TESS data and ground-based observations (see Table 5.4), we see that they are in good agreement. The sizes of the components are comparable yet not the same. The temperatures of the components are also very similar. The values of inclination and eccentricity are also consistent throughout all datasets.

The mass ratio discrepancy can be caused by the different values of exposure times of used TESS datasets 0,1,2, and 3 (1426 s, 465 s, 158 s, 158 s correspondingly). Nevertheless, the mass ratio has a high value in all datasets.

Table 5.4: Pair A – parameters of physical model.

Parameter	TESS 0	TESS 1	TESS 2	TESS 3	filter C	filter R	filter V	error
$\frac{R_1}{a}$	3.77	3.64	3.45	3.57	3.46	3.39	3.66	0.01
$\frac{R_2}{a}$	3.17	3.05	3.04	3.08	2.87	3.15	3.41	0.01
$M_{\text{bol1}}$ [mag]	1.549	1.628	1.744	1.672	1.743	1.785	1.620	0.001
$M_{\text{bol2}}$ [mag]	2.052	1.121	2.145	2.105	2.287	2.263	1.885	0.001
$T_{\text{ef1}}$ [K]	6 200	6 200	6 200	6 200	6 200	6 200	6 200	10
$T_{\text{ef2}}$ [K]	6 030	6 040	6 030	6 030	6 000	5 900	6 040	10
$i$ [°]	88.48	85.92	87.16	89.95	86.00	80.02	84.00	0.01
$q$	0.94	0.90	0.87	0.99	0.92	0.87	0.87	0.87
$e$	0.00	0.00	0.00	0.00	0.00	0.00	0.00	0.00

### 5.4.2 Pair B

Due to the almost integer value of the orbital period of pair B and lack of observational nights, the phase curve of pair B is not fully covered (see Figure 5.7). Therefore, the physical fit was only for TESS measurements. The physical models of pair B can be seen in Figure 5.14, and the values of parameters are listed in Table 5.5.

When comparing values of parameters of the physical fit of pair B, we have to take into account that the fit was done without any stellar spots. Moreover, the exposure times change, as was mentioned in the analysis of the physical fit of pair A. Even though the values of parameters are only estimates, they are consistent throughout all datasets.

The physical fit supports the assumption (based on the shape of minima in phase curves of pair B) that components have significantly different sizes and different effective temperatures. All parameters would be determined more precisely if we had some information about the stellar spots.

Table 5.5: Pair B – parameters of physical model.

Parameter	TESS 0	TESS 1	TESS 2	TESS 3	error
$\frac{R_1}{a}$	3.75	3.61	3.61	3.69	0.01
$\frac{R_2}{a}$	0.77	0.55	0.60	0.60	0.01
$M_{\text{bol1}}$ [mag]	1.165	1.248	1.248	1.198	0.001
$M_{\text{bol2}}$ [mag]	5.764	6.152	6.234	5.977	0.001
$T_{\text{ef1}}$ [K]	6 800	6 800	6 800	6 800	10
$T_{\text{ef2}}$ [K]	5 200	5 600	5 300	5 600	10
$i$ [°]	88.00	88.00	88.00	88.00	0.01
$q$	0.08	0.08	0.08	0.08	0.01
$e$	0.00	0.00	0.00	0.00	0.01

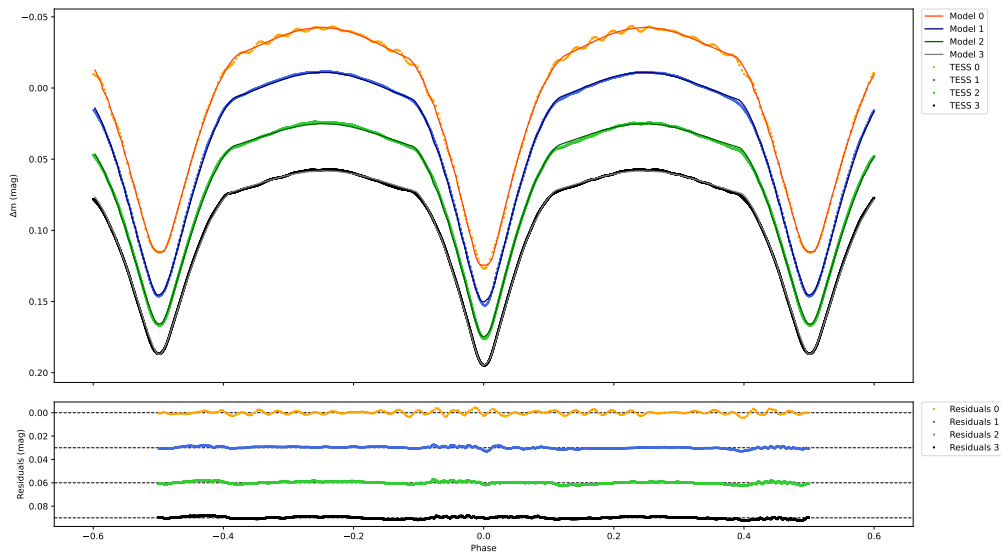


Figure 5.12: Pair A, TESS data - physical model.

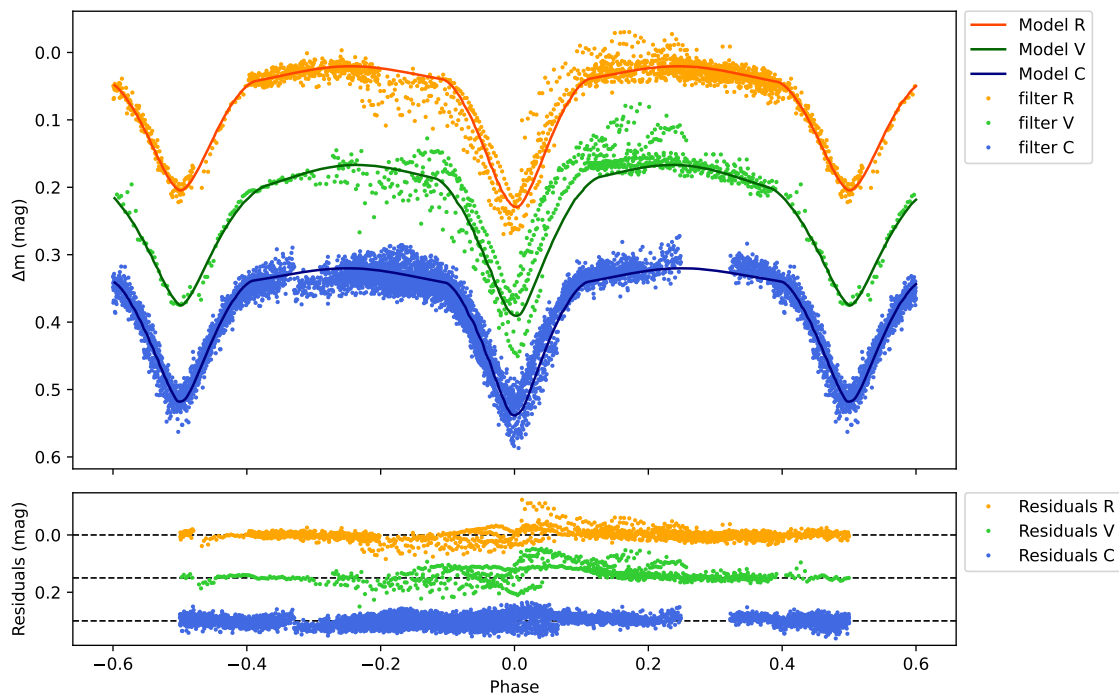


Figure 5.13: Pair A, ground-based data - physical model.

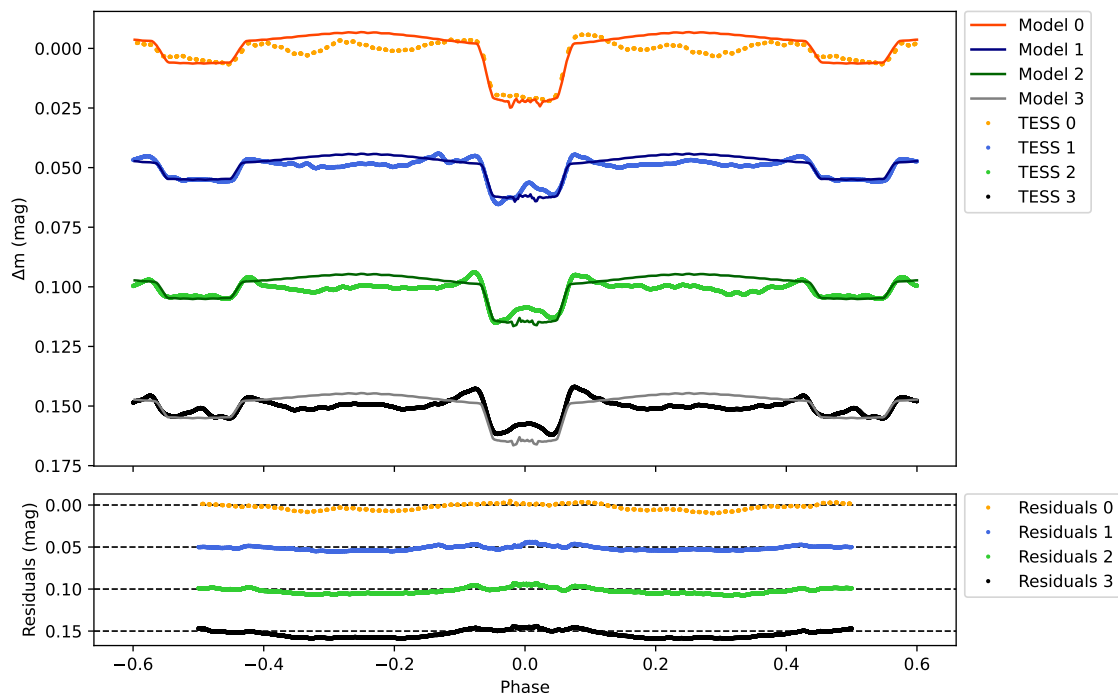


Figure 5.14: Pair B, TESS data - physical model.

## 5.5 Summary

Available photometric measurements of S1 Peg were analysed. By two independent methods (Fourier and iteration method), the phase curves of both pairs were obtained. For pair A, the physical models were calculated for both TESS and ground-based datasets. Due to the almost integer orbital period and lack of observational nights, the phase curve based on ground-based observations of pair B is not fully covered. Nevertheless, the change in brightness is clearly visible.

The timings of minima of both the pairs were determined via SILICUPS software and then plotted via OCFit. In the O-C diagram of both the pairs, the change in the orbital period is seen. In the case of pair A, the position of points resembles a parabola open upwards (the period of pair A is prolonging). On the other hand, the points in the O-C diagram of pair B are along a downward open parabola (the period of pair B is getting shorter). The ephemerides of both the pairs were further specified and are compared with the initial values of ephemerides in Table 5.6.

Even though we lack the spectroscopic data and O-C diagrams of individual pairs do not cover the whole phase of the sine curve, the O-C diagrams of individual pairs clearly go in antiphase. This is a sufficient reason to claim that the system S1 Peg is a doubly eclipsing stellar system.

Table 5.6: Specification of ephemerides of pairs A and B.

<b>Parameter</b>	<b>Pair A - original</b>	<b>Pair A - new</b>
$M_{0A}$ [HJD]	2459207.13900	$2459207.15103 \pm 0.00002$
$P_A$ [d]	0.747245	$0.747264 \pm 0.000001$
<b>Parameter</b>	<b>Pair B - original</b>	<b>Pair B - new</b>
$M_{0B}$ [HJD]	2458726.71000	$2458725.66000 \pm 0.00005$
$P_B$ [d]	2.083732	$2.083265 \pm 0.000003$

# Conclusion

Three candidates for doubly eclipsing stellar systems were studied in this thesis: ASAS J073054-1840.7, V0674 Pup, and TYC 2201-991-1. For this analysis, the photometric and spectroscopic measurements were used.

In the case of ASAS J073054-1840.7 (S2 Pup), the photometric data from the TESS satellite from years 2019, 2021, 2023, and 2025 were analysed. The ground-based observations were measured in 2022-2024 in photometric filters  $V$  and  $I$  at the La Silla observatory. The contributions of individual pairs were identified by two independent methods (iteration and Fourier). After removing pair A and B, in the residuals, the periodic changes in the brightness were found in all examined datasets. The period of these eclipse-like changes in brightness was estimated from the residuals ( $P_C = 10.4$  d), and due to the strong dominance of pair A in this system, no other peaks in the Lomb-Scargle periodogram were observed. The most probable cause of these periodic changes is a mutual eclipse in both pairs.

From the results of disentanglement by iteration method, the phase curves were plotted, and from their shape, the basic parameters of individual pairs were estimated. With this, the initially estimated values of parameters for the physical fits of pairs A and B were calculated using PHOEBE software. The phase curves of both pairs indicate that pair A and pair B are detached eclipsing binaries type Algol.

After that, the timings of minima were identified using SILICUPS software, and O-C diagrams for both pairs were plotted via OCFit. In the O-C diagram of pair A, the LiTE effect was modeled. Concerning the O-C diagram of pair B, a strong apsidal motion was modeled. After the elimination of the apsidal motion, no significant changes in the O-C diagram were observed. The values of ephemerides of pair B were further specified  $P_B=1.728520$  d and  $M_{0B}=2458508.97300$  HJD.

In the spectroscopic measurements, the splitting into four lines is not directly observed. However, the shift in the position of  $H\delta$  (4102 Å) and  $H\gamma$  (4340 Å) lines when one pair is in the eclipse is visible.

To prove whether or not the system S2 Pup is a doubly eclipsing system in the arrangement 2+2 (and its components are gravitationally bound) we would need more photometric data or more precise spectroscopic measurements.

Secondly, the system V0674 Pup (S1 Pup) was examined. The photometric measurements from the TESS satellite were captured in years 2019, 2023, and 2025. Ground-based observations were done in 2023-2025 at Los Leones and Boyden observatories.

By the disentanglement of the contribution of individual pairs, the O'Connell effect in pair A was identified. From the shape of the phase curves, the initial estimates of parameters of physical fit were determined. Due to the presence of the O'Connell effect, the physical model of pair A was only approximate. On the other hand, the physical model of pair B was very consistent throughout the studied datasets.

Using the determined moments of minima, the O-C diagrams of both pairs were plotted and modeled using the LiTE effect. Moreover, the values of ephemerides were specified for both the pairs ( $M_{0A} = 2458497.57501$  HJD,  $P_A = 0.602915$  d,  $M_{0B} = 2458511.44000$  HJD and  $P_B = 6.522901$  d).

The spectroscopic measurements did not show a splitting into four spectral lines, but in the subtraction of spectra, where pair B is in the same phase and pair A in a different phase, there is a significant splitting at hydrogen lines  $H\delta$  (4102 Å) and  $H\gamma$  (4340 Å).

Both photometric and spectroscopic measurements prove that there is a gravitational bond between pair A and pair B, and therefore, S1 Pup is a doubly eclipsing stellar system in the arrangement of 2+2.

Thirdly, the photometric observations of system TYC 2201-991-1 (S1 Peg) were analysed. The TESS data were captured in the years 2019, 2022, and 2024. The ground-based data were measured in 2021-2024.

Via iteration and the Fourier method, the contribution of individual pairs was determined. From the shape of the phase curves, the initial values of parameters in PHOEBE were estimated. In the minima of pair B, there is significant mid-eclipse brightening caused either by stellar spots or dust discs. As we lack information about the size and number of spots as well as the disc, the physical fit of pair B is only approximate. On the other hand, the physical fit of pair A corresponds well with the data.

The moments of minima were determined, and O-C diagrams were plotted for both pairs A and B. The LiTE effect was modeled, and the points in the O-C diagrams resemble parts of the sine curve that go in the antiphase. Therefore, even though we lack spectroscopic measurements for star S1 Peg, the position of points in the O-C diagram proves that it is indeed a doubly eclipsing stellar system in the arrangement 2+2. Moreover, the values of ephemerides were specified ( $M_{0A} = 2459207.15103$  HJD,  $P_A = 0.747264$  d,  $M_{0B} = 2458725.66000$  HJD and  $P_B = 2.083265$  d) using the O-C diagrams.

In conclusion, out of the three analysed candidates, two were proven to be doubly eclipsing systems in the arrangement 2+2. More measurements are essential to prove the gravitational bond in the remaining system.

# Bibliography

- A. Bayo, C. Rodrigo, D. Barrado Y Navascués, E. Solano, R. Gutiérrez, M. Morales-Calderón, and F. Allard. VOSA: virtual observatory SED analyzer. An application to the Collinder 69 open cluster. , 492(1):277–287, Dec. 2008. doi: 10.1051/0004-6361:200810395.
- K. Bernhard and S. Hümmerich. Four Candidate Binary Stars with strong Reflection Effect from the Zwicky Transient Facility. *Open European Journal on Variable Stars*, 206:1–8, Nov. 2020. doi: 10.5817/OEJV2020-0206.
- S. Bloemen, P. Degroote, K. Conroy, K. M. Hambleton, J. M. Giammarco, H. Pablo, and A. Prša. Physics of Eclipsing Binaries: Modelling in the new era of ultra-high precision photometry. In K. Pavlovski, A. Tkachenko, and G. Torres, editors, *EAS Publications Series*, volume 64 of *EAS Publications Series*, pages 269–276, Feb. 2013. doi: 10.1051/eas/1364037.
- Budaj, J. Effects of dust on light-curves of aurigae-type stars. *AA*, 532:L12, 2011. doi: 10.1051/0004-6361/201117320. URL <https://doi.org/10.1051/0004-6361/201117320>.
- Cagaš. Gxc ccd website - CAT187, 2025. URL <https://www.gxccd.com/cat?id=187lang=405>. Accessed: 2025-03-26.
- X. Chen, Z. Liu, and Z. Han. Binary stars in the new millennium. *Progress in Particle and Nuclear Physics*, 134:104083, 2024. ISSN 0146-6410. doi: <https://doi.org/10.1016/j.ppnp.2023.104083>. URL <https://www.sciencedirect.com/science/article/pii/S0146641023000649>.
- P. Gajdoš and Š. Parimucha. OCFit: Python package for fitting of O-C diagrams. *Astrophysics Source Code Library*, record ascl:1901.002, Jan. 2019.
- D. Graczyk. Light-curve solutions for bright detached eclipsing binaries in the small magellanic cloud: absolute dimensions and distance indicators. *Monthly Notices of the Royal Astronomical Society*, 342(4):1334–1348, July 2003. ISSN 1365-2966. doi: 10.1046/j.1365-8711.2003.06636.x. URL <http://dx.doi.org/10.1046/j.1365-8711.2003.06636.x>.
- P. M. Harmanec and P. Zasche. *Dvojhvězdy*. Astronomický ústav Univerzity Karlovy, 2023.
- Z. Henzl. Private communication, 2023.
- R. W. Hilditch. *An introduction to close binary stars*. Cambridge University Press, 2001.

- S. Jester, D. P. Schneider, G. T. Richards, R. F. Green, M. Schmidt, P. B. Hall, M. A. Strauss, D. E. Vanden Berk, C. Stoughton, J. E. Gunn, J. Brinkmann, S. M. Kent, J. A. Smith, D. L. Tucker, and B. Yanny. The Sloan Digital Sky Survey View of the Palomar-Green Bright Quasar Survey. , 130(3):873–895, Sept. 2005. doi: 10.1086/432466.
- J. Kolář. Private communication, 2023.
- J. Kolář, M. Zejda, A. Richterková, P. Dvořák, R. F. Auer, Z. Henzl, R. Dřevěný, S. Pačková, and M. Uhlár. Period ratios and observation of noticeable resonance at 3:2 for 2+2 quadruple systems. *Monthly Notices of the Royal Astronomical Society*, 538(2):1160–1166, 03 2025. ISSN 0035-8711. doi: 10.1093/mnras/staf364. URL <https://doi.org/10.1093/mnras/staf364>.
- V. B. Kostov, B. P. Powell, G. Torres, T. Borkovits, S. A. Rappaport, A. Tokovinin, P. Zsche, D. Anderson, T. Barclay, P. Berlind, P. Brown, M. L. Calkins, K. A. Collins, K. I. Collins, D. M. Conti, G. A. Esquerdo, C. Hellier, E. L. N. Jensen, J. Kamler, E. Kruse, D. W. Latham, M. Mašek, F. Murgas, G. Olmschenk, J. A. Orosz, A. Pál, E. Palles, R. P. Schwarz, C. Stockdale, D. Tamayo, R. Uhlář, W. F. Welsh, and R. West. TIC 454140642: A compact, coplanar, quadruple-lined quadruple star system consisting of two eclipsing binaries. *The Astrophysical Journal*, 917(2):93, Aug. 2021. ISSN 1538-4357. doi: 10.3847/1538-4357/ac04ad. URL <http://dx.doi.org/10.3847/1538-4357/ac04ad>.
- S. Kouzuma. Mass ratio estimates for overcontact binaries using the derivatives of light curves, 2023. URL <https://arxiv.org/abs/2311.10949>.
- Q.-Y. Liu and Y.-L. Yang. A possible explanation of the o’connell effect in close binary stars. *Chinese Journal of Astronomy and Astrophysics*, 3:142, 04 2009. doi: 10.1088/1009-9271/3/2/142.
- Z. Mikulášek and M. Zejda. *Proměnné hvězdy*. ÚTFA PřF MU, Brno, 2013.
- E. A. Milne. The reflection effect in eclipsing binaries. *Monthly Notices of the Royal Astronomical Society*, 87(1):43–55, 11 1926. ISSN 0035-8711. doi: 10.1093/mnras/87.1.43. URL <https://doi.org/10.1093/mnras/87.1.43>.
- D. Motl. Muniwin v2.1. <http://c-munipack.sourceforge.net>, 2010. Accessed: 2025-04-21.
- D. J. K. O’Connell. The so-called periastron effect in close eclipsing binaries ; New variable stars (fifth list). *Publications of the Riverview College Observatory*, 2(6):85–100, Aug. 1951.
- K. Oláh, B. Seli, A. Haris, S. Rappaport, M. Tuomi, R. Gagliano, T. L. Jacobs, M. H. Kristiansen, H. M. Schwengeler, M. Omohundro, I. Terentev, A. Vanderburg, B. Powell, V. Kostov, and Z. Kóvári. Starspots on eclipsing giant stars i.: The sample and eclipse mapping examples, 2025. URL <https://arxiv.org/abs/2504.15389>.
- B. P. Powell, V. B. Kostov, S. A. Rappaport, T. Borkovits, P. Zsche, A. Tokovinin, E. Kruse, D. W. Latham, B. T. Montet, E. L. N. Jensen, R. Jayaraman, K. A. Collins, M. Mašek, C. Hellier, P. Evans, T.-G. Tan, J. E. Schlieder, G. Torres, A. P. Smale, A. H. Friedman, T. Barclay, R. Gagliano, E. V. Quintana, T. L. Jacobs, E. A. Gilbert, M. H. Kristiansen, K. D. Colón, D. M. LaCourse, G. Olmschenk, M. Omohundro, J. D.

- Schnittman, H. M. Schwengeler, R. K. Barry, I. A. Terentev, P. Boyd, A. R. Schmitt, S. N. Quinn, A. Vanderburg, E. Palle, J. Armstrong, G. R. Ricker, R. Vanderspek, S. Seager, J. N. Winn, J. M. Jenkins, D. A. Caldwell, B. Wohler, B. Shiao, C. J. Burke, T. Daylan, and J. Villaseñor. Tic 168789840: A sextuply eclipsing sextuple star system. *The Astronomical Journal*, 161(4):162, Mar. 2021. ISSN 1538-3881. doi: 10.3847/1538-3881/abddb5. URL <http://dx.doi.org/10.3847/1538-3881/abddb5>.
- A. Prša, G. Matijevic, O. Latkovic, F. Vilardell, and P. Wils. PHOEBE: PHysics Of Eclipsing BinariEs. Astrophysics Source Code Library, record ascl:1106.002, June 2011.
- A. Richterková. *Studium vybraného vícenásobně zákrytového systému*. Masarykova univerzita, 2023.
- K. Serkowski. Determination of differential limb darkening of eclipsing binaries from multicolor photometric observations. I. , 66:405, Oct. 1961. doi: 10.1086/108445.
- L.-Y. Song and Z.-J. Tian. Period–luminosity–metallicity–color relations of late-type contact binaries in the big data era. *The Astrophysical Journal*, 961(2):248, jan 2024. doi: 10.3847/1538-4357/ad12c0. URL <https://dx.doi.org/10.3847/1538-4357/ad12c0>.
- R. E. Wilson. Eccentric orbit generalization and simultaneous solution of binary star light and velocity curves. *The Astrophysical Journal*, 234:1054–1066, 1979.
- P. Zasche. Private communication, 2024.
- P. Zasche, D. Vokrouhlický, M. Wolf, H. Kučáková, J. Kára, R. Uhlař, M. Mašek, Z. Henzl, and P. Cagaš. Doubly eclipsing systems. *Astronomy & Astrophysics*, 630:A128, 2019.
- P. Zasche, Z. Henzl, H. Lehmann, J. Pepper, B. P. Powell, V. B. Kostov, T. Barclay, M. Wolf, H. Kučáková, R. Uhlař, M. Mašek, S. Palafouta, K. Gazeas, K. G. Stassun, B. S. Gaudi, J. E. Rodriguez, and D. J. Stevens. Czev1731: The unique doubly eclipsing quadruple system. *AA*, 642:A63, 2020. doi: 10.1051/0004-6361/202038656. URL <https://doi.org/10.1051/0004-6361/202038656>.
- P. Zasche, Z. Henzl, and M. Mašek. Multiply eclipsing candidates from the tess satellite. *AA*, 664:A96, 2022. doi: 10.1051/0004-6361/202243723. URL <https://doi.org/10.1051/0004-6361/202243723>.
- P. Zasche, Z. Henzl, M. Mašek, R. Uhlař, J. Kára, J. Merc, and H. Kučáková. Detection of seven 2+2 doubly eclipsing quadruple systems. *Astronomy amp; Astrophysics*, 675:A113, July 2023. ISSN 1432-0746. doi: 10.1051/0004-6361/202346848. URL <http://dx.doi.org/10.1051/0004-6361/202346848>.

# Appendices

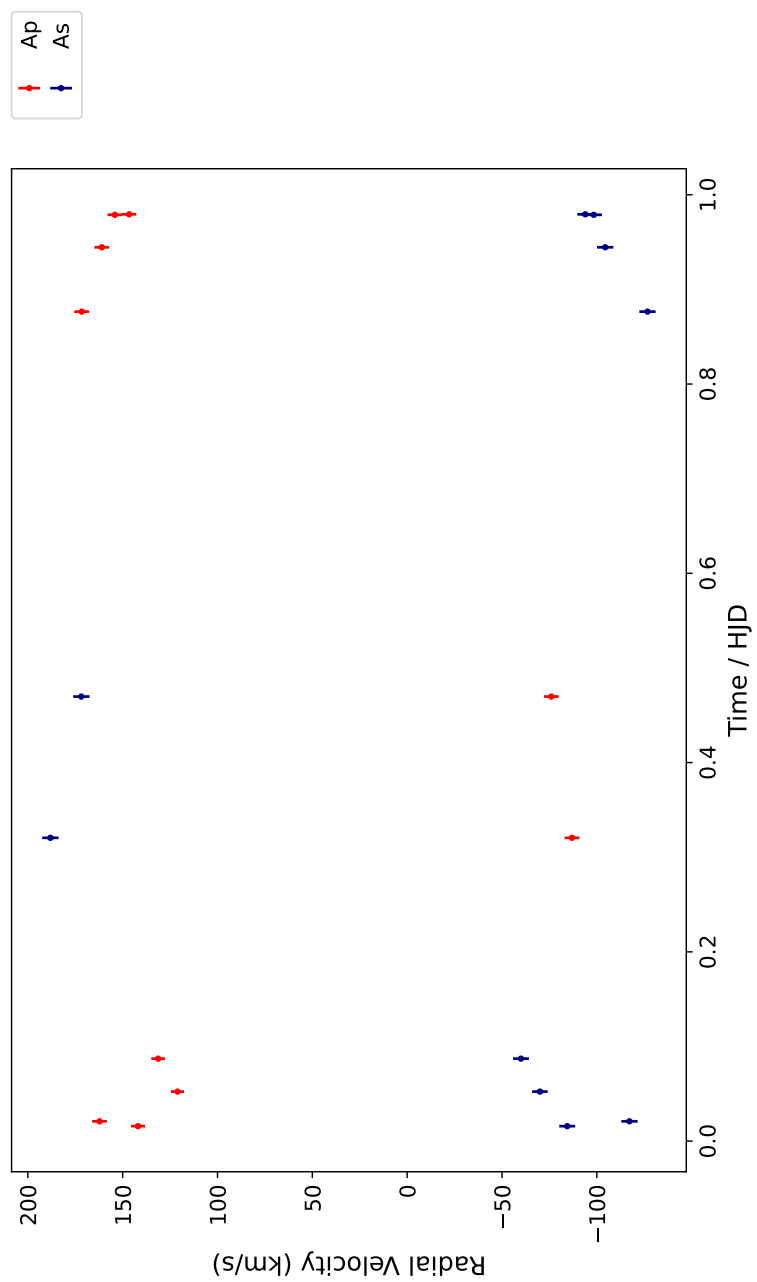


Figure 5.15: Pair A - radial velocity curve.

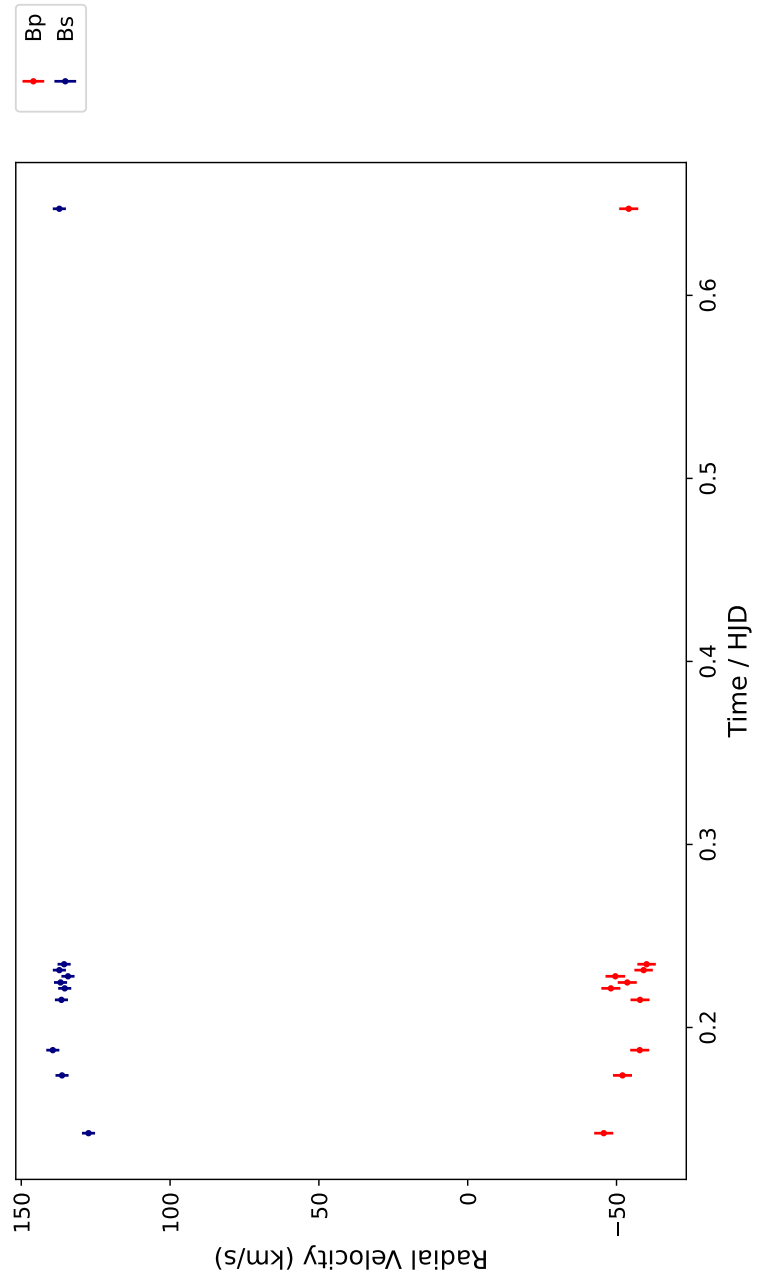


Figure 5.16: Pair B - radial velocity curve.

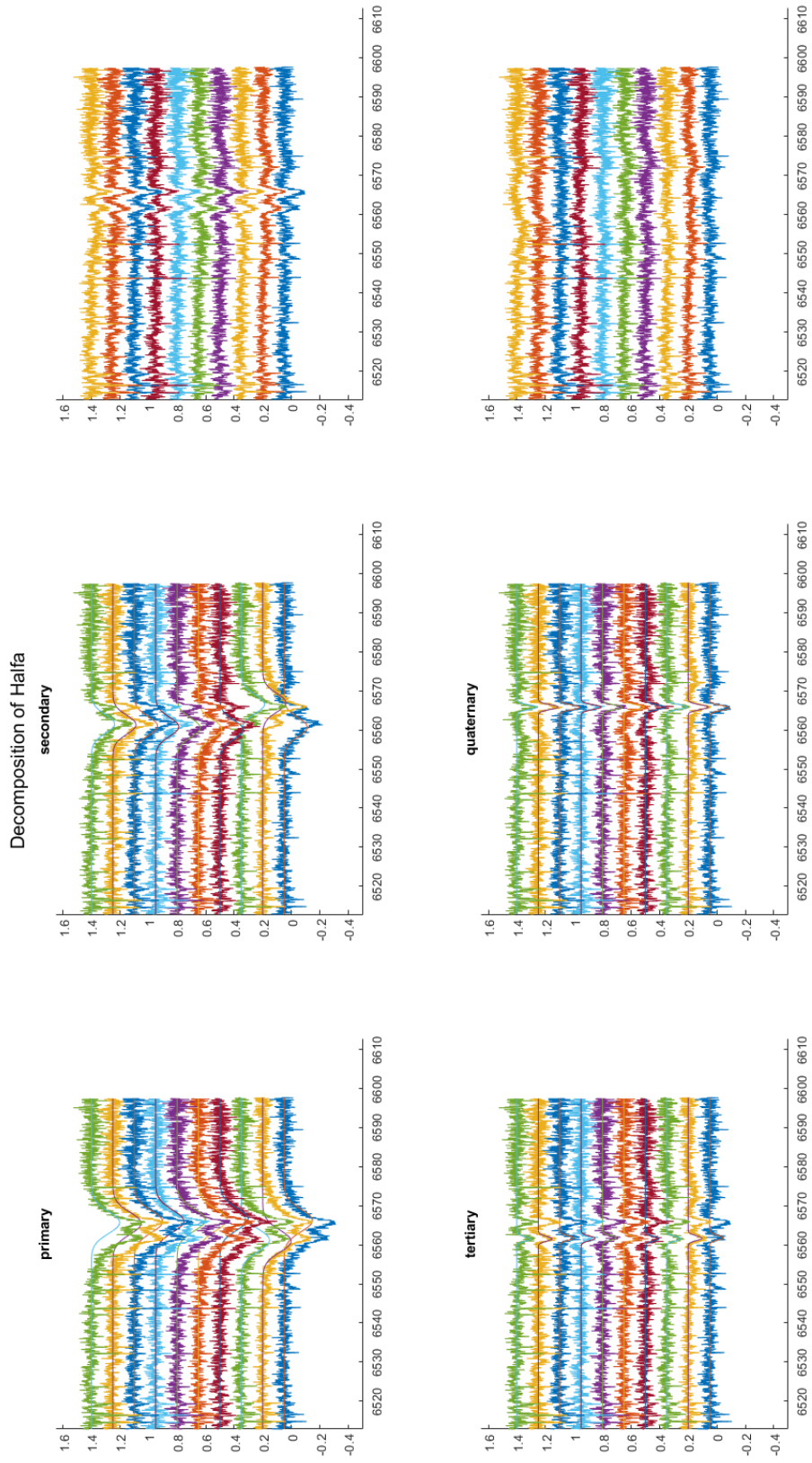


Figure 5.17: S1 Pup - splitting into 4 spectral lines.